DEVELOPMENT OF FAILURE CRITERIA AND EXPERIMENTAL TESETING FOR COMPOSITE ADHESIVELY BONDED SCARF REPAIRS UTILIZING STRUCTURAL PASTE ADHESIVES

by

Tammy Nicole Ritchey

A thesis submitted in partial fulfillment
of the requirements for the degree

of

Master of Science

in

Mechanical Engineering

MONTANA STATE UNIVERSITY

Bozeman, Montana

May 2014

ACKNOWLDEGMENTS

A special thank you to my committee members, Dr. Douglas Cairns, Dr. David Miller, and Dr. Jared Nelson for their guidance and mentorship throughout the course of this research. Daniel Samborsky was instrumental in the experimental portion. Finally, thank you to the Montana State University composites group for the hard work dedicated to the completion of this research.

TABLE OF CONTENTS

TABLE OF CONTENTS - CONTINUED

TABLE OF CONTENTS - CONTINUED

TABLE OF CONTENTS - CONTINUED

LIST OF TABLES

Table Page

LIST OF TABLES – CONTINUED

Table Page

LIST OF FIGURES

Figure Page

LIST OF FIGURES – CONTINUED

Figure Page

LIST OF FIGURES – CONTINUED

Figure Page

LIST OF FIGURES – CONTINUED

Figure Page

LIST OF FIGURES – CONTINUED

Figure Page

LIST OF FIGURES – CONTINUED

Figure Page

ABSTRACT

Rapid growth of composite application in wind energy has strained the wind turbine blade service industry as blades continually fail prior to life cycle expectations. Minimal research surrounding composite repair has led to gaps in the ability to characterize, analyze, and predict composite repair behavior. Certification standards derived from two dimensional simplified geometric configurations are speculated to be conservative. In this study, coupon level adhesively bonded composite scarf repair specimens are developed and tested to failure under static tensile loads. Based on experimental results, a geometry independent failure criteria is proposed and validated through finite element modeling. Specimen failures are compared against current repair standards and analysis techniques. The proposed maximum Von Mises Strain failure criteria has potential to provide a preliminary decision making framework for the service industry reducing time, cost, and resources.

INTRODUCTION

Composite wind turbine blades are designed to last 20 years in the field.[1] Since inception, service life of these blades continually falls short of design life. With the rapid growth of composite application in wind energy, the service industry has become strained as generations of blades are failing as they approach 10 to 15 years of field life. In recent years, the need for repair is becoming industry recognized, but documentation of parameters detailing efficient repair methods, materials, and effect are lacking in the face of demand. Due to the lack of research surrounding composite repair, standards for certification of a wind turbine blade repair are derived from two dimensional analyses of simplified geometric configurations.[2] Absent of experimental data collected from test specimens that accurately represent a repair scheme, these standards are speculated to be conservative.

The goal of this research is to collect tensile data on coupon level repair specimens by first developing a geometrically accurate repair specimen. An adhesively bonded scarf repair scheme is utilized. The results are then compared against industry standards and results from tensile joint testing, the simplified version of an adhesively bonded repair. A geometry independent failure criterion based on the repair coupon experimental data is sought. This failure criteria is then integrated into a two-dimension finite element model to test its accuracy at predicting failure in the repaired composite. A secondary goal of this research is to visually capture the strain field through the thickness of the repair to better understand the damage progression in the composite under a tensile load.

The parameters of this study include varying scarf angles, composite adherend layups in joints, amount of material and number of plies removed, and types of two-part paste adhesives. A joint is a form of repair in which damage is incurred throughout the full thickness of the composite. Repair specimens representative of damage occurring in a fraction of the composite plies require a removal of only those damaged plies. These specimens are referred to as non-through thickness repairs. Only adhesively bonded joints and scarf repairs with composite adherends and two-part paste adhesives are considered. This study assumes a constant nominal adhesive thickness and does not encompass a full adhesive parametric analysis. In addition, finite element modeling is limited to 2D. Experimental testing considers only tensile loading and does not involve compressive, bending, shear, or torsional forces.

The objective of this research is three-fold:

I) Quantify the effects of scarf angle, depth of repair, and material compatibility on failure in adhesively bonded joints and repair coupons to enhance decision making for the service industry.

II) Validate current composite repair standards in the use of 2D joint models to analyze 3D repair scenarios and derive a geometry independent failure criterion to more accurately predict the adhesive failure in the bondline of a scarf repair and correlate the criterion with finite element modeling.

III) Visually characterize the strain field and damage progression through the thickness of an adhesively bonded scarf repair and joint using ARAMIS data image correlation.

This research is intended to contribute to the database of knowledge surrounding composite repair, setting the stage for further developments in optimized repair design and the predicative capabilities of finite element modeling.

BACKGROUND

Composite Damage and Analysis

Impact damage, manufacturing defects, and environmental wear drive the need for the repair industry. The most common types of damage include crushing, surface scraping, gouging, erosion, fatigue, thermal cycling, puncture holes, pitting, delamination, cracking, disbonding and spar separation.[1] A few examples of in-field blade damage are shown in Figure 1. Composite blades see a considerable amount of

Figure 1: Wind Turbine Blade Damages

damage before being put into service. Defects such as porosity, voids, delamination, and fiber waviness resulting from manufacturing reduce the composite's material properties. Impact damage resulting from transportation by road, rail, and crane from the manufacturing facility to the field sight is observed regularly. Delamination generally causes compressive and shear issues, matrix damage results in a loss of stiffness, and fiber damage reduces strength.[3] Repair of these defects and damaged areas is completed before the blade is put into service.

Damage analysis is based on the stress state around the damaged area compared to the laminate's original ultimate strength.[4] Left un-repaired damage will continue to progress through three distinct stages. Stage one is defined by multiple cracking and characterized by a random pattern of damaged scattered over the laminate. In stage two, delamination initiation begins and damage localizes at free edges or interfaces. Finally, during stage three, the fibers fracture and the laminate fails.[3] A repair is intended to restore a laminate at any damage progression stage to a new laminate free of any cracking or indication of damage. A repaired composite will, in theory, have restored strength greater than the knocked down properties of the damage or defect, but less strength than the original undamaged and unflawed composite.

Composite Repair Methods

Current repair methods begin with inspection, damage assessment, and surface preparation.[1] The repair scheme is then applied taking into account parent resin and fiber material properties and orientation, followed by post-repair inspection, documentation, and monitoring.[3] Small repairs do not require fiber reinforcement and are typical with matrix cracks. Low viscous resins are used to fill the damaged area with a standard cartridge gun and sometimes sealed with a [+45/-45] external patch for the purposes of environmental protection.[4]

Structural restoration repairs resulting from fiber damage require more invasive techniques. The two most prominent techniques are the external patch, Figure 2, and the scarfed patch repair scheme. In both methods, the damaged section is removed.

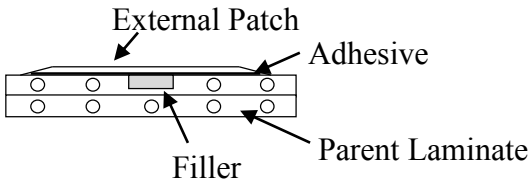

Figure 2: External Patch Composite Repair Scheme

However, the patch method employs a filler in the removed section over which a tapered external patch is bonded with adhesive. The external patch may or may not have the same lay-up as the parent.

In a scarf repair, Figure 3, the parent laminate receives a tapered angle as the damaged section is removed and the repair patch, which has the same lay-up as the

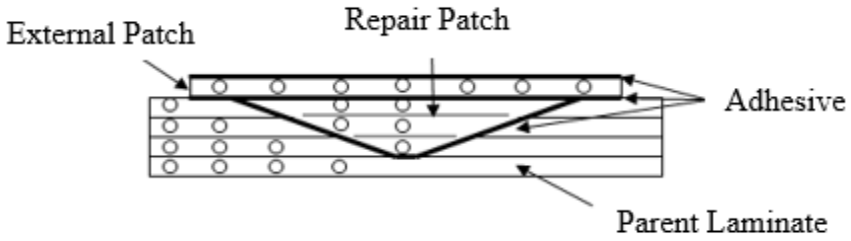

Figure 3: Scarfed Patch Composite Repair Scheme

parent, is stepped.[4] Parent and patch are bonded with a layer of adhesive. The scarf is then completed with the 2-ply ±45 external patch environmental seal similar to small repair schemes. Images of this repair scheme are shown in Figure 4. Scarf repairs are more difficult and time consuming and therefore best suited for a factory setting vs. in-field service. A scarf is ideal for repairing defects caused during the manufacturing of the blade or for repairing damaged incurred before the blade becomes operational. The

external patch is more commonly used for field repairs of damage caused by environmental wear, fatigue, lightning and bird strikes.

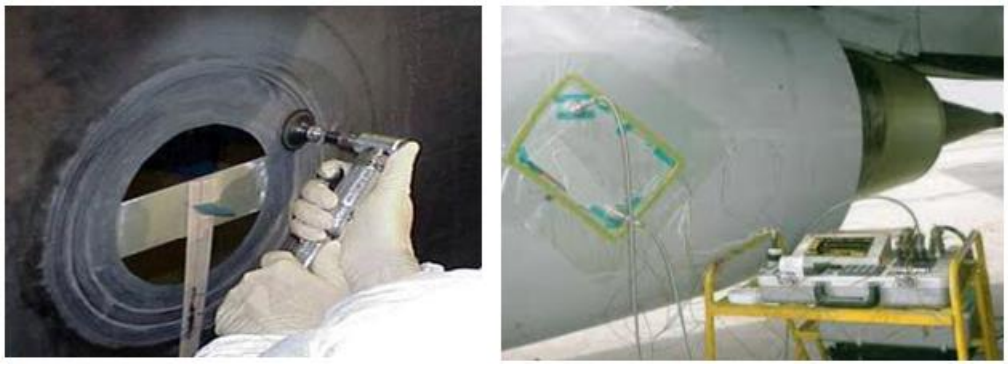

Figure 4: Images of Composite Repair Procedure
Left: Scarf Material Removal; Right: Vacuum Co-cure of Scarfed Repair Patch

The repair patch can either be "soft" or "hard." A soft patch is comprised of a composite pre-preg or a wet lay-up and co-cured with the adhesive in place. The hard patch is molded and cured prior to the adhesive bonding. This process requires a mold, takes more time and therefore, is more expensive than the soft patch approach. However, utilizing the hard patch approach ensures a higher quality patch, no distortion of plies, lower adhesive driven temperatures can be used while curing, and prior non-destructive testing (NDI) is possible. All of which can be downfalls of a soft patch.[5]

Understanding Joints as a Simplified Repair

Bonded Joint Configurations and Stress States

Structural restoration repair schemes are typically analyzed as a bonded joint due to the adhesive layer. Joint types, Figure 5, include single lap, double lap, scarf, stepped lap, bevel, and butt. Basic loads seen in adhesive bonded joints are tension, compression,

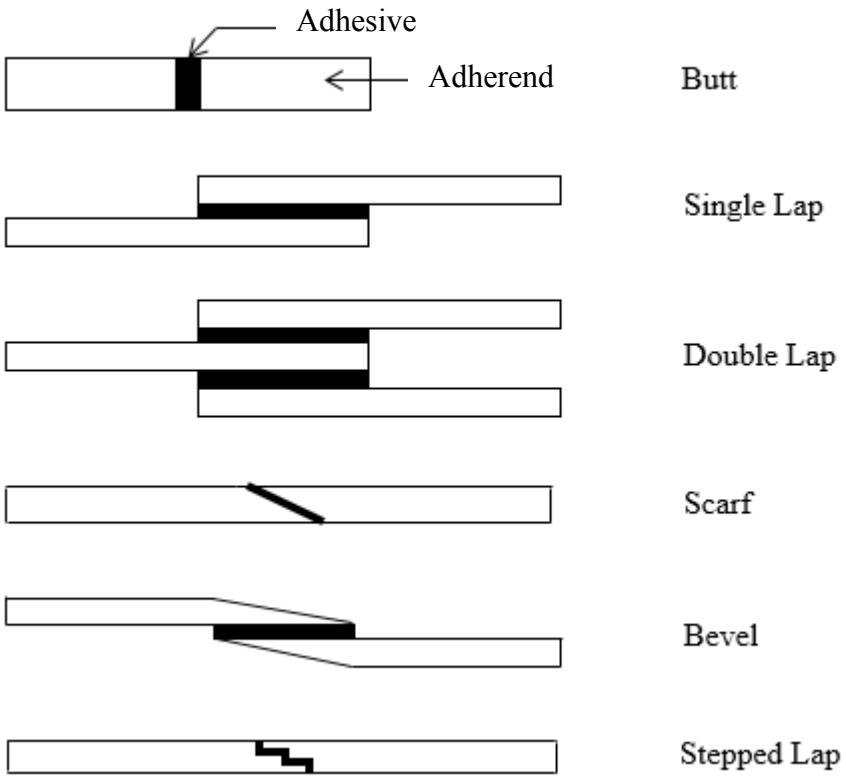

Figure 5: Basic Joint Types

shear, cleavage, and peel, Figure 6.[6] The most intense loads are the cleavage and peel conditions as the applied force is concentrated into a "single line of high stress."[7] A bond

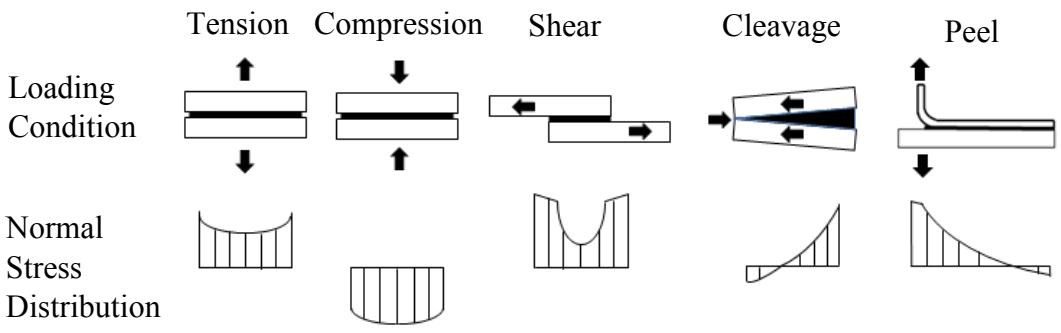

Figure 6: Basic Joint Stresses Induced by Typical Loading Conditions

will experience a combination of loading conditions. Therefore to achieve maximum strength, peel and cleavage stresses are sought to be minimized. A scarfed patch, as previously described, is more efficient than an external patch as the shear stress in the adhesive layer is uniformly distributed. An external patch is subject to severe bending and buckling instability as well as peeling stresses in the adhesive.[3] Thus, in composite repair patches it is advantageous to add a tapper to the adjacent material. The added angle strengthens the design by transferring some of the cleavage and peel loads to tension, compression, and shear stresses.

Failure Modes

There are three modes of failure associated with a bonded joint. An adhesive failure, Figure 7, occurs on the bond-substrate interface due primarily to a lack of chemical bonding. During this failure mode, the adhesive separates clean from one or both surfaces

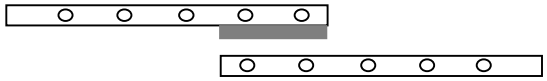

Figure 7: Adhesive Failure Mode

and is more likely the result of poor surface preparation or lack of suitability between adhesive and substrate.

A failure occurring primarily in the adhesive layer is called a cohesive failure, Figure 8. This is the preferred type of failure in a bonded joint and is the mode that drives the predicted load in the design of the joint. A joint that experiences a cohesive failure well below the predicted load is likely the result of poor curing process,

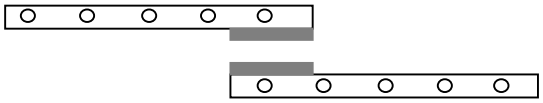

Figure 8: Cohesive Failure Mode

introduction of contaminants in the adhesive, or influence of environmental conditions such as moisture and temperature.

A substrate failure, the third common failure mode depicted in Figure 9, is characterized by an interlaminar fracture in the composite. The fracture typically occurs

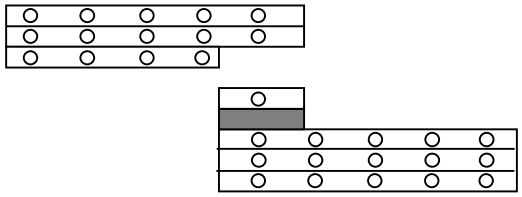

Figure 9: Substrate Failure Mode

between the first and second layer closest to the bondline and is most prevalent with composites containing brittle epoxies.

Repair Design Parameters

Design parameters for the optimal blade repair include repair type and dimensions, materials, cure conditions, internal stresses due to material interface chemistry, energy dissipation, and geometry and layup of the parent.[8] Significant factors influencing the strength of a repair are listed in Table 1 and discussed in the following sections.

Table 1: Composite Repair Design Factors

Parameter	Scope of Research	Design Goals
Patch Type – External vs Scarfed & Hard vs Soft	No	Optimize design based on repair location: in-field vs factory
Scarf Angle	Yes	Reduced peel and cleavage stresses
Bondline Thickness	No	Maximize repair patch strength and cohesive failure modes
Local Variations in Scarf Angle and Bondline Thickness	No	Optimize strength to material removal ratio
Depth of Damage/Repair	Yes	Understand ultimate strength of structure
Adhesive Type	Yes	Increase adhesion characteristics/ Reduce application flaws
Adherend Thickness	No	Attain optimal cohesive failure mode
Parent Composite Layup	Yes	Minimize stress concentrations on outer plies
Adhesive-Adherend Compatibility	No	Increase adhesion characteristics
Cure/Co-Cure Conditions	No	Increase adhesion characteristics

Film and Paste Adhesives

Film adhesives are traditionally used to bond the parent and patch. These high-performance structural pre-preg adhesives can be epoxy, bismaleimide- (BMI), phenolic-, polyimide- and cyanate ester-based, and they are distributed in film form or on a roll with varying thicknesses available. Simple to apply, they are noted for their high peel strength, but require an elevated temperature cure cycle such as use of an autoclave.[6] The use of structural paste adhesives in place of film adhesives may offer some distinct advantages. Structural paste adhesives are noted for their excellent peel strength, the most intense loading condition seen in a joint, and are less subject to distortions than films[4]. Bondlines up to 30mm can be employed which is beneficial for thick composites often seen in the wind turbine and aerospace industries. Though more difficult to apply

than a film, local variations in bondline thickness around the scarf can be explored in an effort to optimize the repair. Some paste adhesives can be cured at room temperature, while others can be cured using a tempered vacuum bag method. Temperatures needed to cure these pastes are far less than film adhesives.

A variety of structural paste adhesives are suitable for the adhesively bonded repair application. Paste adhesives are either one-part or two-part with a resin, part A, and hardener, part B mixed by a manufacturer prescribed ratio. Toughened adhesives are available for epoxy and acrylic-based adhesives. A toughed adhesive contains rubber-like particles dispersed within the matrix resulting in increased resistance to crack propagation. Epoxy-based adhesives are the most widely used in industry primarily due to their high mechanical and thermal properties, water resistance, and low cure shrinkage.[9] Polyurethane adhesives are most noted for high peel strengths and increased toughness. Other mechanical properties such as tensile strength are moderate. Limited working time makes polyurethane difficult to implement for in-field and large repairs. Less surface prep is required for polyurethane vs epoxy and these adhesives can be cured at room temperature. They are naturally crack resistant and therefore do not need to be toughened. High strain to failure, ease of mixing, and low peak exothermic temperatures makes this adhesive a suitable choice for composite repair.[10] Another typical adhesive system used in the wind turbine industry is methacrylate, MA. This acrylic-based adhesive can be toughened and has better adhesion characteristics than other structural adhesives. High resistance to temperature, humidity, and UV makes MA durable in harsh environmental conditions subjected on wind turbine blades.

Bondline Thickness

Bondline thickness is a crucial parameter in the design of a joint. The strength of the bond at the interface between the substrate and the adhesive is stronger than the bond within the adhesive itself. Therefore, shear strength greatly diminishes with a thick bondline. Figure 10, published by Huntsman, reveals that the shear strength drop occurs

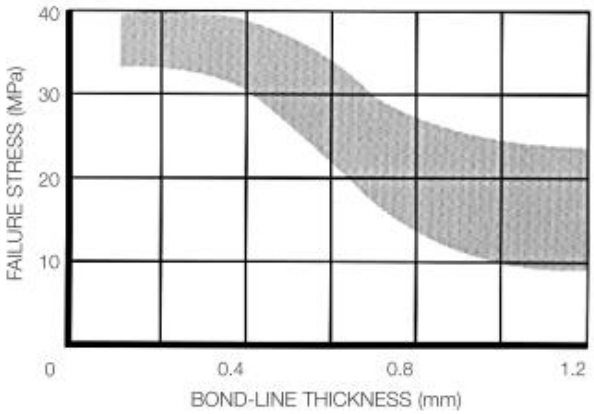

Figure 10: Effect of Bondline Thickness on Failure Stress in Single Lap Joints[7]

between 0.4mm and 1.0mm, depending on adhesive's characteristics, after which the strength remains approximately the same. Toughened adhesives are reported to maintain strength longer in a thicker bondline while rigid adhesives will drop more quickly. Huntsman recommends an optimum bondline thickness of 0.1mm to 0.3mm. A previous study published by the International Journal of Adhesion and Adhesives shows that thin bondlines, between 0.3mm and 0.6mm, have higher failure loads and shear strength than thick bondlines.[8] The study analyzed a butt-joint with a two part epoxy adhesive and aluminum alloy adherend under pure tension and pure shear. Failures in thick bondlines, considered greater than 1mm, tend to be less brittle and thus less catastrophic in nature.

Adherend Thickness

A study conducted by the FAA on a single lap joint using a two part epoxy paste adhesive and fiberglass and carbon fiber laminate adherends noted that adhesive joints with composite adherends, regardless of bondline thickness, experience failure in the adherend material, not at the adhesive or interface.[11] The substrate failures all occurred between the first two plies closest to the adhesive joint. This indicates that the failure mode is more influenced by the thickness of the substrate vs. the thickness of the adhesive. Substrate thickness also affects joint shear strength as it is highly dependent on the bending stiffness of the parent. Reduced bending stiffness increases the peel stresses in the bondline. Thick bondlines exhibit a similar and more pronounced load path distribution than thin bondlines which is thought to be the main contributor to decreased strength in thicker bonds. Shear and tensile strength test results on varying bondline thickness are shown in Figure 11. The majority of previous research has been conducted on single lap joints. The purpose of a chamfered scarf joint is to reduce peel stresses by transferring these stresses to a higher concentration of tension, compression, and shear.

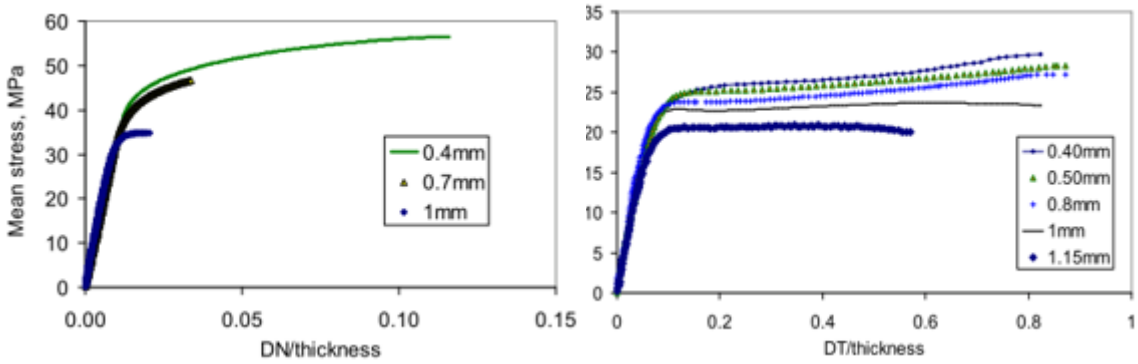

Figure 11: Influence of Bondline Thickness on (a) Tensile and (b) Shear Strength in Butt Joints[8]

Cure Conditions

In thin bondlines there is a risk of unfilled regions resulting in substrate-to-substrate contact, which will significantly reduce the strength of the bond. Careful application of the adhesive and use of spacers between the substrate can mitigate this risk. Application of pressure and elevated temperature during the cure cycle can increase bond strength and should be consistent with manufacturer recommendations. A uniform distribution of pressure on the bond is an important factor on optimizing the strength of a bonded joint. Use of vacuum while curing is one method of achieving uniform pressure. A side effect of curing adhesive bonds at elevated temperatures is a defect known as micro-voiding. Characterized by a significant number of small voids, Figure 12, the total

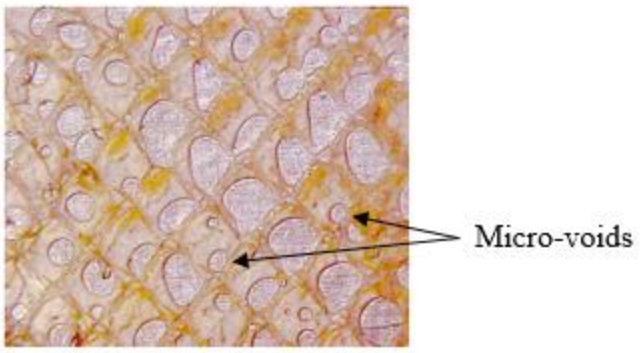

Figure 12: Micro-voids Observed in a Lap Joint Adhesive[7]

sum of the area of the voids can be enough to cause significant strength degradation of up to 53% of peel strength in the adhesive.[8] Micro-voids are a byproduct of gasses, namely water as steam, released during the curing cycle after the temperature reaches boiling point. Adding vacuum to the process may draw out some voids near the edge of the adhesive, but excessive pressure actually worsens the situation as a whole by making the

majority of the micro-voids larger. Controlling the temperature and vacuum parameters while the bond is curing can minimize the occurrence of this phenomenon. An article written by Adhesion Associates, a specialist in composites, adhesive bonding, and aircraft repair technologies, recommends limiting the applied vacuum to 25mmHg and controlling the temperature elevation rate as specified by the manufacturer, which is typically 3°C to 6°C.[8]

Repair Analysis Criterion

Certification Standards

Considered conservative, repair analysis criterion considers strength restoration, buckling resistance, fatigue, and deflection limitations. International industry standards for repairs are outlined by the EIC and certified by agencies such as Germanischer Llyod. Section three, "Repair of Components," in Rules for Classification and Construction, Materials and Welding (Non-metallic materials), outlines the requirements for repair of composite materials that must be met for certification purposes. Of notable interest are the following rules:

> (1.1) Damaged material, or material which no longer exhibits complete bonding, shall be removed from the area to be repaired.
>
> (1.2) The region adjacent to the damaged area shall be chamfered. The Chamfer ration (chamfer length l_s to chamfer thickness t_s) depends on the tensile strength of the repair material, σ_{Mat}, in the chamfer direction and the permissible shear stress, τ. The minimum chamfer ratio shall be calculated by means of the

following formula:

$$\frac{\sigma_{Mat}}{\tau} = \frac{l_s}{t_s} * \chi \quad (1)$$

x = 1 for hand laminate
x = 1.05 in case of tempering
x = 1.15 for curing under vacuum and tempering

The permissible shear stress shall be 9 MPa (1.3 ksi) for repairs in the shop and 7 MPa (1.0 ksi) for repairs in the field.[12]

Application of Standards to Composite Laminates

Applications of this standard to four composite layups for a hand laminate with a permissible shear stress of 9 MPa are shown in Table 2. A joint configuration is assumed and the chamfer thickness set to the average thickness of the 4-ply laminate.

Table 2: G-L Required Scarf Angles for Composite Test Specimens

Layup (4-ply)	**Chamfer Thickness (t_s)**	σ_{Mat}	**Chamfer Length (l_s)**	**Required Scarf Angle (deg)**
Glass Uni	0.12 in	146 ksi	13.4 in	0.5
Carbon Uni	0.15 in	206 ksi	23.7 in	0.35
Glass Triax	0.19 in	119 ksi	17.3 in	0.65
Hybrid Triax	0.20 in	151 ksi	23.2 in	0.5

Most repairs are completed by a trained technician using an angled grinder. Due to the lack of precision tooling during repair work, the accepted industry standard for scarf angles is between one and three degrees. In order to achieve the scarf angle required by these standards, a significant amount of undamaged material must be removed, especially in the case of thick laminates. Conservative failure criteria leads to an overdesigned repair, shallower scarf angle, removal of unnecessary material, and ultimately more time

and higher cost. Little research has been conducted on composite repair. Therefore an effective and optimal failure criteria has yet to be proven. It is possible that current standards are too conservative for the implementation of composite repair schemes in the wind turbine industry.

Failure Criteria

An important part of the design process is to define an upper bound on the stress state of the structure thereby defining its point of failure. This point becomes difficult to define when the structure is subjected to multi-axial loading. Failure criterion that address a multi-axial stress state include maximum-shear stress theory, maximum-distortion-energy theory, maximum-normal-stress theory, and the strain energy release rate approach. The former two criteria are best applied to ductile materials, for which failure is defined by yield initiation. The latter two describe brittle failures characterized by fracture of the material.

Tresca Yield Criterion. Maximum-shear-stress theory or Tresca yield criterion states that yielding begins when the absolute maximum shear stress in the material reaches the shear stress that causes the same material to yield when it is subjected only to axial tension. Therefore, the absolute max shear stress must be less than or equal to half the axial tensile stress.[13]

Von Mises Hencky Theory. Maximum-distortion-energy, or Von Mises Hencky, theory relates to the distortion caused by strain energy once the material has reached its ability to store energy internally throughout its volume when subjected to a stress

condition. This theory states that yield occurs when the distortion energy per unit volume of the material equals or exceeds the distortion energy per unit volume of the same material when subjected to yielding in a tension test.[13]

Maximum Normal Stress Theory. Brittle materials tend to fail suddenly with no apparent warning or observed yielding. While most adhesives exhibit ductile properties, structural paste adhesives like some epoxies, fail in a brittle fashion. Maximum-normal stress theory states that a brittle material will fail when the maximum principle stress in the material reaches a limiting value that is equal to the ultimate normal stress the material can sustain when subjected to tension.[13] For materials that exhibit similar properties in tension and compression stress-strain diagrams, this criteria has shown good agreement with experimental testing.

Strain-Energy Release Rate. The previous failure criteria are developed from the knowledge of principal stresses from which the critical failure point is determined. These methods can be difficult to apply to anisotropic materials, and complex loading and geometry cases. The strain-energy release rate failure criteria based on crack growth is suited for these applications. Energy release rate is the change in potential energy, U, during an increment of crack area, A. It states that a crack is expected to propagate when the strain energy release rate, G_I, exceeds its critical point, G_{Ic}, a material property related by fracture toughness, K_{Ic}, and Young's modulus, E.[14]

$$G_I \geq G_{Ic} \tag{2}$$

$$G_I = -\frac{\partial U}{\partial A} \tag{3}$$

$$G_{Ic} = \frac{1}{E} K_{Ic}^2 \tag{4}$$

For a plane stress assumption, these four failure criteria can be summarized by Table 3.

Table 3: Summary of Failure Criteria Characteristic Equations

Failure Criteria	Characteristic Equation	Material/Failure Application
Tresca yield Criterion	$\tau_{max} = \frac{\sigma_Y}{2}$	Ductile/Yield
Von Mises-Hencky Theory	$\sigma_1^2 - \sigma_1\sigma_2 + \sigma_2^2 = \sigma_Y^2$	Ductile/Yield
Maximum-Normal-Stress Theory	$\lvert\sigma_1\rvert = \sigma_{ult}$ $\lvert\sigma_2\rvert = \sigma_{ult}$	Brittle/Fracture
Strain Energy Release Rate	$\frac{P}{2t}\frac{\partial u}{\partial a} \geq \frac{1}{E} K_{Ic}^2$	Anisotropic/Crack Propagation

Literiature Review

Development and Testing of Adhesively Bonded Repair Specimen

A study conducted by the Advanced Composites Division, CSRI-National Laboratories attempted to develop and evaluate an adhesively bonded scarf repair specimen utilizing destructive and non-destructive testing.[15] Static tensile testing was conducted on scarf joint carbon fiber reinforced plastic (CFRP) adherends bonded with an epoxy based adhesive. Damaged specimen strengths were compared with the repaired joint strengths. The artificially damaged laminates were represented by a 50mm diameter hole in the center. The repair specimens received a 3 degree taper around the same size hole, Figure 13, and repaired with two different methods: a wet layup of carbon fiber and carbon Prepreg material. This design accounts for possible load shedding by surrounding the perimeter of the damage with the original parent plies. However, the damage is

carried through the entire thickness of the laminate ruling out any possible load shedding onto undamaged parent plies underneath the thickness of the patch. When compared against the damaged laminate, this study concluded that the repaired laminate was 2.6%

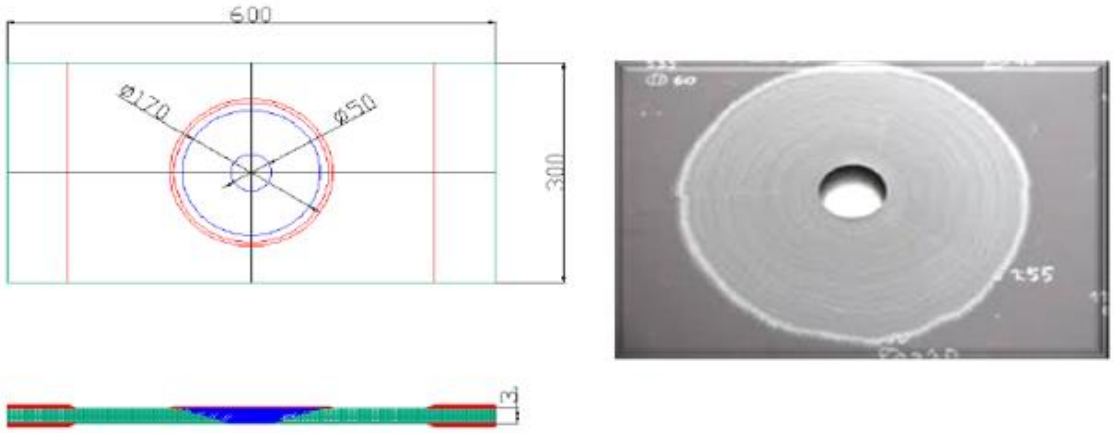

Figure 13: Scarf Repair Test Specimen Scheme for CSIR-National Aerospace Laboratories Research on Development of Damage Tolerant Adhesive Bonded Repair[15]

stronger in static tensile loading with failure occurring within the adhesive bond. The repaired laminate resulted in a strength knockdown of 14% while the damaged laminate resulted in a strength knockdown of 16%. These results can be compared with a 3 degree full-width joint to better understand the impact of load shedding on the surrounding parent laminate. In order to develop a more damage tolerant repair, two external cover plies were added, increasing the strength of the repair by 12% compared to the damage specimens.[15] Load shedding around the perimeter of the repair does not appear to be a significant factor in increasing repair strength when compared to the damaged parent strength.

Adhesively Bonded Composite Scarf Joint Testing

Research conducted on adhesively bonded CFRP composite scarf joints tested configurations comprised of unidirectional carbon reinforced epoxy adherends bonded with a film adhesive in uniaxial tensile loading.[16] Substrate failures were observed in scarf angles less than 2 degrees, while cohesive failures were observed in angles larger than 2 degrees. The largest scarf angle tested, 5 degrees, resulted in a strength knockdown of 89% compared with a neat composite absent of a joint.[16] In relation to the previously discussed study in which a 3 degree scarf repair resulted in a 14% knockdown, it appears that the surrounding undamaged parent plies create a load shedding phenomenon making a full-width joint a conservative representation of the strength of a scarf repaired structure.

Composite Repair Finite Element Modeling

The application of a finite element modeling to the design of structural composite repairs is an efficient method for optimizing strength and cost in an industry setting. FEA models are often validated through experimental testing. Currently, limited data on coupon level repair specimens has stunted confidence in the use of these models to determine industry standards. Previous research on finite element analysis of scarf-patch-repaired composite laminates looked 2D and 3D models of joint and non-through thickness repair configurations. The study concluded that 2D analysis was sufficient for isotropic materials, such as adhesive failure but insufficient in characterizing the behavior of orthotropic or other non-isotropic materials, such as damage progression in the composite laminate. The difficulty with finite element models and scarf repair lies in the

ability to accurately reflect small angle geometries of less than two degrees without singularities affecting convergence. Acute angles within the mesh along the edges of the adhesive bondline are created when small angles are induced in the geometry. As a result, "numerical results tend to display extreme values near the taper tip." High stress gradients should be identified and ignored in the failure analysis. This study concludes that a complete 3D modeling representation for strength analysis in a composite repair takes into account "(i) the characteristics of the adhesive, (ii) high stress/strain gradient and concentrations within the adhesive caused by partial failure of the 90-degree plies and (iii) the edge effect contributed by the stacking sequence of orthotropic composites."[17]

Testing and Modeling of Repairs in Composite Sandwich Structures

Federal Aviation Administration (FAA) sponsored research on bonded repair of aircraft composite structures investigated variables in repair including scarf overlap, core cell size, and impact damage, and compared analytical models to experimental results.[18] Multiple repair techniques were examined with varying scarf overlap in four-point bending and tensile load configurations. A schematic of the coupon configuration is shown in Figure 14. This study concluded "that there was no variation in strength and strain capacity as a function of increasing scarf overlap" for the majority of repair

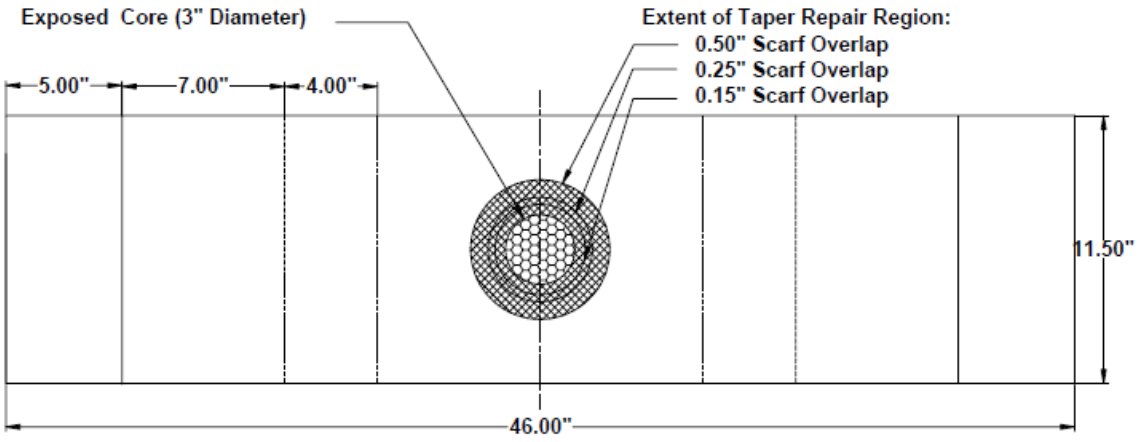

Figure 14: Repair Coupon Configuration for Varying Scarf Overlap in Composite Sandwich Structures[18]

procedures and loading conditions. Core size was revealed to be the primary influencer on strength values in the repaired coupons. Investigation of analytical models compared laminate models to substrate failures and adhesive models to adhesive failures. All but one laminate model over predicted the strength of the repair regardless of repair system and loading condition with the exception resulting in a conservative analysis. Adhesive models failed to take peel stresses and strain concentrations into account resulting in a "positive strength margin, with respect to laminate strength, which excludes the possibility of an adhesive failure."[18] The two adhesive models are designed from scarf joints and include the Delta Design Spreadsheet strength model, a mechanics of materials approach, and the Hart-Smith's model which involves stiffness imbalances and thermal mismatch. These models failed to properly characterize the failure mode of the experimental repair coupons.[18]

Scope of Immediate Research

The application of composite materials over a broad range of industries from aerospace to renewable energies to sporting goods has resulted in diverse implementation and configurations. Recent demand for repair on these diverse structures drives the need for research on each variable and combination of variables for the proper characterization of strength in a restored structure. Repair schemes, methods, laminate materials and layups, sandwich cores, and adhesives are just a few variables that influence the design of a composite repair. This paper seeks to investigate composite repairs utilizing structural paste adhesives in soft patch scarf repair schemes for employment of factory repairs of manufacturing defects and pre-operational damages on composite wind turbine blades.

MANUFACTURING AND TESTING

Development of Experimental Joint Specimens

Joint Coupon Configurations

The initial objective for manufacturing and testing is to develop a broad database for characterizing the behavior of a scarf joint with a composite substrate and structural adhesive bond. While there are numerous factors influencing the behavior in a scarf joint, this study focuses on understanding the effects of scarf angles and substrate material properties on the strength and deformation of a joint. Figure 15 depicts the

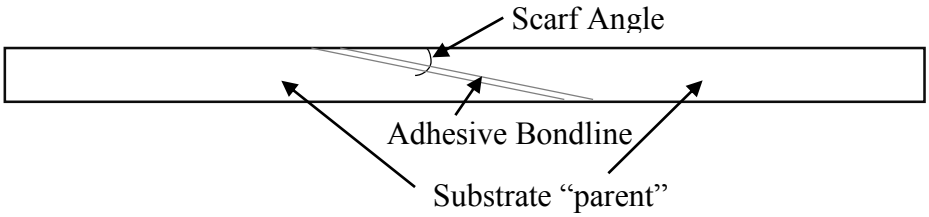

Figure 15: Elements in a Scarf Joint

elements of a basic scarf joint. A taper of equal angle is introduced to the substrates and joined by an adhesive forming a bondline between the substrates. Composite substrate, or "parent" laminates include unidirectional carbon fiber and glass, glass triax, and a carbon/glass hybrid triax. A single triax ply is composed of a unidirectional ply combined with a ±45 ply. In the case of the hybrid layup, the unidirectional material is carbon and the ±45 material is glass. All laminates are of 4-ply construction. Scarf angles of 5, 15, and 25 degrees are introduced to each of these laminates. Table 4 is a

summary of the manufactured joint specimen layups and configurations. Three specimens of each configuration are manufactured.

Table 4: Experimental Joint Layups and Configurations

Material	Layup	Scarf Angle (deg)
Glass Uni	$[0_2]_s$	5
		15
		25
Carbon Uni	$[0_2]_s$	5
		15
		25
Glass Triax	$[(0/\pm45)_2]_s$	5
		15
		25
Hybrid Triax	$[(0/\pm45)_2]_s$	5
		15
		25

Layup Background and Motivation. The four layups are motivated by previous research conducted by the Montana State University Composites Group as part of the Blade Reliability Collaborative (BRC) aimed at improving reliability in wind turbine blades delivered to field in order to achieve lifecycle expectations. Data of undamaged and unflawed specimens of identical geometry and materials can be used as a baseline for comparison of restored strength from a scarf joint. In addition, testing joints in laminates of varying stiffness aids in understanding the effect of the substrate to adhesive stiffness gradient. Stiff substrates are proposed to apply greater peel stresses on the adhesive resulting in more brittle failures and lower strengths. Table 5 gives the material specifications and previously tested strength values for the control specimens.

Table 5: Fiber and Resin Specifications for Composite Substrates and Previously Tested Data for Undamaged/Unflawed Specimens

Layup (4-ply)	Fiber	Resin	Failure Stress (ksi)
Glass Uni	PPG 1250 UD 2025	Hexion Epikote MGS RIMR 135, RIMH 1366	146
Carbon Uni	Vectorply CLA 2012	Hexion Epikote MGS RIMR 135, RIMH 1366	206
Glass Triax	PPG 1250 UD 2025/ PPG 810 Biax 2002	Hexion Epikote MGS RIMR 135, RIMH 1366	119
Hybrid Triax	Vectoryply CLA 2012/ PPG 810 Biax 2002	Hexion Epikote MGS RIMR 135, RIMH 1366	151

Scarf Angle Motivation. The scarf angles are driven by both manufacturing and equipment constraints. The smaller the angle, the longer the tapered section of the specimen. Due to data acquisition measuring volume constraints and the criteria to collect data through the entirety of the bondline, the longest scarf length is limited to that resulting from a 5 degree angle. Using this as a lower bound, angles were incremented by 10 degrees to give a broad understanding of trends as the angle is increased.

Manufacturing Technique for
Scarfed Parent Composite

Vacuum assisted resin transfer method (VARTM) is used to manufacture a large flat plate of each layup. A schematic of the VARTM method is shown in Figure 16. The plate is cured under vacuum for 48 hours at 25°C and then post cured for 8 hours at 70°C, after which it is cut into two and a half inch wide coupons of lengths determined by the intended scarf angle, Table 6. The scarf length is determined by using the tangent trig function given by

$$Scarf\ Length = \frac{t_l}{\tan(\alpha)} \quad (5)$$

Where t_l is the laminate thickness and α is the scarf angle. Five inches is added to the scarf length for a particular angle in order to eliminate edge effects and allow for tabs on each end of the specimen.

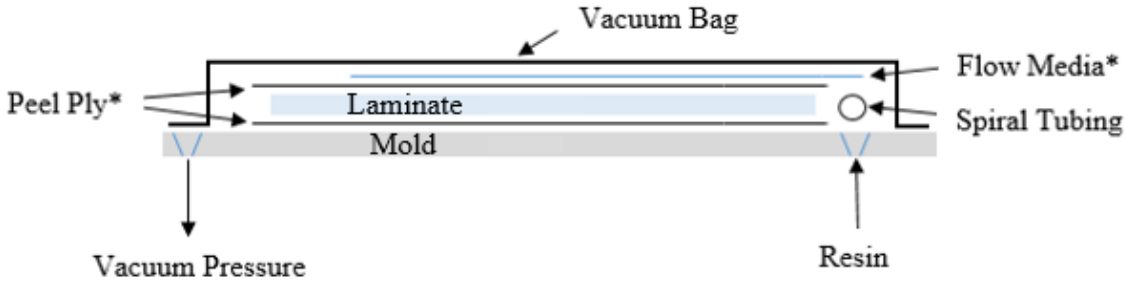

Figure 16: Schematic of VARTM

Table 6: Specimen Length Dimensions

Layup	Layup Thickness (in)	Scarf Angle (deg)	Scarf Length (in)	Un-scarfed Material Length (in)	Total Length of parent section (in)
Glass Uni	0.15	5	1.72		6.71
		15	0.56		5.56
		25	0.32		5.32
Carbon Uni	0.12	5	1.37		6.37
		15	0.45		5.45
		25	0.26		5.26
Glass Triax	0.19	5	2.17		7.17
		15	0.71		5.71
		25	0.41		5.41
Hybrid Triax	0.2	5	2.29		7.29
		15	0.75		5.75
		25	0.43		5.43

Scarf Angles are machined into the parent sections utilizing a Smithy Mill with a ½ inch carbide end mill at 900 revolutions per minute (RPM) as depicted in Figure 17.

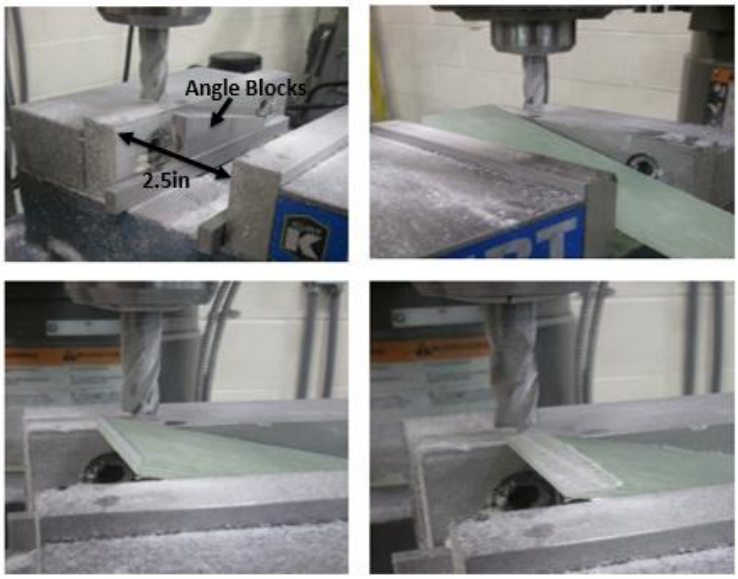

Figure 17: Milling Process
Top Left: Angled Blocks placed in clamps; Top Right and Bottom Left: Specimen clamped on angled blocks; Bottom Right: Width Wide Passes

The specimens are clamped in place with a trued vice on angled blocks to establish the desired angle. Width-wide passes dropping 0.015 inches in thickness per pass of the end mill are made until the angle is fully machined. Verification of angles is completed with a protractor.

Bonding of Joint Specimens

Adhesive Selection. The joint is formed by bonding two scarfed specimens using a structural paste adhesive. The wind turbine industry primarily relies on film and paste adhesives for construction and repair. Paste adhesives allow for local variation in bondline thickness, an area which has seen little research. Using a structural adhesive of

constant thickness will establish baseline data for further research on bondline variations and is thus chosen for the adhesive type in this immediate study. A two part epoxy adhesive is utilized as it is widely and commonly used in industry. Nomenclature and material properties can be seen in Table 7.

Table 7: Mechanical Properties for two-part Paste Epoxy Adhesive[20]

Epoxy Resin	Epikote MGS 135G
Hardener	Epikure MGS BHP 137G
Tensile Shear Strength (ksi)	1.9
Peel Strength (ksi)	0.22
Tensile Strength (ksi)	9
Tensile Modulus (ksi)	613.5
Tensile Ultimate Strain (%)	2.9
Bending Strength (ksi)	11.2
Bending Modulus (ksi)	496
Bending Ultimate Strain (%)	2.7

Bondline Thickness. Bondline thickness, defined normal to the scarf angle, is another significant factor in joint design and can greatly impact the strength of the bondline. Thin bondlines less than 0.6mm, run a greater risk of unfilled areas of adhesive leading to substrate to substrate contact. As bondlines reach a thickness greater than 1mm there is a significant strength reduction due to a more eccentric load path. A 0.6mm bondline with a ±25% tolerance is chosen for this study in order to increase effectiveness of adhesive application without sacrificing strength. With the given tolerance all bondlines are considered thin.

Surface Preparation. The substrate sections of the specimen are prepped for bonding by sanding the scarfed regions with 80 grit sandpaper, washed with water, and dried completely creating a lightly abrased finish. Teflon spacers 0.8mm tall are fastened with superglue to one of the substrates in the pair. Placement of the spacers, as seen in Figure 18, is in the center of the scarfed region lengthwise, and within ¼ inch of each edge widthwise. The spacers are allowed to cure for 24 hours before adhesive is applied.

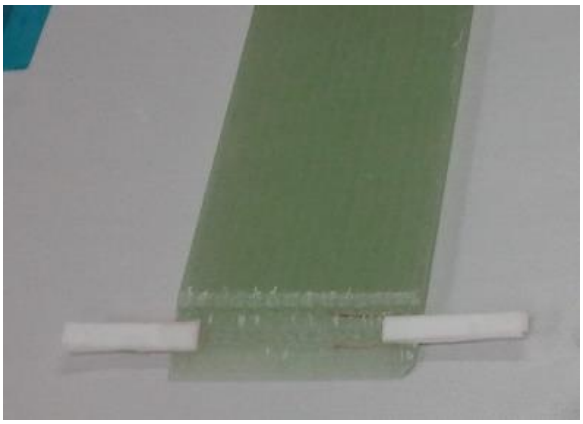

Figure 18: Location of Spacers in Scarfed Region Used to Control Bondline Thickness

Adhesive Application and Curing. The two parts of the epoxy adhesive are weighed out at a 100:45 resin to hardener ratio and mixed by hand until the color becomes uniform. The adhesive is applied to the substrate with the spacers and spread along the width using a spatula. The second substrate in the pair is then mated along the scarfed region and pressed firmly until flush. Flash, access adhesive, is cleaned off with the spatula. Up to six specimens are bonded with a given epoxy mix limited by the 45 minute approximate working time of the adhesive. The specimens are placed on a peel ply lined mold with an aluminum strip butted lengthwise along the specimens in order to

maintain alignment as seen in Figure 19. A layer of peel ply is placed over the specimens and vacuum pulled to 22mmHg in order to prevent micro voids from forming in the adhesive. The specimens are cured for 24 hours at 25°C and then post cured for 8 hours at 70°C.

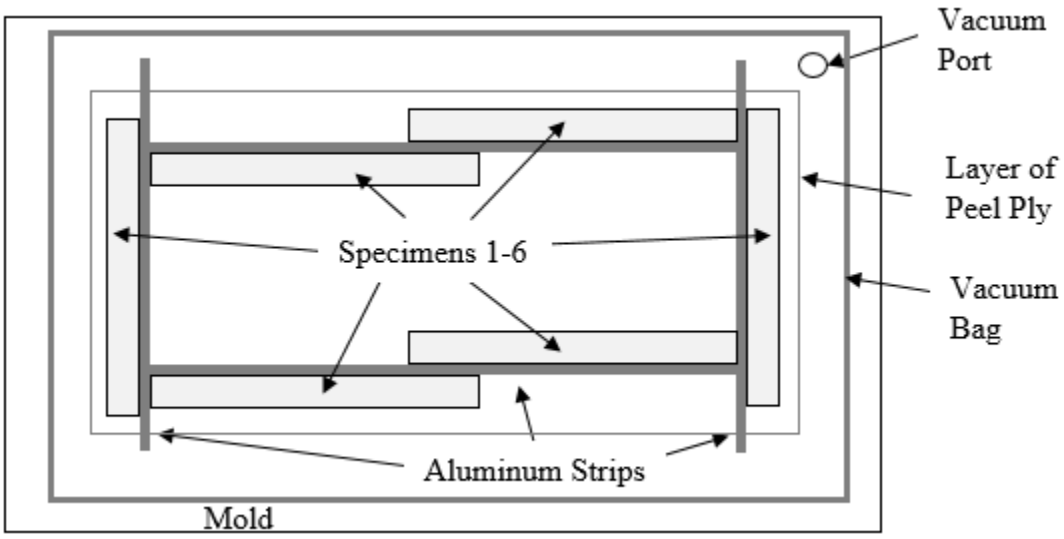

Figure 19: Schematic of Specimen Layout on Mold During Vacuum Cure Cycle

Finishing and Verification. Following the cure process specimens are trimmed 0.25 inches along the lengthwise edges removing the spacers, Figure 20. Once the spacers are removed the bondline becomes clearly visible and each specimen is measured for width, thickness, scarf angle, and bondline thickness. Bondline thickness is measured normal to the scarf angle and the angle is verified with a protractor as seen in Figure 21. Three measurements of each parameter are averaged for the final value.

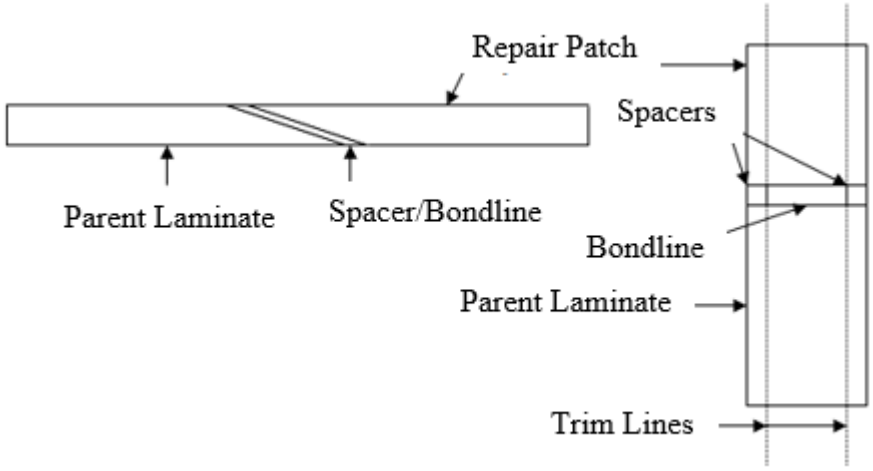

Figure 20: Schematic of Trim Lines Intended To Remove Spacers

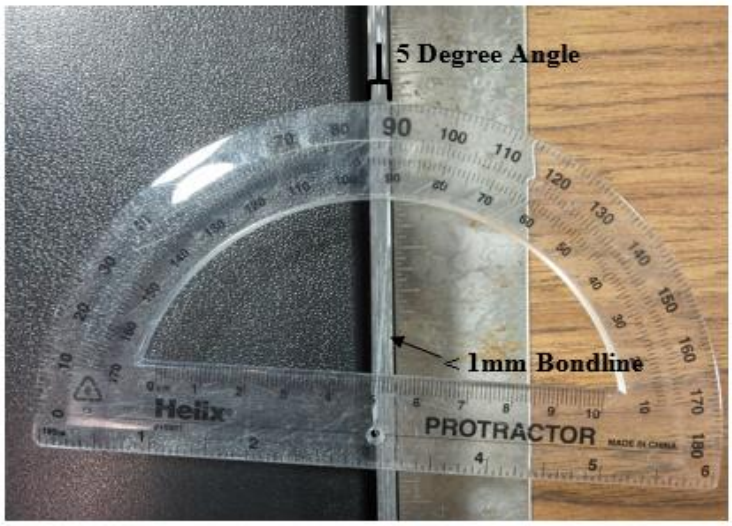

Figure 21: Measuring of Scarf Angle and Bondline Thickness of a Joint Specimen

Three inch tabs are then bonded with epoxy, sandwiching the ends of the specimens while leaving two inches between the end of the joint and the beginning of the tab, Figure 22. The tabs allow for easier placement within the grips of the testing machine and for an even distribution of clamp pressure, thus reducing the chance of the grips slipping, crushing of the laminate, or failure of the grips during testing. The two

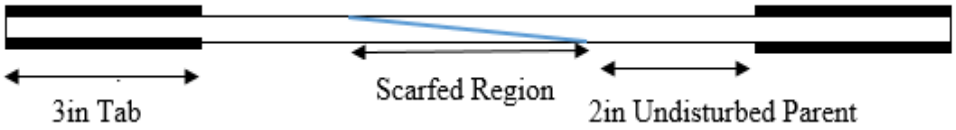

Figure 22: Visualization of Tabs

inch section of undisturbed laminate between the end of the scarf and tab allows for far-field strains to be analyzed.

Test Setup and Data Acquisition

The samples are tested to failure in tension with an Instron 8872 servo-electric testing machine at a feed rate of 0.01 inches per minute. The Instron 8872 has a 100kN load capacity and a 100mm (4 inch) maximum stroke. Ambient temperature of the facility during testing is 24°C with a relative humidity of 28%.

Data acquisition is controlled through ARAMIS 3D digital image correlation (DIC) measuring system. Benefits of the DIC method include non-specimen contact and high sensitivity.[25] Load data from the Instron is fed into ARAMIS and deformation data is collected and calculated within the DIC. Images are taken in two second increments over a defined control volume. For this research, the control volume is defined as the length of the scarf joint. The DIC then divides each image into smaller sub-images. User specified control points in the initial image are used to determine the correlation of subsequent sub-images. Deformation is calculated based on this correlation, leading to realized parameters of displacement and strain.[19] The specimens are imaged along the thickness to capture strain distributions along the joint. The high sensitivity of DIC makes it an ideal data acquisition method allowing the user to capture the strain

distributions over a small volume. Figure 23 is a depiction of the test set up. Failure mode of the joint is visually observed and recorded after each test is complete.

Figure 23: Static Tension Test Set Up for Joint Specimens

After initial testing is complete a quick data reduction to determine ultimate failure stress is performed using a simple mechanics of materials approach of load divided by the cross sectional area.

$$\sigma = \frac{P}{A} \tag{6}$$

If the standard deviation between the three specimens of each joint configuration is too great, a fourth specimen is manufactured and tested. Table 8 is a comprehensive list of the tested joints.

Table 8: Scarf Joint Specimen Test Matrix

Layup*	Scarf Angle (deg)	#	Bondline Thickness (mm)	Ave Width (in)	Ave Thickness (in)	Surface Area (in^2)	Actual Failure Load (kip)	Failure Mode
GU	5	1	0.8	1.95	0.140	0.274	6.91	Adhesive
GU	5	2	0.8	1.90	0.143	0.272	5.95	Adhesive
GU	5	3	0.8	1.89	0.143	0.271	6.22	Adhesive
GU	15	1	0.6	1.93	0.138	0.266	2.63	Adhesive
GU	15	2	0.6	1.95	0.139	0.270	2.91	Cohesive
GU	15	3	0.8	1.98	0.138	0.273	3.34	Adhesive
GU	25	1	0.8	2.06	0.140	0.288	2.19	Adhesive
GU	25	2	0.6	2.04	0.138	0.282	3.70	Cohesive
GU	25	3	1.0	2.03	0.137	0.278	2.73	Cohesive
GTr	5	1	1.0	2.04	0.200	0.407	7.71	Adhesive
GTr	5	2	1.0	2.04	0.207	0.422	7.33	Adhesive
GTr	5	3	1.0	2.12	0.202	0.428	9.15	Adhesive
GTr	15	1	0.6	2.06	0.208	0.427	5.10	Adhesive
GTr	15	2	0.8	1.95	0.201	0.392	5.65	Adhesive
GTr	15	3	0.6	2.07	0.207	0.429	5.75	Adhesive
GTr	25	1	0.8	2.10	0.201	0.422	5.36	Cohesive
GTr	25	2	0.8	2.15	0.203	0.437	4.70	Cohesive
GTr	25	3	1.0	2.09	0.200	0.417	4.02	Cohesive
CU	5	1	0.6	1.85	0.150	0.277	9.04	Cohesive
CU	5	2	0.6	2.00	0.153	0.306	11.13	Cohesive
CU	5	3	0.6	1.81	0.156	0.282	7.74	Cohesive
CU	5	4	0.8	1.70	0.148	0.251	9.98	Cohesive
CU	15	1	0.6	2.12	0.159	0.338	5.84	Cohesive
CU	15	2	0.6	1.79	0.152	0.273	3.96	Cohesive
CU	15	3	0.6	2.04	0.157	0.321	4.45	Cohesive
CU	15	4	0.8	2.03	0.158	0.321	4.53	Cohesive
CU	25	1	0.8	1.99	0.156	0.310	2.29	Not Through
CU	25	2	0.6	2.04	0.155	0.315	3.00	Cohesive
CU	25	3	0.6	1.96	0.160	0.313	2.97	Cohesive
CU	25	4	0.8	2.02	0.154	0.311	3.02	Cohesive
HTr	5	1	1.0	1.75	0.211	0.371	10.10	Cohesive
HTr	5	2	1.0	1.95	0.208	0.404	9.58	Substrate
HTr	5	3	1.0	2.00	0.217	0.432	11.32	Substrate
HTr	15	1	0.6	2.02	0.203	0.411	4.96	Cohesive

Table 8 Continued

HTr	15	2	0.6	1.94	0.205	0.396	6.16	Cohesive
HTr	15	3	0.6	1.86	0.204	0.380	4.25	Cohesive
HTr	15	4	0.8	2.13	0.207	0.441	5.46	Cohesive
HTr	25	1	1.0	2.14	0.207	0.443	2.94	Not Through
HTr	25	2	0.8	2.12	0.211	0.444	4.51	Cohesive
HTr	25	3	0.6	2.12	0.212	0.448	4.12	Cohesive

*GU = Glass Uni, GTr = Glass Triax, CU = Carbon Uni, HTr = Hybrid Triax

Development of Experimental Non Through Thickness Repair Specimen

Repair Coupon Configurations

Through Thickness and Scarf Angles. The second objective of manufacturing and testing is to apply the knowledge gained from joint testing and design coupon level composite repair specimens. These specimens are defined as non-through thickness since only a percentage of the plies are removed at a tapper in a similar fashion as the joint specimens. For this stage, all substrates, or "parents", are composed of 4-ply Vectorply CLA 2012 unidirectional carbon fiber infused with Hexion Epikote MGS RIMR 135, RIMH 1366 resin/hardener. One layup was chosen in order to control the stiffness mismatch and chemical composition or compatibility effect between substrate and adhesive. Unidirectional carbon exhibited the greatest number of cohesive failures during joint testing. This is the desired failure mode in an adhesive, therefore this layup is utilized in repair specimen manufacturing. Configurations of 5 and 15 degree scarf angles and 50% and 75% repairs are manufactured as depicted in Figure 24. The 25 degree joint specimens exhibited low strength values and are not considered in the non

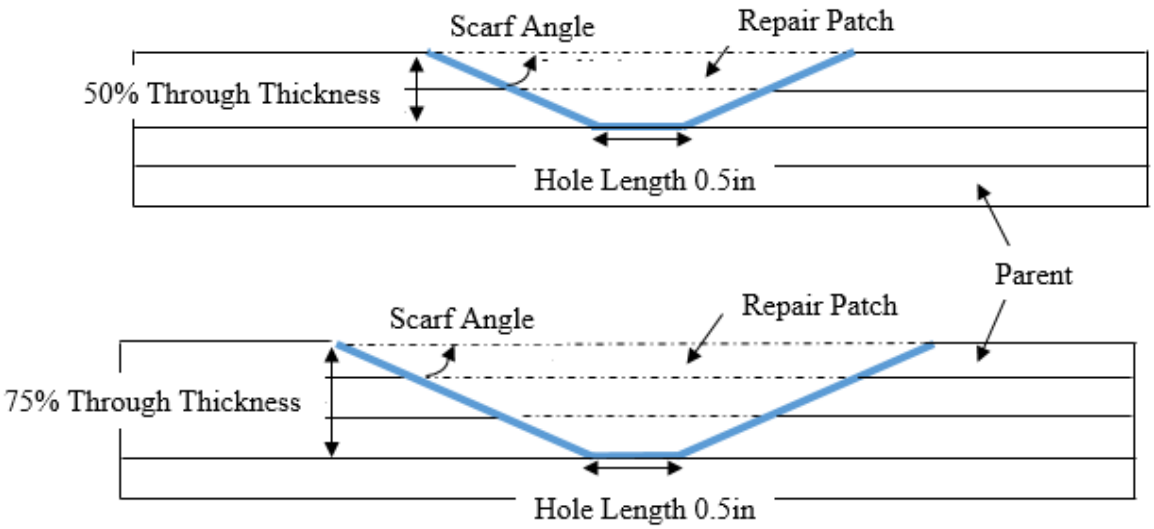

Figure 24: Non Through Thickness Schematic: Upper Diagram is 50% Repair, Lower Diagram is 75% Repair

through thickness study. For this study, a 50% repair is the removal of two of the four plies and a 75% repair is the removal of three of four plies.

Adhesive Selection. Three two-part paste adhesives are compared: epoxy, polyurethane, and methacrylate (MA). Table 9 is a summary of the mechanical properties comparing the three adhesives.

Table 9: Comparison of Structural Paste Adhesive Mechanical Properties

	EPOXY[20]	**Polyurethane[21]**	**MA[22]**
Resin	Epikote MGS 135G	Permabond PT 326 A	Plexus MA550
Hardener	Epikure MGS BHP 137G	Permabond PT 326 B	Plexus MA320 White Activator
Tensile Shear Strength (ksi)*	1.9 (double lap shear)	1.3-1.6 (ISO4587)	1.3-1.8 (ASTM D1002)
Peel Strength (ksi)	0.22	--	--

Table 9 Continued

Tensile Strength (ksi)**	9 (ISO 527)	2.3-3.6 (ISO37)	1.75-2.0 (ASTM D638)
Tensile Modulus (ksi)	613.5	--	40-50
Tensile Ultimate Strain (%)	2.9	15	35-45
Bending Strength (ksi)	11.2 (ISO178)	--	--
Bending Modulus (ksi)	496	--	--
Bending Ultimate Strain (%)	2.7	--	--

While tensile shear strengths and tensile strengths are reported through different testing standards, the resulting mechanical values allow the adhesives to be compared. The Polyurethane and MA adhesives are chosen for their comparable shear strengths, two-part paste architecture, and suitable applications in the wind turbine industry. For the adhesive comparison, only configurations of 50% through thickness and 15 degree scarf angle are tested. In addition, a scarfed specimen of this same configuration is tested absent of repair patch or adhesive. The purpose of this is to isolate and understand the damage progression and failure of the parent. A summary of the test specimen configurations are shown in Table 10. Three specimens of each are tested.

Table 10: Repair Specimen Configurations

Configuration	Lay Up	Scarf Angle (deg)	Adhesive	Bondline Thickness (mm)
Repair: 50%	Carbon Uni	15	Epoxy	>1mm
Repair: 75%	Carbon Uni	15	Epoxy	>1mm
Repair: 50%	Carbon Uni	5	Epoxy	>1mm
Repair: 75%	Carbon Uni	5	Epoxy	>1mm
Repair: 50%	Carbon Uni	15	N/A (No patch)	>1mm
Repair: 50%	Carbon Uni	15	MA	>1mm
Repair: 50%	Carbon Uni	15	Polyurethane	>1mm

Manufacturing Technique for
Scarfed Parent Composite

Large flat plates are manufactured using VARTM as described in the above "Manufacturing and Testing of Joint Specimens" section and cut into two and a half inch wide specimens. Material is removed in lengthwise passes with a carbide end mill at 900 RPM dropping 0.015 inches each pass. Hole length, Figure 24, for each specimen is 0.5 inches and the angles are created by clamping the specimen on angled blocks, Figure 17. The finished milled repair sample is shown in Figure 25. The scarfed region is sanded

Figure 25: Edge View Milled Repair Specimen, 15 Degree Scarf Angle, 50% Through Thickness Repair (Painted white for ARAMIS DIC imaging purposes)

with 80 grit sandpaper and 0.8 mm Teflon spacers are adhered to the middle of each scarf and hole length within 0.25 inches of the edge with superglue, Figure 26. The superglue is cured at room temperature for 24 hours.

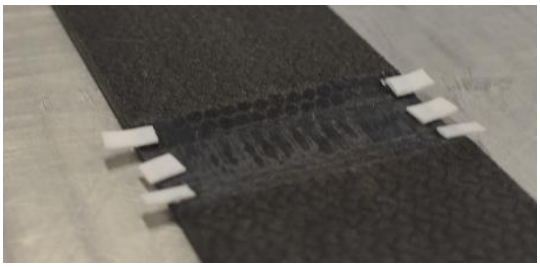

Figure 26: Teflon Spacer Locations for Repair Specimens

Repair Patch Bonding Method

A wet layup is performed to fill the scarfed region with repair patch plies identical material as the parent. The adhesive bondline and repair patch are co-cured in place.

Material Preparation. For the 50% non through thickness specimens two repair plies form the patch while the 75% non through thickness specimen patches consist of three plies. The plies are cut at different lengths, outlined in Table 11 and shown in Figure 27, in order to taper the patch as it fills the scarfed region.

Table 11: Repair Ply Lengths for All Specimen Configuration

Scarf Angle/ % Repair	Outer Ply Length (in)	Middle Ply Length (in)	Inner Ply Length (in)
5deg/50%	1.6	--	0.75
5deg/75%	2.5	1.6	0.75
15deg/50%	0.9	--	0.6
15deg/75%	1.2	0.9	0.6

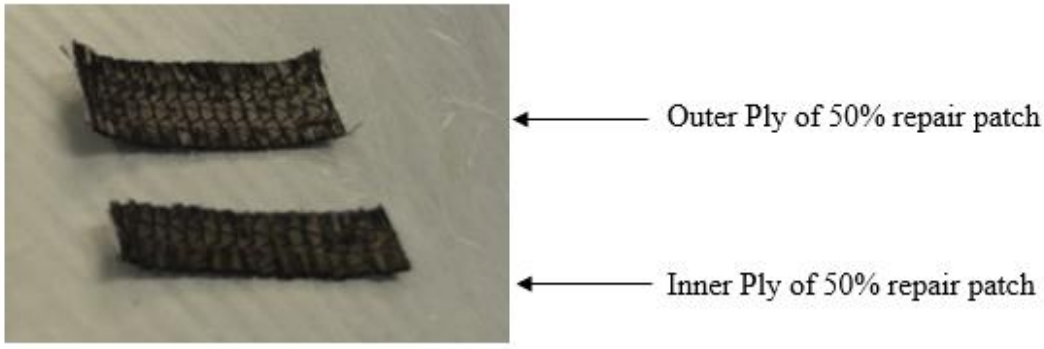

Figure 27: Repair Patch Plies Cut to Different Lengths to Fill Tapered Region in Parent

A maximum of six specimens are repaired for a given resin/adhesive mix. The specimens are placed on a mold lined with peel ply, Figure 28.

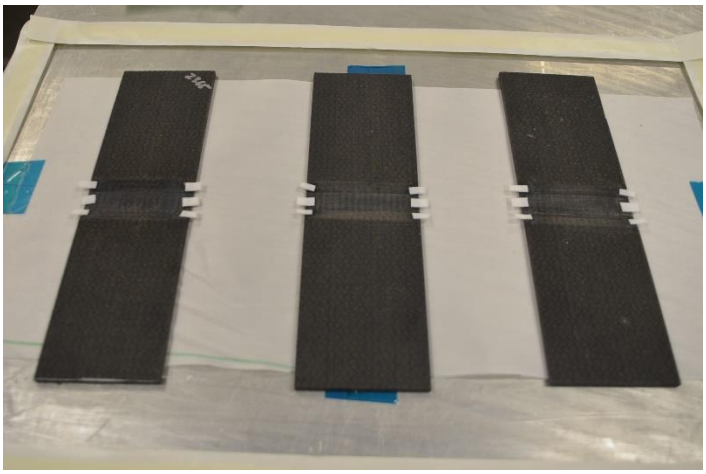

Figure 28: Three Repair Specimens in Preparation for Wet Layup Repair Patch

Wet Layup and Adhesive Application. The resin and hardener are mixed with a static mixer for 8 minutes at 220 rpms, then degassed for 8 minutes. During the degassing process, the epoxy adhesive is measured at a 100:45 resin to hardener ratio and mixed by hand until the color is uniform. The polyurethane and MA adhesives are administered with a dual cartridge static mixer nozzle applicator gun provided by the manufacturer, an example of which can be seen in Figure 29. All three adhesives are

Figure 29: Static Nozzle Mixer and Dual Cartridge Applicator Gun

mixed, administered, and cured within tolerances specified by the adhesive manufacturer. A 1.5 inch standard paintbrush with trimmed bristles for the wet layup, wide spatula for bondline adhesive application, and the repair plies are arranged for quick work, Figure 30.

Figure 30: Preparation of Repair Plies, Spatula, and Brush for Wet Layup

The adhesive bondline is applied utilizing the spacers to control the amount so as to reduce flash. Epoxy is dripped over the repair plies and spread with the trimmed brush until all fibers are visibly saturated. The plies are then aligned in the parent, working from the inner shortest ply to the outer longest ply. Once the repair plies are in place a layer of peel ply is added over the top and a vacuum bag affixed, as shown in Figure 31.

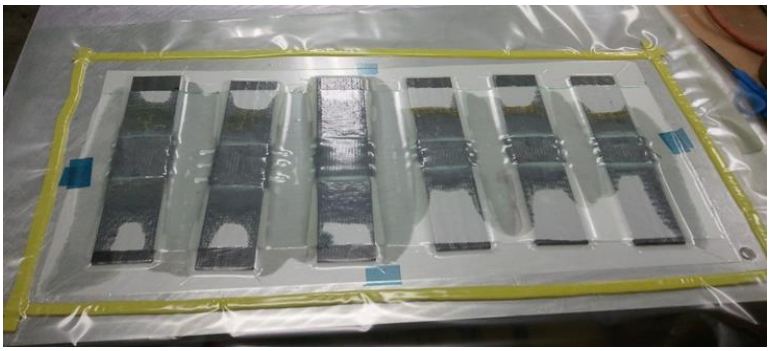

Figure 31: Repair Test Coupons Co-curing Under Vacuum Bag

The specimens are cured under 22mmHg vacuum pressure for 48 hours at 25°C and post cured for 8 hours at 70°C. Vacuum pressure is limited to prevent micro voids in the adhesive.

Finishing and Validation. After post-cure, the edges along the length are trimmed by 0.25 inch in the same manner as the joints thereby removing the spacers. Figure 32

Figure 32: Edge View of Completed PMMA 50% Repair Specimen with 5 Degree Scarf Angle

shows an edge-wise view of a MA specimen with a 50% through thickness repair and 15 degree scarf angle after the spacers are trimmed. Tabs are bonded in a sandwich configuration to the ends with epoxy and cured for 24 hours. A minimum of 1.5 to 2 inches of un-scarfed 4-ply parent material is accounted for between the end of the scarf and the tab on each side of the repair. This area will be utilized in measuring far-field strain values. Three measurements are averaged to find realized values for width, thickness, scarf angle, and bondline thickness. The realized bondline thickness for the repair specimens is 1mm.

Test Setup and Data Acquisition

Testing is conducted using an Instron 8802 servo hydraulic machine with 250kN load capacity and a 150mm (6 inch) maximum stroke, Figure 33. Feed rate for the repair testing is 100 inches per minute. Ambient temperature of the facility during testing is 24°C with a relative humidity of 28%.

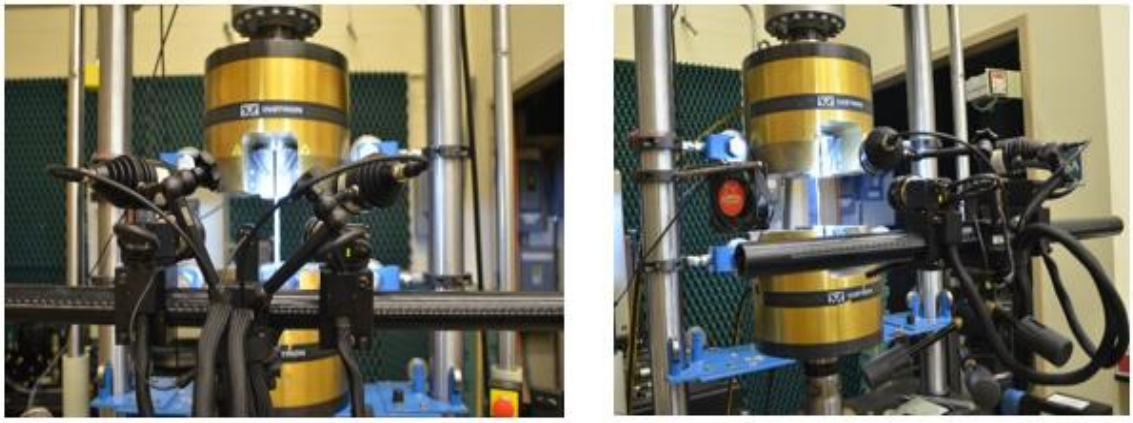

Figure 33: Repair Specimen Test Setup with Instron 8802 and ARAMIS DIC

The specimens were tested to failure in static tension. Load and deformation data is acquired using the ARAMIS DIC as described in the joint manufacturing and testing section. Specimens are viewed with the DIC along the thickness edge. Six specimens at random are affixed with a strain gauge for validation of the DIC strain measurements. The gauges are oriented in the y-direction, centered on the width-wise face behind the repair patch on the parent laminate. Adhesive failure mode is observed visually and recorded after each test. Table 12 is a summary of the measured values of the repair specimens along with recorded ultimate loads and observed adhesive failure modes. Refer to Experimental Test Results section for interpretation adhesive failure modes. Refer to Experimental Test Results section for interpretation and analysis of failure data.

Table 12: Test Matrix for Carbon Uni Repair Specimens with 1mm Bondline Including Ultimate Failure Load and Adhesive Failure Mode

Adhesive	Scarf Angle (deg)	% Laminate Repaired	#	Ave Width (in)	Ave Thickness (in)	Surface Area (in^2)	Actual Failure Load (kip)	Failure Mode
Epoxy	5	50%	1	1.851	0.173	0.321	24.45	Cohesive
Epoxy	5	50%	2	1.889	0.171	0.322	28.39	Cohesive
Epoxy	5	50%	3	1.811	0.167	0.303	25.33	Cohesive
Epoxy	5	75%	1	1.939	0.170	0.330	16.40	Cohesive
Epoxy	5	75%	2	1.968	0.172	0.338	15.31	Cohesive
Epoxy	5	75%	3	1.912	0.168	0.321	10.50	Cohesive
Epoxy	15	50%	1	1.949	0.165	0.322	26.17	Cohesive
Epoxy	15	50%	2	2.173	0.167	0.362	31.05	Cohesive
Epoxy	15	50%	3	1.905	0.168	0.320	26.22	Cohesive
Epoxy	15	75%	1	1.784	0.168	0.300	10.73	Cohesive
Epoxy	15	75%	2	1.945	0.171	0.332	14.87	Cohesive
Epoxy	15	75%	3	1.895	0.161	0.305	13.71	Cohesive
Polyurethane	15	50%	1	1.581	0.154	0.244	21.40	Adhesive
Polyurethane	15	50%	2	1.588	0.162	0.258	25.34	Adhesive
Polyurethane	15	50%	3	1.606	0.158	0.254	23.77	Adhesive
MA	15	50%	1	1.941	0.160	0.310	26.97	Cohesive
MA	15	50%	2	1.815	0.148	0.269	23.63	Cohesive
MA	15	50%	3	damaged during manufacturing - not tested				
No Patch	15	50%	1	2.011	0.151	0.304	28.67	N/A
No Patch	15	50%	2	1.741	0.151	0.263	25.71	N/A
No Patch	15	50%	3	1.943	0.163	0.316	28.95	N/A

FINITE ELEMENT MODEL DEVELOPMENT

Background and Previous Work

Within a scarf, whether a joint or a repair, the applied load is carried through the adhesive suggesting that strength is independent of how far through the thickness the scarf extends. Thus, previous finite element modeling (FEA) and coupon level testing has used 2D joints as an applicable simplified version of a 3D repair. Wang and Gunnison propose that a load shedding phenomenon may occur in a repair in which loads are diverted around the adhesive and into to the adjoining composite substrate giving the repair more strength than suggested by a 2D joint model (FEA1). This research also references a report by Soutis and Hu stating that "2D joint analysis underestimated the strength of the repair patch by more than 40% when adherend failure limits the joint and repair strengths."[2] It is of note that analysis was not extended to composite adherends. After comparing a FEA model of 2D joint and 3D repair with a 5 degree scarf angle and composite adherends, Wang and Gunnison, found the difference closer to 10% concluding that a 2D joint produces a good strength prediction.[2] This can be attributed to the varying stress concentrations within a composite laminate. For this reason, the immediate study limits FEA to two dimensions. Considering both the joint and non through thickness repair configurations, the objective is to correlate the results with experimental test data for the unidirectional carbon adherend specimens.

MATLAB PDE Model Development

Geometry and Boundary Conditions

The Matlab partial differential equation (PDE) tool, an intrinsic FEA program, with strictly two dimensional space and time solving capability, is used for the finite element analysis. Geometry, shown in Figure 34, reproduces the length vs thickness

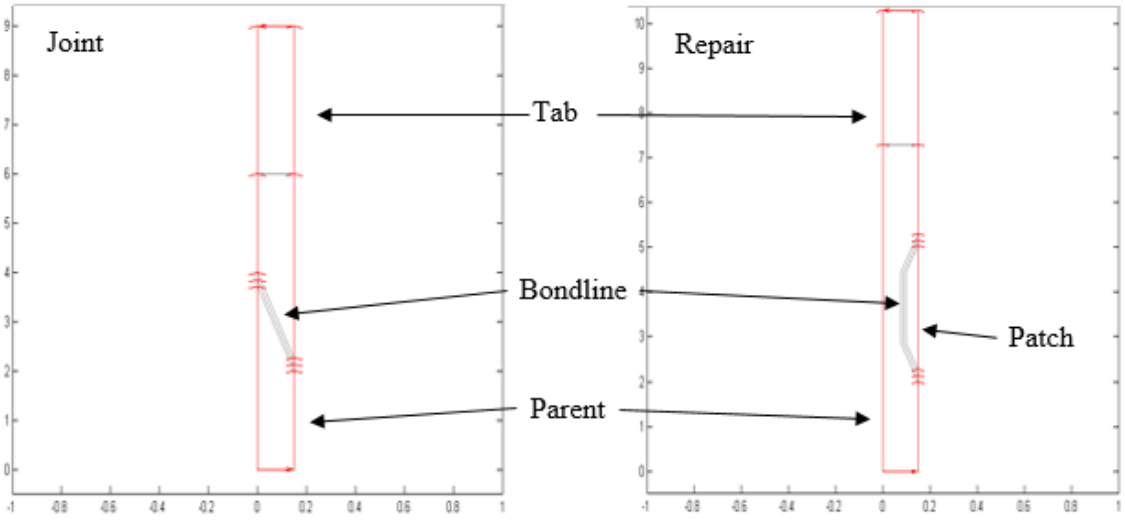

Figure 34: Thickness vs Length Cross Sectional Geometry of 2D Scarf Joint and Repair Finite Element Model

cross section including one of the tabbed sections of both a scarf joint and scarf repair. The model is oriented vertically to match the test setup orientation allowing for easier comparisons. A bondline thickness of 0.6mm is held constant for all model configurations. Dirichlet boundary conditions are imposed on the model. The bottom edge is fixed, or pinned, in both the x-direction and y-direction. The tab section is constrained only in the x-direction to simulate the condition imposed by the Instron grips and the force applied in the y-direction. The limitations of two dimensional modeling

eliminate any torque induced by the loading condition and are therefore not considered in the analysis. The remaining boundary edges are not constrained allowing for deformation in both x and y directions. Figure 35 depicts the boundary condition and loading condition of the joint model. A volume force, K_Y, is applied to the tab section in the y-direction loading the model in tension.

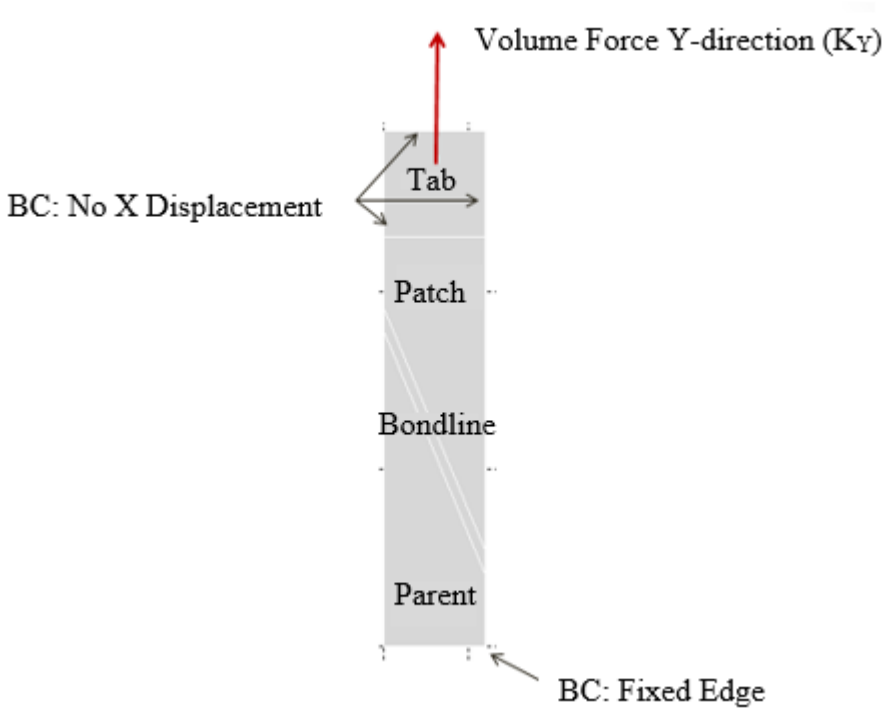

Figure 35: Boundary and Loading Conditions of 2D Joint FEA Model in Matlab

Mechanical Properties

Mechanical properties of elastic, bulk, modulus and Poisson's ratio for the composite laminate and adhesive are applied to each respective section. The carbon bulk modulus is an approximation taken from previous BRC tests conducted at Montana State University of a 4-ply control layup of identical materials and manufacturing technique.

The Poisson's ratio for the laminate is a commonly reported number for an average unidirectional carbon layup. Material properties for the Momentive Epikote MGS BPR 135G3/MGS 137G epoxy adhesive are obtained from the Montana State University material database and are the result of extensive internal testing. Plexus MA550 and Permabond PT326 Polyurethane adhesive data is specified by the manufacturer's technical data sheet. An average value of the given range is applied to the model. Table 13 is a summary of the mechanical properties used in the model.

Table 13: Mechanical Properties Used in FEA Model

Material	**Elastic Modulus [E] (GPa / ksi)**	**Poisson's Ratio [υ]**
Carbon Uni Laminate[19]	67.8 / 9833.56	0.3
Epoxy Adhesive[24]	4.23 / 613.15	0.35
MA Adhesive[22]	0.31 / 44.96	0.38

Governing Equations: Plane Strain

The application mode of the elliptical PDE system is set to Structural Mechanics, Plane Strain, a condition in which x and y displacements are not a function of z and no deformation in the z-direction occurs.[13] The stress-strain relationship, Equation 7, is written assuming isotropic and isothermal conditions.

$$\begin{bmatrix} \sigma_x \\ \sigma_y \\ \gamma_{xy} \end{bmatrix} = \frac{E}{1-\upsilon^2} \begin{bmatrix} 1 & \upsilon & 0 \\ \upsilon & 1 & 0 \\ 0 & 0 & \frac{1-\upsilon}{2} \end{bmatrix} \begin{bmatrix} \epsilon_x \\ \epsilon_y \\ \gamma_{xy} \end{bmatrix} \tag{7}$$

Where σ_x and σ_y denote normal stresses and γ_{xy} denotes the shear stress. The elastic modulus, E, and Poisson's ratio, υ, are material properties listed in Table 13.

Deformation, or strain, is defined by *u* and *v*, displacements in the x and y directions respectively.

$$\varepsilon_x = \frac{\partial u}{\partial x} \tag{8}$$

$$\varepsilon_y = \frac{\partial v}{\partial y} \tag{9}$$

$$\gamma_{xy} = \frac{\partial u}{\partial y} + \frac{\partial v}{\partial x} \tag{10}$$

Volume, body, forces are described with the force balance equations.

$$K_X = \frac{-\partial \sigma_x}{\partial x} - \frac{\partial \gamma_{xy}}{\partial y} \tag{11}$$

$$K_Y = \frac{-\partial \gamma_{xy}}{\partial x} - \frac{\partial \sigma_y}{\partial y} \tag{12}$$

Combining the stress-strain and balance force equations, a relationship for displacement can be written.

$$-\nabla \cdot (c \otimes \nabla u) = k \tag{13}$$

Where volume forces, k, are defined as

$$k = \begin{bmatrix} K_X \\ K_Y \end{bmatrix} \tag{14}$$

And *c* is a rank four tensor represented by four two-by-two matrices.

$$c_{11} = \begin{bmatrix} 2G + \mu & 0 \\ 0 & G \end{bmatrix} \tag{15}$$

$$c_{12} = \begin{bmatrix} 0 & \mu \\ G & 0 \end{bmatrix} \tag{16}$$

$$c_{11} = \begin{bmatrix} 0 & G \\ \mu & 0 \end{bmatrix} \tag{17}$$

$$c_{22} = \begin{bmatrix} G & 0 \\ 0 & 2G + \mu \end{bmatrix} \tag{18}$$

Shear modulus, *G*, is given by

$$G = \frac{E}{2(1+\nu)} \tag{19}$$

And intrinsically, μ is given by

$$\mu = 2G\left(\frac{\nu}{1-2\nu}\right) \tag{20}$$

Solving Equation 13, fifteen scalar Tensors can be calculated as outputs in MATLAB including displacements, principal, shear, and Von Mises effective stresses and strains.

Mesh Generation

A triangular mesh is initialized and then refined by bisecting the longest edge in the element. MATLAB's innate functions limit the mesh to triangular elements and therefore no other options are explored. Mesh refining is repeated until solver results change by less than 5% ensuring the model is mesh independent. A summary of the results from the mesh dependence test are shown in Table 14. For the joint and repair model, the mesh, Figure 36, is refined seven times. A nonlinear solver is employed to prevent noisy results due to improperly modeled non-linearity.

Table 14: Mesh Dependence Test Iterations for 5 Degree, 50% Through Thickness Repair Model

Iteration	Resulting Far-field Strain (%)	% Difference
Refinement 1	0.63	--
Refinement 2	0.54	17%
Refinement 3	0.45	20%
Refinement 4	0.35	29%
Refinement 5	0.32	9%
Refinement 6	0.27	19%
Refinement 7	0.26	4%

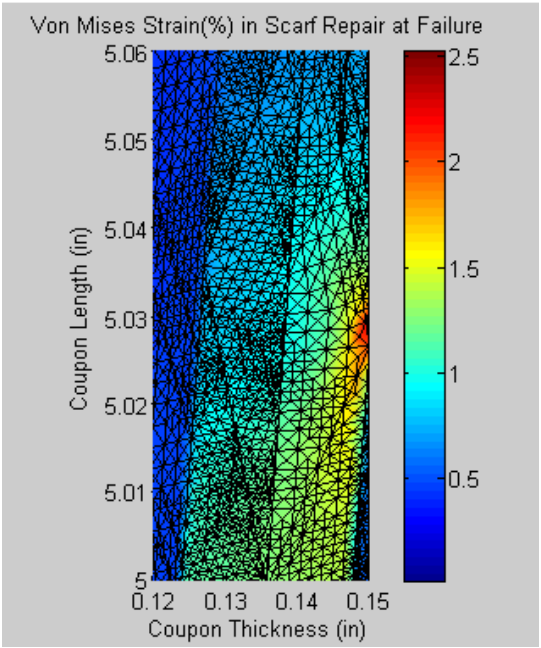

Figure 36: Mesh Overlay of Failed Adhesive Portion in 5 Degree Scarf Repair Model

Implementation of Failure Criteria

MATLAB code is formulated to increase the volume force from 0.0 by a step of 0.05 until the failure criteria is met. Failure criteria, based on the Von Mises-Hencky, or maximum-distortion-energy theory, is derived from the experimental portion of this

study. This criteria states that "yielding in a ductile material occurs when the distortion energy per unit volume of the material equals or exceeds the distortion energy per unit volume of the same material when it is subjected to yielding in a simple tension test."[13] Strain-energy density can be decomposed into two parts: 1) the energy necessary to cause volume change with no change in element shape and, 2) the energy necessary to distort the element's shape. Applying Hooke's law under the assumption that material behavior is linear-elastic to an element subjected to three principle stresses, strain-energy density can be defined by

$$u = \frac{1}{2E}\left[\sigma_1^2 + \sigma_2^2 + \sigma_3^2 - 2\upsilon(\sigma_1\sigma_2 + \sigma_1\sigma_3 + \sigma_2\sigma_3)\right] \tag{21}$$

The energy necessary to cause volume change is caused by the average principle stress and therefore, the energy needed to distort the element is the result of the remaining portion of the stress: $(\sigma_1 - \sigma_{ave})$, $(\sigma_2 - \sigma_{ave})$, and $(\sigma_3 - \sigma_{ave})$. To find distortion energy per unit volume, these stresses are substituted into Equation 22 for the principal stresses, $\sigma_1, \sigma_2,$ and σ_3.

$$u_d = \frac{1+\upsilon}{6E}\left[(\sigma_1 - \sigma_2)^2 + (\sigma_2 - \sigma_3)^2 + (\sigma_3 - \sigma_1)^2\right] \tag{22}$$

For this plane stress – plane strain model, $\sigma_3 = 0$

$$u_d = \frac{1+\upsilon}{3E}\left[{\sigma_1}^2 - \sigma_1\sigma_2 + {\sigma_2}^2\right] \tag{23}$$

And under uniaxial tension, $\sigma_1 = \sigma_Y, \sigma_2 = \sigma_3 = 0$, therefore,

$$(u_d)_Y = \frac{1+\upsilon}{3E}\sigma_Y^2 \tag{24}$$

The maximum-distortion-energy theory, states that $u_d = (u_d)_Y$ and so

$$\sigma_Y = \sqrt{\sigma_1^2 - \sigma_1\sigma_2 + \sigma_2{}^2} \tag{25}$$

Equation 25 is depicted in Figure 37 representing an elliptical curve. The maximum-distortion-energy, or Von Mises, failure criteria, conditions that if an element is stressed

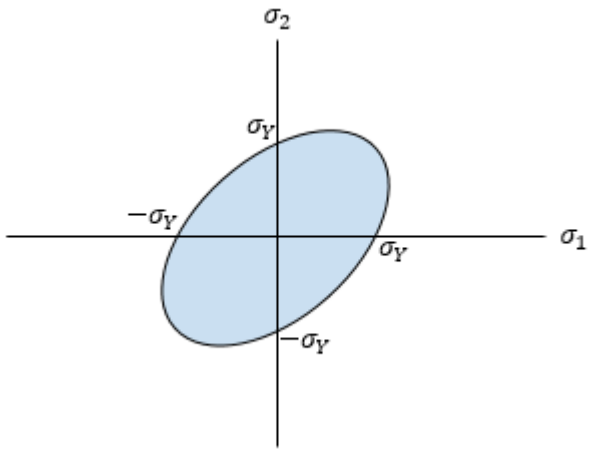

Figure 37: Elliptical Boundary of Maximum-distortional-energy, Huber-Henky-Von Mises Theory[13]

in a manner that (σ_1, σ_2) is plotted on or outside the boundary, the material fails[13]. The same derivation can be completed using principal strains in place of principal stresses. Thus, failure criteria can be developed using a maximum Von Mises strain which is applied to this FEA model. The maximum-distortion-energy theory is only valid for isotropic materials and best applied to ductile materials. Since the failure criteria is solely applied to the adhesive, which characteristically exhibits high strain to failure and isotropic properties, the application of this theory is valid.

Model Runs

Finite element analysis models are compiled for unidirectional carbon joints of 5, 15, and 25 degree scarf angles, non-through thickness repair configurations of 5 and 15 degree scarf angles for both 50% and 75% through thickness with an epoxy adhesive, and a 15 degree, 50% through thickness configuration for Polyurethane and MA adhesive. Table 15 is a summary of model runs completed for the FEA study.

Table 15: Summary of Finite Element Analysis Model Runs

Configuration	**Scarf Angle**	**Composite/Adhesive**	**Design Parameter**
Joint	5	Carbon Uni/Epoxy	Scarf Angle
Joint	15	Carbon Uni/Epoxy	Scarf Angle
Joint	25	Carbon Uni/Epoxy	Scarf Angle
75% Repair	5	Carbon Uni/Epoxy	Scarf Angle/Repair Depth
75% Repair	15	Carbon Uni/Epoxy	Scarf Angle/Repair Depth
50% Repair	5	Carbon Uni/Epoxy	Scarf Angle/Repair Depth
50% Repair	15	Carbon Uni/Epoxy	Scarf Angle/Repair Depth/Adhesive Type
50% Repair	15	Carbon Uni/MA	Adhesive Type
50% Repair	15	Carbon Uni/Polyurethane	Adhesive Type

Algorithm Application

The model runs are correlated to experimental data by comparing far-field strain in the y-direction as well as the Von Mises strain distribution through the center of the adhesive at failure. Failure in the FEA model is defined as the point which the maximum Von Mises strain in the adhesive reaches the value derived from experimental data. Failure in the experimental test specimen is noted at the first visual observance of damage in the adhesive bondline.

Far-field strain data is averaged over a 0.075 in^2 area located 0.5 inches below the tab and centered through the thickness, Figure 38. This strain represents the average

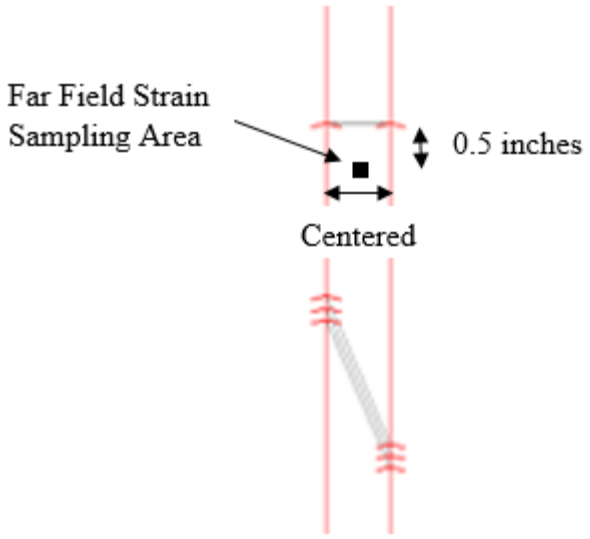

Figure 38: Location of Far-field Strain Sampling Area

strain in the y-direction of the composite adherend, thus characterizing the general strain conditions a structure can undergo before the adhesive in a joint or repair will fail. The location is such that the scarfed region does not directly or sympathetically affect the strain field. Far-field is defined such that the distance in which an object no longer affected by a discontinuity is equal to one half the size of the discontinuity in the respective direction. In this case, the far-field area is a minimum distance of one half the scarf length from the end of the scarf. The tabs used in experimental testing and modeled in MATLAB eliminate effects of the grip on the strain field. Therefore, proximity to the tabs and grips is arbitrary. The same measuring area and location is used to determine the far-field strain in both the FEA model and test specimens. Average stress in the y-

direction is also calculated over this measuring area and compared to test data. FEA results from the joint model vs non-through thickness repair model are compared for respective 5 and 15 degree scarf angles.

EXPERIMENTAL TEST RESULTS

The purpose of this research was to develop coupon level specimens to more accurately represent a repaired composite structure than the current joint methodology and to propose a geometry independent failure criteria based on experimental testing. Joint coupons of varying adherend layups and scarf angles, as well as non-through thickness repair coupons of varying scarf angles and depths, were tested in tension. Strength and strain data from these configurations was compared in order to determine the validity of joint geometry in the characterization of a scarf repair. A 2D finite element model was developed to correlate test results with the proposed geometry independent failure criterion.

Joint Specimen Results

Strength Results and Failure Modes

Scarf joint configurations consisted of 5, 15, and 25 degree angles bonded by Hexion Epikote MGS RIMR 135 structural epoxy adhesive. 4-ply Carbon Uni, Glass Uni, Glass Triax, and Carbon/Glass hybrid Triax composite adherend layups were used. Strength results and failure modes are shown in Table 16. Failure stress was averaged over all the coupons tested for each respective configuration and was calculated from a mechanics of materials method by taking the maximum load upon failure divided by the average cross sectional surface area of the specimen as described by Equation 6. Control data listed in column one represents the average failure stress of an undamaged, unflawed 4-ply coupon tested in previous research at MSU. Five degree angles, the strongest of the

tested joints, restored approximately 15% of strength of the damage free control specimen.

Table 16: Summary of Failure Strength and Modes for Joint Specimens

	Scarf Angle (deg)	Ave Failure Stress (ksi)	Standard Deviation	Failure Mode
Glass Uni Control: 146 ksi	5	23.2	1.8	Adhesive
	15	10.9	1.2	Adhesive & Cohesive
	25	10.0	2.8	Adhesive & Cohesive
Carbon Uni Control: 206 ksi	5	31.8	4.5	Cohesive
	15	15.5	2.5	Cohesive
	25	8.7	1.3	Cohesive
Glass Triax Control: 119 ksi	5	19.1	2.0	Adhesive
	15	13.2	1.1	Adhesive
	25	10.2	0.6	Cohesive
Hybrid Triax Control: 151 ksi	5	25.6	0.4	Adhesive & Cohesive
	15	12.9	2.3	Cohesive
	25	10.5	1.3	Cohesive

Cohesive and adhesive failure modes were observed during testing. A cohesive failure, the desired mode, is a failure within the adhesive and is characterized by adhesive residue on both sides of the joint, Figure 39. The Carbon Uni (CU) and Hybrid Triax (HTr) specimens presented mostly cohesive failures with the Carbon Uni adherend layup being the most consistent. The Glass layups resulted in an increased number of adhesive failures in which the bond failed between the adhesive and adherend. As observed in Figure 40, the adhesive is fully intact on one side of the joint and the other side shows a clean adherend.

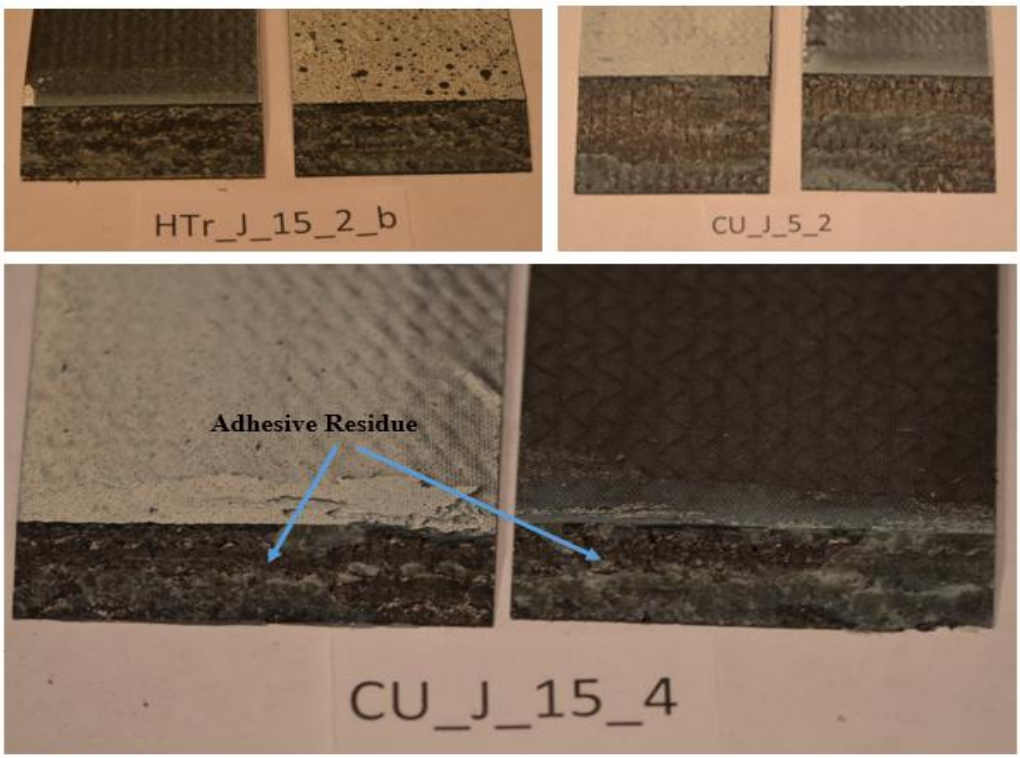

Figure 39: Cohesive Failures in Carbon Uni (CU) and Hybrid Triax (HTr) 2 inch Wide Joint Specimens

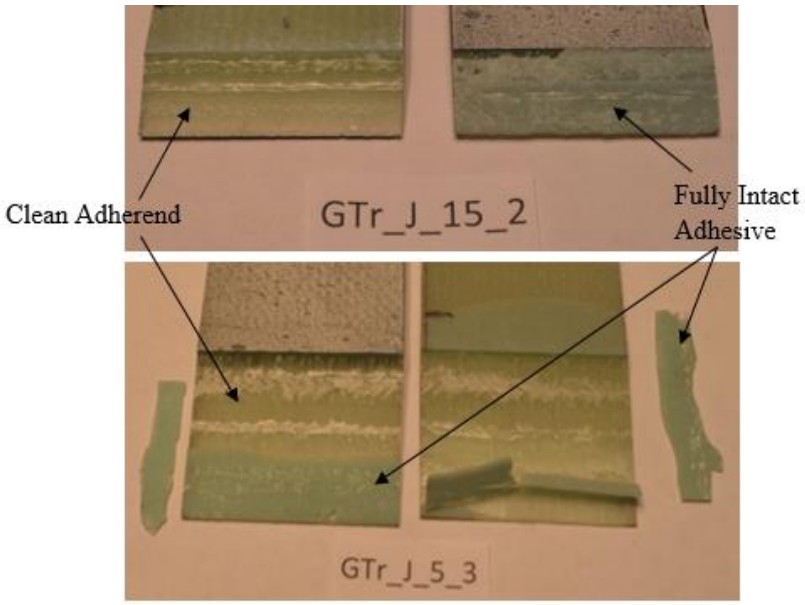

Figure 40: Adhesive Failures in Glass Triax (GTr) 2 inch Wide Joint Specimens

Chemical compatibility between adhesive and adherend is a contributing factor in joint strength. Optimizing this compatibility should be considered in adhesively bonded joints. Results suggest that a two-part epoxy based structural adhesive pairs better with Carbon laminates than Glass. Poor surface prep may have also played a role in the failure modes. However, all surfaces were prepared with the same process thus limiting this factor.

Strain Results

Strain data was collected through ARAMIS data image correlation (DIC) measuring system. Far-field strain in the y-direction and maximum Von Mises strain in the adhesive was recorded at coupon failure and shown in Table 17.

Table 17: Strain Results of Scarf Joint Specimens at Failure

Layup (4-ply)	Scarf Angle (deg)	Ave Far Field Strain Y (%)	Max Adhesive Von Mises Strain (%)
Glass Uni	5	0.36	2.76
	15	0.16	2.23
	25	0.20	0.96
Carbon Uni	5	0.27	2.62
	15	0.16	2.56
	25	0.11	2.79
Glass Triax	5	0.43	2.69
	15	0.28	2.63
	25	0.22	2.32
Hybrid Triax	5	0.34	3.03
	15	0.15	2.80
	25	0.14	2.68

Stress vs Far Field Strain. A plot of Stress vs Far-field strain, Figure 41, for the Carbon Uni joints reveals that varying the angle of the joint does not change the coupon

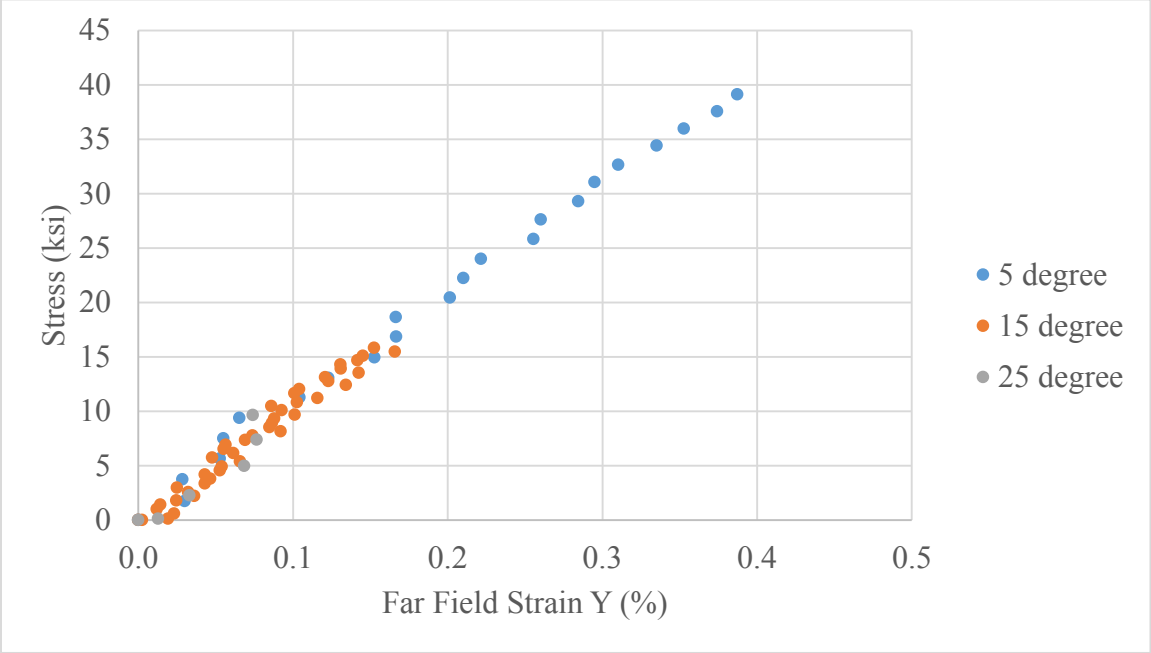

Figure 41: Stress vs Far Field Strain Y for Unidirectional Carbon/Epoxy Adhesive Joint Specimens of Varying Scarf Angle

properties. All adherend layups exhibited the same consistency in material properties. Failure strength and strain generally decreases as scarf angle increases. Results from the 15 and 25 degree angles are more closely coupled than the 5 and 15 degree angles suggesting there is a scarf angle for which the ratio between the amount of material removed to the strength restored is optimized. Additional tests for angles between 5 and 15 degrees would be required for this to be conclusive.

Von Mises Strain vs Far Field Strain. Figures 42 and 43 plot the maximum Von Mises strain in the adhesive against far-field strain-y in the coupon for the Carbon Uni

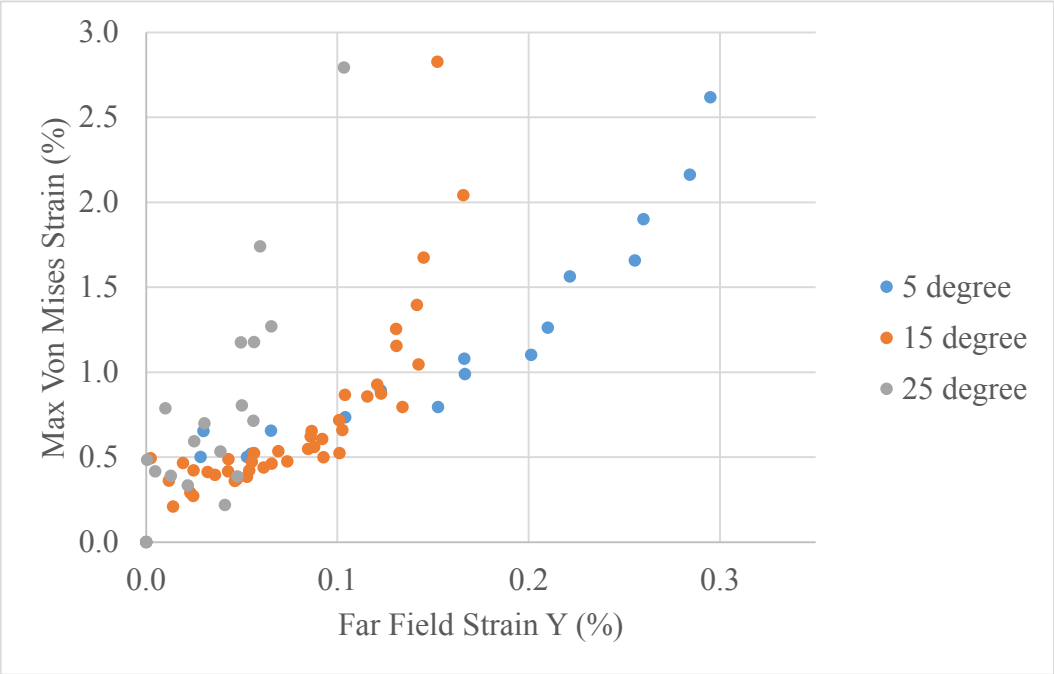

Figure 42: Max Von Mises Strain vs Far Field Strain Y in Bondline for Carbon Uni Scarf Joints with Epoxy Adhesive

and Hybrid Triax layups. Max Von Mises strain was consistent between all angles and adherend layups. One outlier, the 25 degree Glass Uni joint, failed at a much lower max Von Mises strain averaging 0.96%. This is likely due to the observed failure mode and lack of proper adherence between the epoxy and parent laminate. The average far-field strain in the specimen increases as the scarf angle decreases. Decreasing the scarf angle in a joint allows the structure to endure higher strain fields before the adhesive reaches a

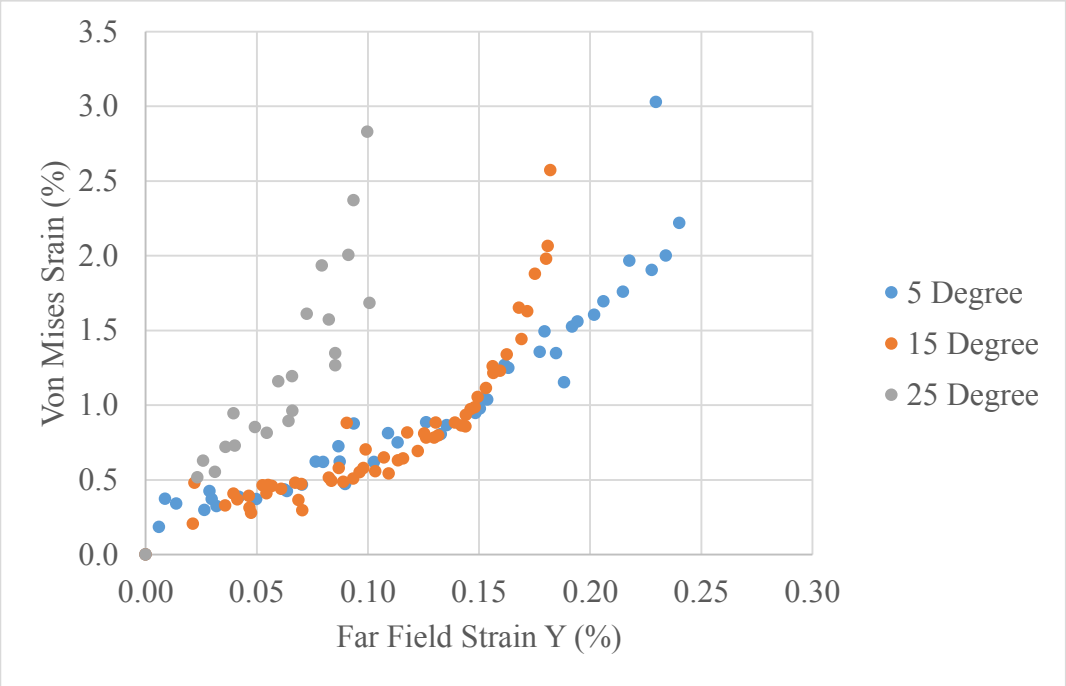

Figure 43: Max Von Mises Strain vs Far Field Strain Y in Bondline for Hybrid Triax Scarf Joints with Epoxy Adhesive

failure strain condition. Larger angles in the joint result in more brittle failures characterized by the steeper slope of the 25 degree joints when compared to the 5 and 15 degree joints.

Adherend Comparison. Comparison of the stress-strain relationship for the adherend layups of identical scarf angle reveal the stiffness differentiation between laminates. As shown in Figure 44, The Carbon Uni is the stiffest of the laminates with the steepest slope and lowest strain at failure. Glass Triax is the least stiff with the shallowest slope and highest strain at failure. These differences in strain at failure are plotted against max Von Mises strain in the adhesive in Figure 45 for the same 15 degree joints. The adhesive fails at the same Von Mises strain values, but the far-field strain

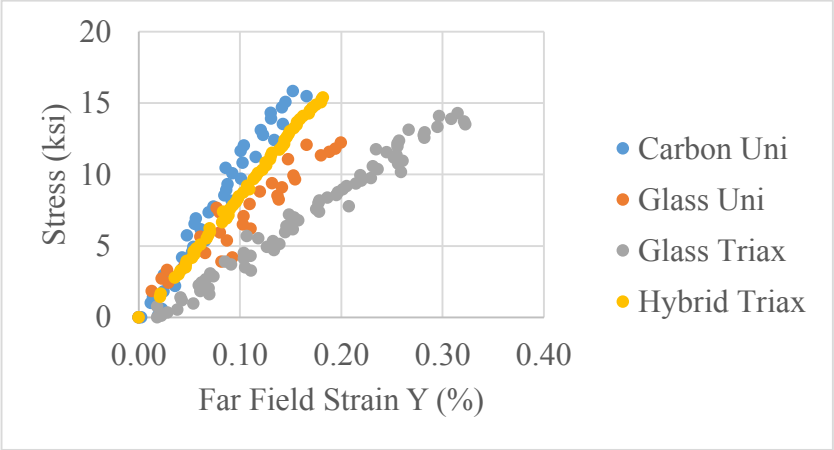

Figure 44: Stress vs Far-field Strain for 15 Degree Joints of Varying Adherend Laminates

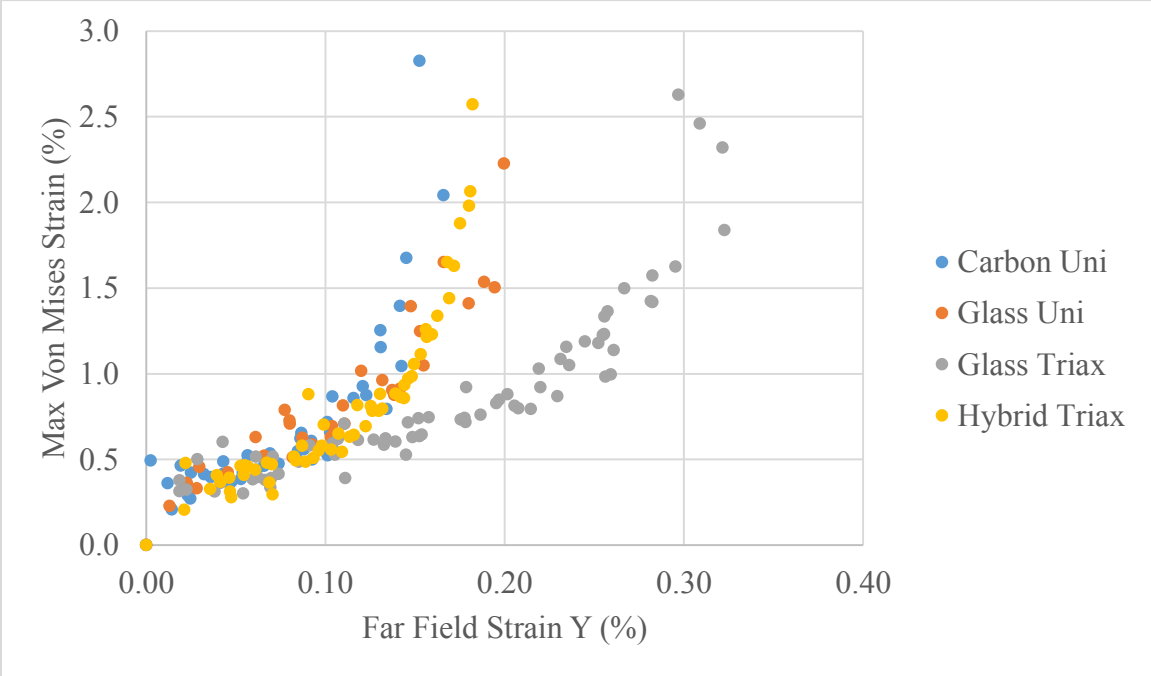

Figure 45: Max Von Mises Strain vs Far-field Strain Y for 15 Degree Joints of Varying Adherend Laminates

values vary per layup. The stiffer the parent, the smaller the far-field strains at adhesive failure. The Glass Triax, being the least stiff laminate, results in far-field strains nearly twice as large as the other laminates when subjected to similar tensile loads.

Non Through Thickness Repair Specimen Results

To compare against scarf joints, non through thickness Carbon Uni-Epoxy Adhesive repair specimens of 5 and 15 degrees with a 50% repair (two out of four plies) and a 75% repair (three out of four plies) were tested in tension. Two additional adhesives, polyurethane and methacrylate (MA) were tested in a 15 degree scarf, 50% repair configuration.

Damage Progression

Unlike the joints, damage initiation to ultimate failure advanced through multiple stages of damage progression as shown in Figure 46. The first sign of damage, frame 1,

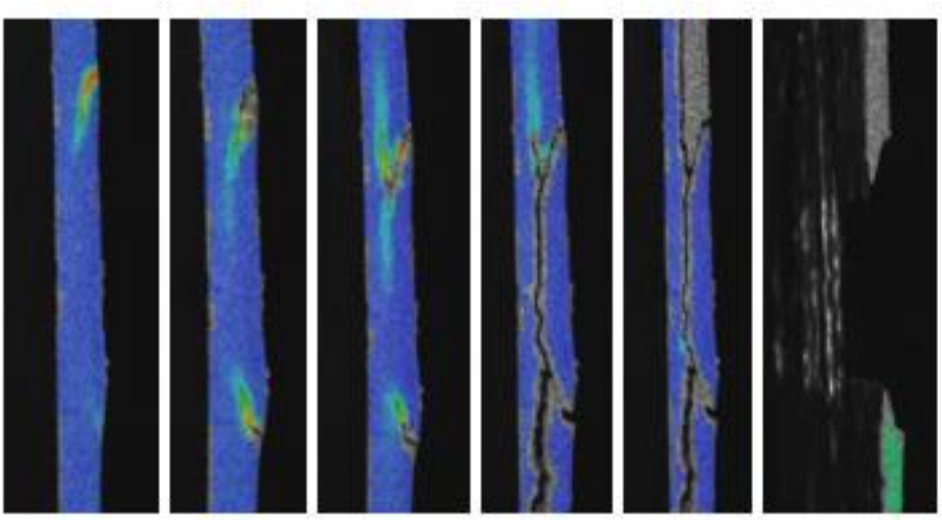

Figure 46: Damage Progression of a 15degree Scarf, 50% Repair Specimen with a Von Mises Strain Overlay Loaded in Tension

occurs in adhesive between the parent and repair patch on one edge of the specimen. For this analysis, this stage is considered the adhesive failure. The opposite scarfed edge fails

and the damage progresses through the bondline, frame 2. In frame 3, a crack begins to form in the parent between the plies that were scarfed out and those left un-scarfed. The crack progresses through the parent, frames 4 and 5, until it propagates to the tabs leaving only the un-scarfed plies to carry the load. When the remaining plies fail, frame 6, the specimen is considered to have reached ultimate failure. Figure 47 depicts the post failure of the un-scarfed plies. Figures 48 and 49 show side view of post-test specimens detailing the location of the adhesive failure and crack propagation in the parent.

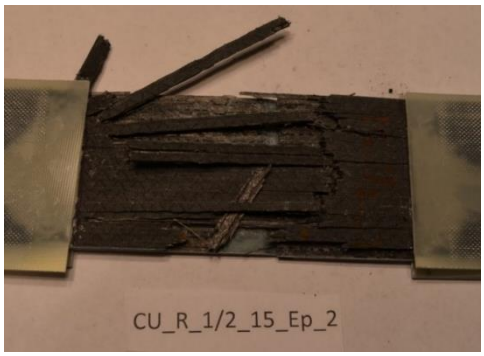

Figure 47: Post Test Damage in a 5 Degree Scarf, 75% Repair Carbon Uni-Epoxy Adhesive Repair Specimen

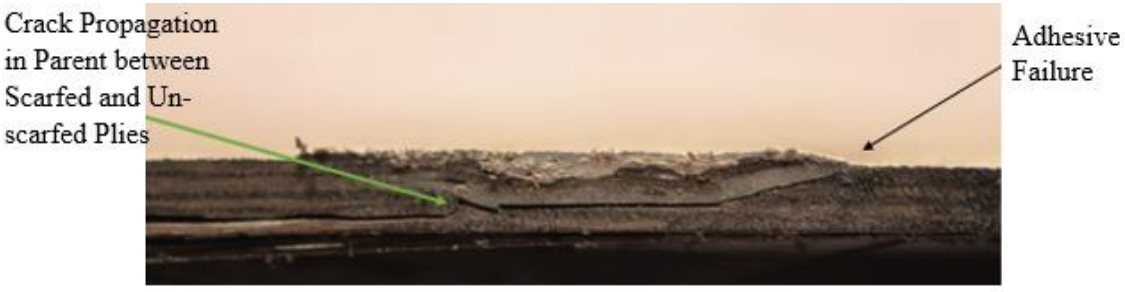

Figure 48: Failure of Un-scarfed Plies Leading to Ultimate Failure in a 15 Degree, 50% Repair Specimen

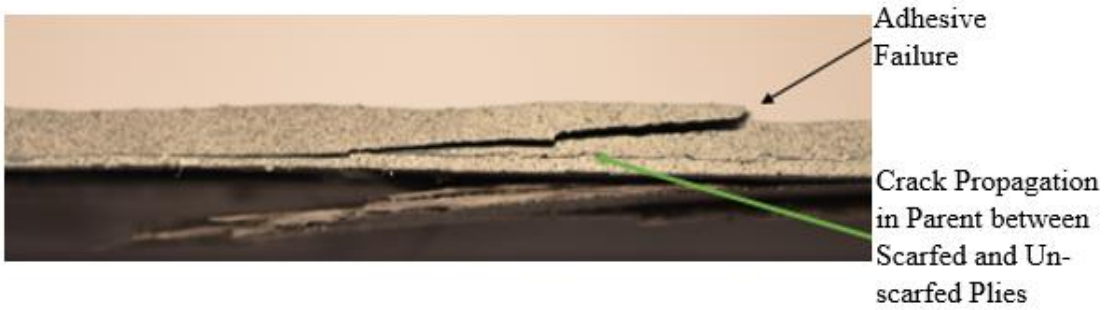

Figure 49: Post Test Damage in a 15 Degree Scarf, 75% Repair Carbon Uni-Epoxy Adhesive Repair Specimen

Strength Results

Strength values are calculated by dividing the load by the cross sectional area, Equation 6, and are evaluated at the adhesive failure stage and ultimate failure stage. Stress results are shown in Table 18. Ultimate failure strength was dependent on the

Table 18: Strength Results for Carbon Uni/Epoxy Adhesive Repair Specimens

	5 Degree Scarf Angle				15 Degree Scarf Angle			
	50% Repair	Std Dev	75% Repair	Std Dev	50% Repair	Std Dev	75% Repair	Std Dev
Ultimate Strength (ksi)	82.08	5.89	42.39	8.84	82.74	2.56	40.16	6.96
Strength-Adhesive Failure (ksi)	25.53	3.97	25.23	0.43	14.27	2.14	10.17	2.92

depth of repair and the strength of the adhesive was dependent on scarf angle. Higher ultimate strength was seen in 50% through thickness specimens because two un-scarfed plies carried the load vs one ply in the 75% through thickness specimens. The smaller the scarf angle the stronger the adhesive bond, similar to the joint results. Depth of repair does not appear to influence the adhesive bondline strength for the 5 degree specimens. However, depth may be a factor as scarf angle increases.

While the adhesive failure strength for the 15 degree 50% and 75% repair specimens are within one standard deviation of each other, these standard deviations are large, approximately 20% the strength value. Additional testing is necessary to lower the standard deviations and determine the influence of depth on adhesive bondline strength.

Strain Data Collection

Far-field strain was difficult to measure with the DIC due to the abundant crack propagation observed through the thickness of the specimens. A sampling of strain data was taken from multiple locations, Figure 50, in an effort to fully characterize the strains

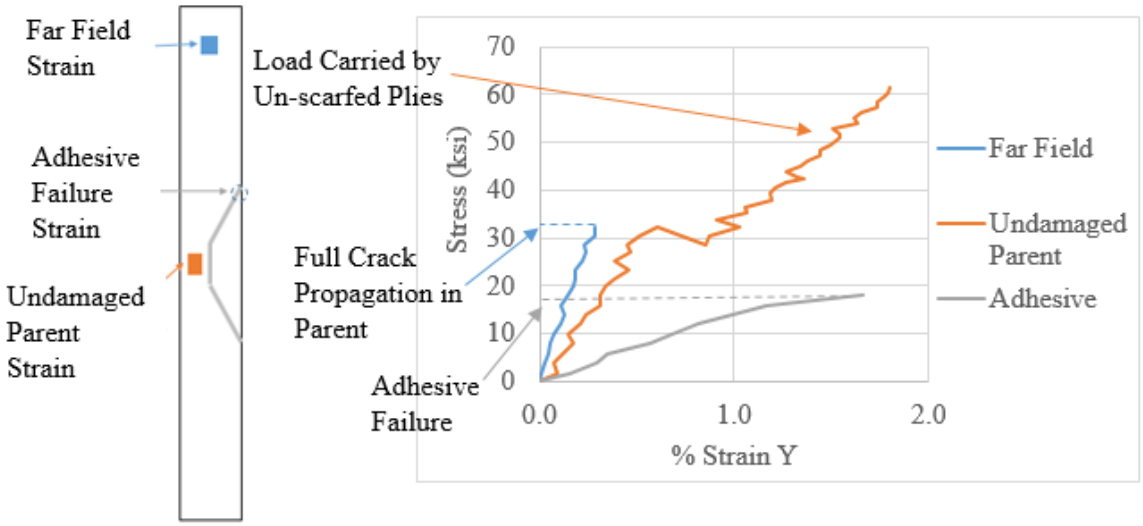

Figure 50: DIC Edge Wise Strain Sampling Locations in a 5 Degree, 50% Repair Carbon Uni/Epoxy Adhesive Specimen

as damage progressed. Far-field strain and undamaged parent strain are average strains in the y-direction, while the adhesive failure strain is a maximum strain value in the y-direction. Strain in the adhesive is collected until damage is visually observed in the ARAMIS images. While strain-y is presented in this figure, maximum Von Mises strain

will be used to analyze the adhesive for a failure criteria. The far-field sampling area remains active until the crack in the parent separating the scarfed and un-scarfed plies propagates to the tabs. The intent of the undamaged parent sampling area was to understand the effect of the load on the remaining un-scarfed plies. In the 50% repair configurations this area remained active for the majority of the test. The final stages were unable to be imaged. This is of no implication to the analysis of the adhesive. During these final stages the adhesive is significantly damaged and outside the elastic range. For the 75% repair configurations, limited data was captured since only one ply remained to carry the load resulting in a small imaging area. The undamaged parent sampling area has a less steep stress-strain relation than the far field sampling due to the proximity to the damaged region.

ARAMIS Strain Validation

Mechanics of Materials. Far-field strain DIC data is validated using a mechanics of materials approach in which an approximate elastic modulus of 67.8GPa based on 4-ply Carbon Uni control testing defines strain by

$$\epsilon = \frac{P}{AE} \tag{26}$$

Where P is the load, A is the cross sectional area, and E is the elastic modulus. The resulting calculated strains are plotted in a stress-strain curve against ARAIMIS DIC results in Figure 51. The excellent correlation of slopes validates the DIC far-field strain data. The uncertainty of the ARAMIS measuring system is +/-0.25 microns with under a 500microstrain potential error.

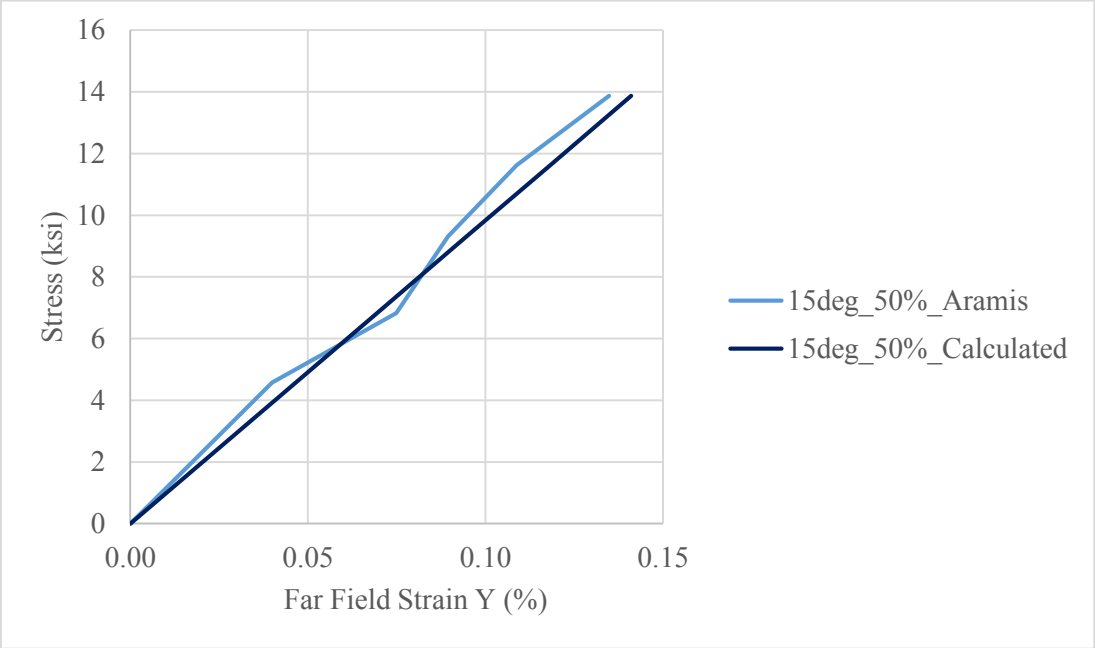

Figure 51: Far-field Strain ARAMIS Validation for 15 Degree, 50% Repair Experimental Data

Strain Gauge. Strain gauges were affixed to six repair samples on the width-wise face directly behind the repair patch and the results compared to the undamaged parent ARAMIS strain data for validation. A schematic of strain gauge location in relation to the undamaged parent sampling area is depicted in Figure 52. Comparison of strain gauge and ARAMIS DIC data for non-patched specimens is shown in Figure 53. The

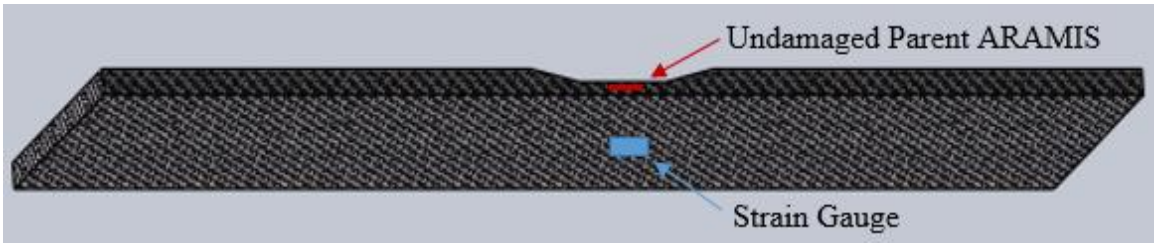

Figure 52: Strain Gauge and Undamaged Parent Sampling Location on Repair Specimen

DIC strain data gives a reasonable correlation to the strain gauge data and therefore can be used to characterize the behavior in the un-scarfed parent plies under the repair patch. Strain gauge data is shifted to the left as expected. The location of the data collection is subject to bending forces induced by the decreased thickness of the parent in the scarfed region. The strain gauges are affixed to the outer composite ply which realizes the highest amount of compression, resulting the curve shift in comparison to the ARAMIS data.

For a given stress value in Figure 50, the undamaged parent strain values are larger than the far-field strains. The parent material under the repair is experiencing more elongation than the parent material away from the proximity of the repair. One possible explanation for this is that load shedding is occurring and as the adhesive is stressed some

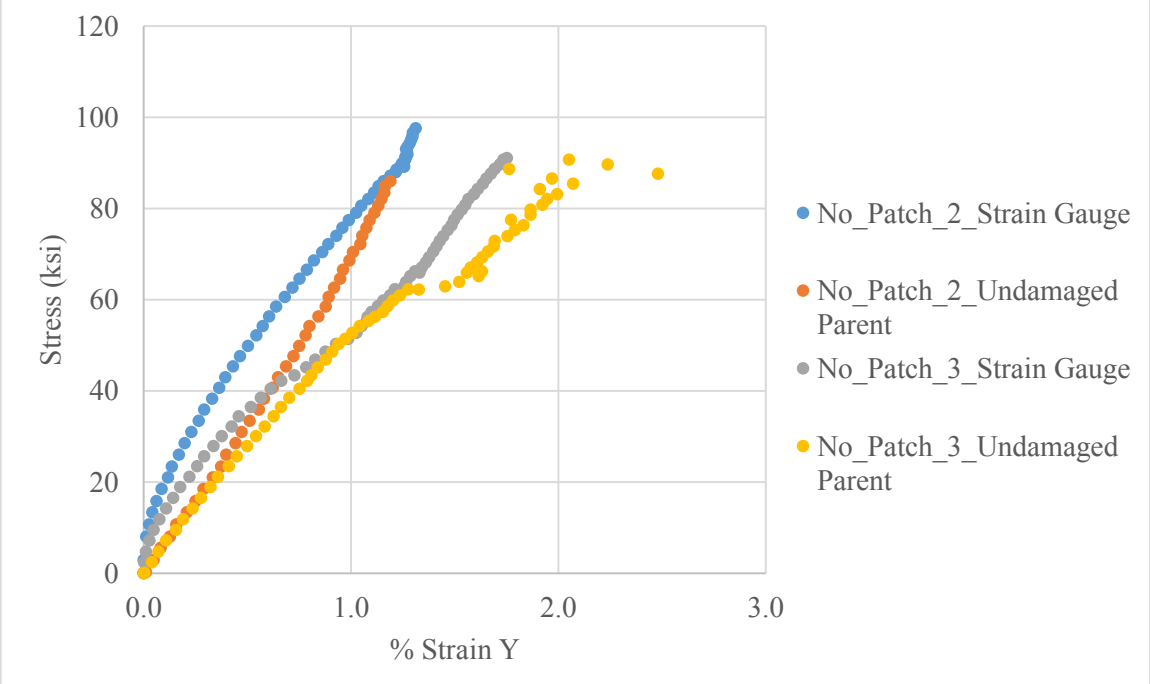

Figure 53: Correlation of ARAMIS Undamaged Parent Strain Data with Strain Gauge Data for a 15 Degree 50% Repair Specimen with no Adhesive or Patch

of the load is diverted into the surrounding parent plies. Another explanation is that the adhesive disrupts the continuity of the cross section and, as Equation 6 illustrates, as cross sectional area decreases, strain increases.

Strain Results

Table 19 displays strength and far-field strain values of the epoxy repair specimen as well as maximum Von Mises strain in the bondline at the adhesive failure stage. This

Table 19: Carbon Uni/Epoxy Adhesive Repair Data at Adhesive Failure

	5 Degree Scarf		15 Degree Scarf	
	50% Repair	75% Repair	50% Repair	75% Repair
Strength (ksi)	25.53	25.23	14.27	10.17
Far Field Strain Y (%)	0.25	0.23	0.13	0.12
Max Von Mises Strain (%)	2.52	2.68	2.75	2.63

data is plotted in a stress-strain curve, Figure 54, and represented in Figure 55 as maximum Von Mises vs Far-field strain. The repairs of all angles and depths present similar characteristic behaviors with adhesive failure stress and far-field strain a product remained consistent for all epoxy repair specimen. The maximum value was the last value recorded prior to the first visual observation of damage in the adhesive and was located on the top outside edge of the adhesive in all cases. The results, presented in of scarf angle. The maximum Von Mises strain recorded at the adhesive failure stage Table 20, are the average max values of all specimens tested for each configuration.

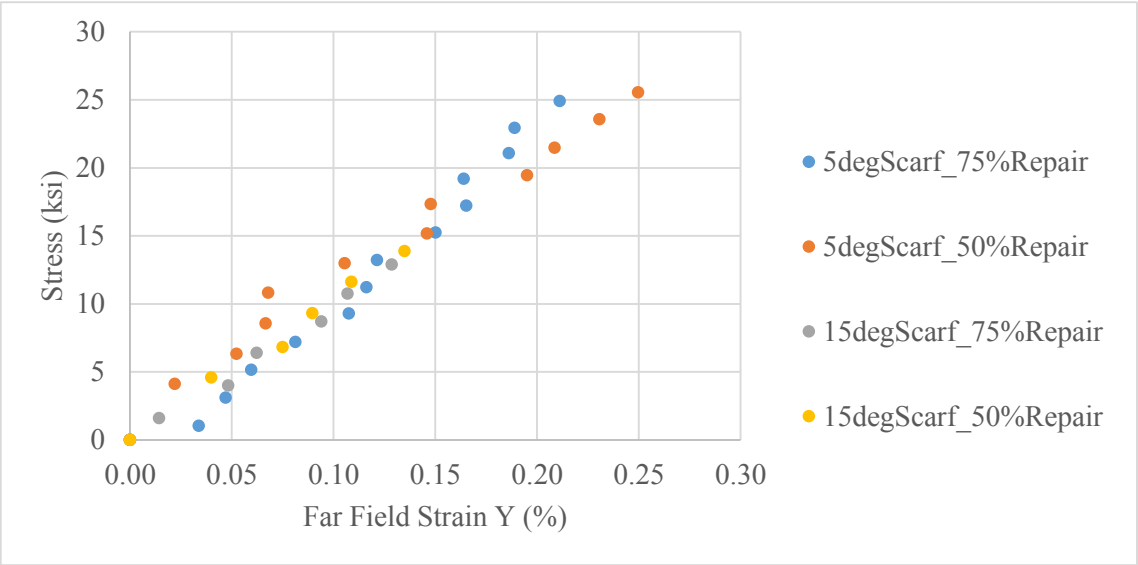

Figure 54: Stress vs Far-field Strain for Carbon Uni/Epoxy Adhesive Repair Specimens at Adhesive Failure

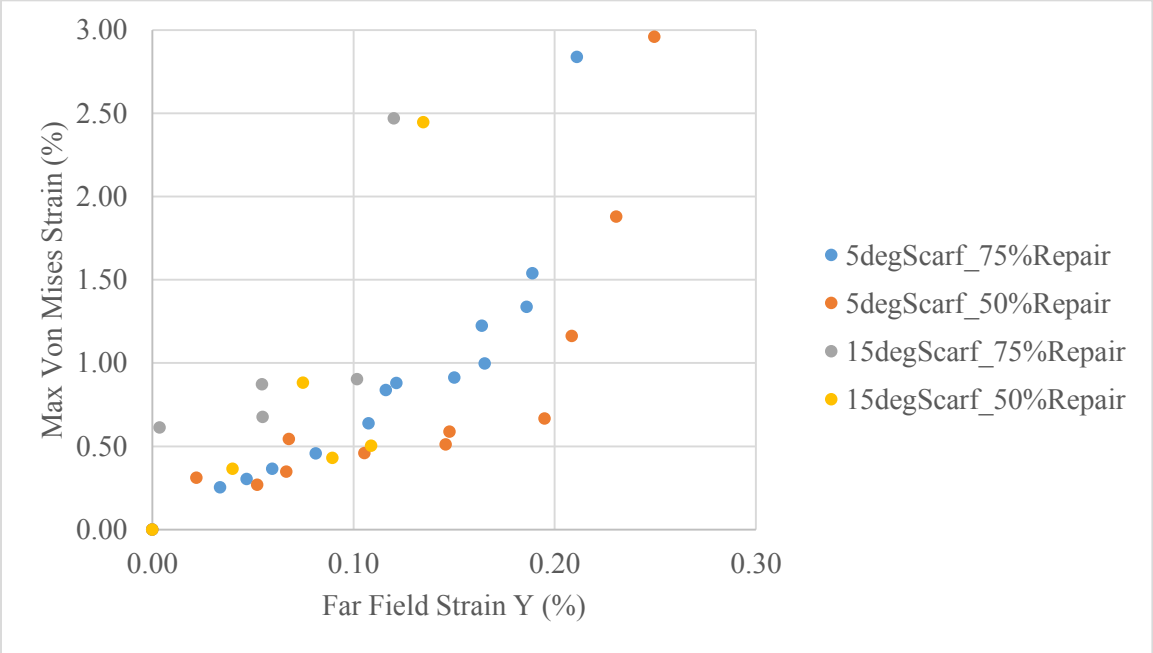

Figure 55: Max Von Mises vs Far-field Strain for Carbon Uni/Epoxy Adhesive Repair Specimens at Adhesive Failure

Table 20: Maximum Von Mises Strain in Epoxy Adhesive for Repair Specimens

Scarf Angle (deg)	% Repair of 4ply	Failure Von Mises Strain (%)	Std Dev
5	50%	2.52	0.62
	75%	2.88	0.60
15	50%	2.75	0.44
	75%	2.63	0.18
All Average		**2.70**	**0.16**

The average value for all configurations was 2.7% with a standard deviation of 0.16. The standard deviation is 5.8% of the reported average value and thus proves the maximum Von Mises strain values in the adhesive at failure are reasonably independent of geometry. Due to the isotropic nature of the adhesive, Von Mises strains can be utilized to evaluate the material. Since Von Mises theory, Equation 25, takes into account strains in two principal directions, it captures both the shear and peel strains induced by the scarf angle when loaded in tension, Figure 56. Thus scarf angle does not

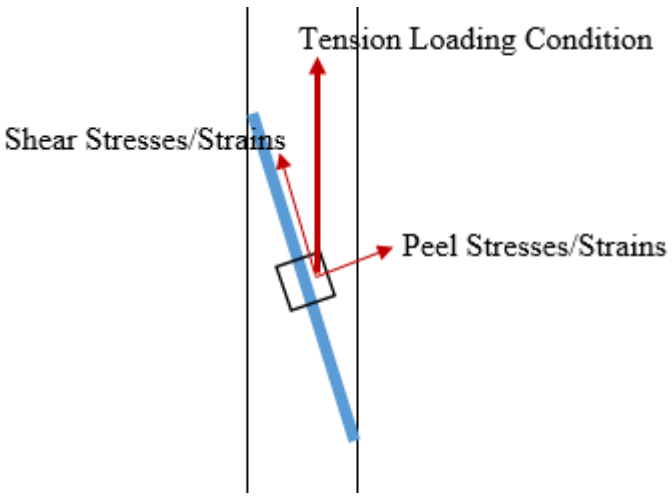

Figure 56: Peel and Shear Stresses Induced by a Scarf Angle when Loaded in Tension

affect Von Mises and, as previously shown, depth of repair does not affect the failure of the adhesive, making Von Mises strain a geometry independent failure criteria for failure in the adhesive bondline. While the repair specimens continued to carry loads after the adhesive failed, analysis of the specimens is limited to the adhesive failure stage. In industry practice, once damage is observed, the structure is removed from service. Therefore, for design purposes, it is applicable to analyze the specimens to the point which the repair patch fails. Observing the repair specimens until ultimate failure in the parent aids in understanding the damage progression of the structure if repair design limitations are exceeded and the structure remains in service.

ANALYSIS OF RESULTS

Adhesive Comparison

Failure Modes

Upon examining the scarfed region after the specimen had failed, it was noted that all epoxy and MA adhesive specimens, Figure 57, presented a cohesive failure in the adhesive. The MA adhesive appears white in color. The Carbon Uni parent laminate in

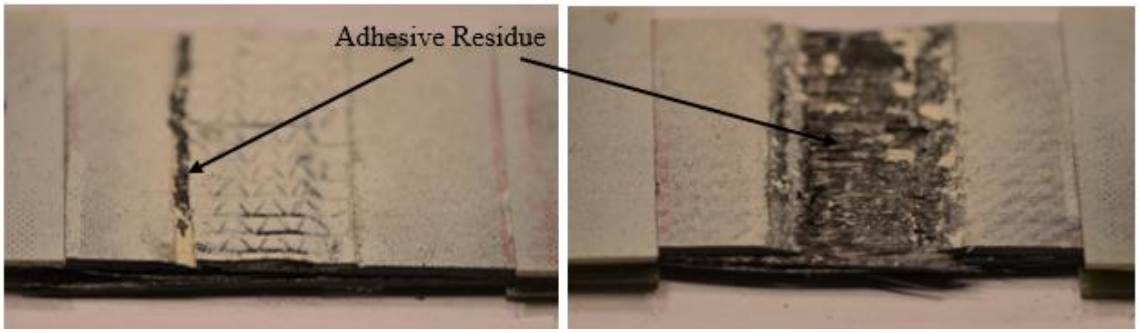

Figure 57: Cohesive Failures in the MA Adhesive Specimens

Figure 57 is painted white for the DIC measuring system. All three polyurethane adhesive specimen tests resulted in adhesive failure modes. The polyurethane appears black in color and can best be seen in the top right image of Figure 58. It is uncertain as to the root cause of this undesirable failure mode. Manufacturer specifications were followed in the preparation, application, and curing of the adhesive. Due to the accelerated cure times in comparison to the epoxy and MA adhesives, it is possible that the adhesive began to cure before the repair patch was fully applied and therefore the adhesive and wet layup resin were not co-cured as intended. The particular polyurethane adhesive used may also have been poorly suited for the application. In general, this type

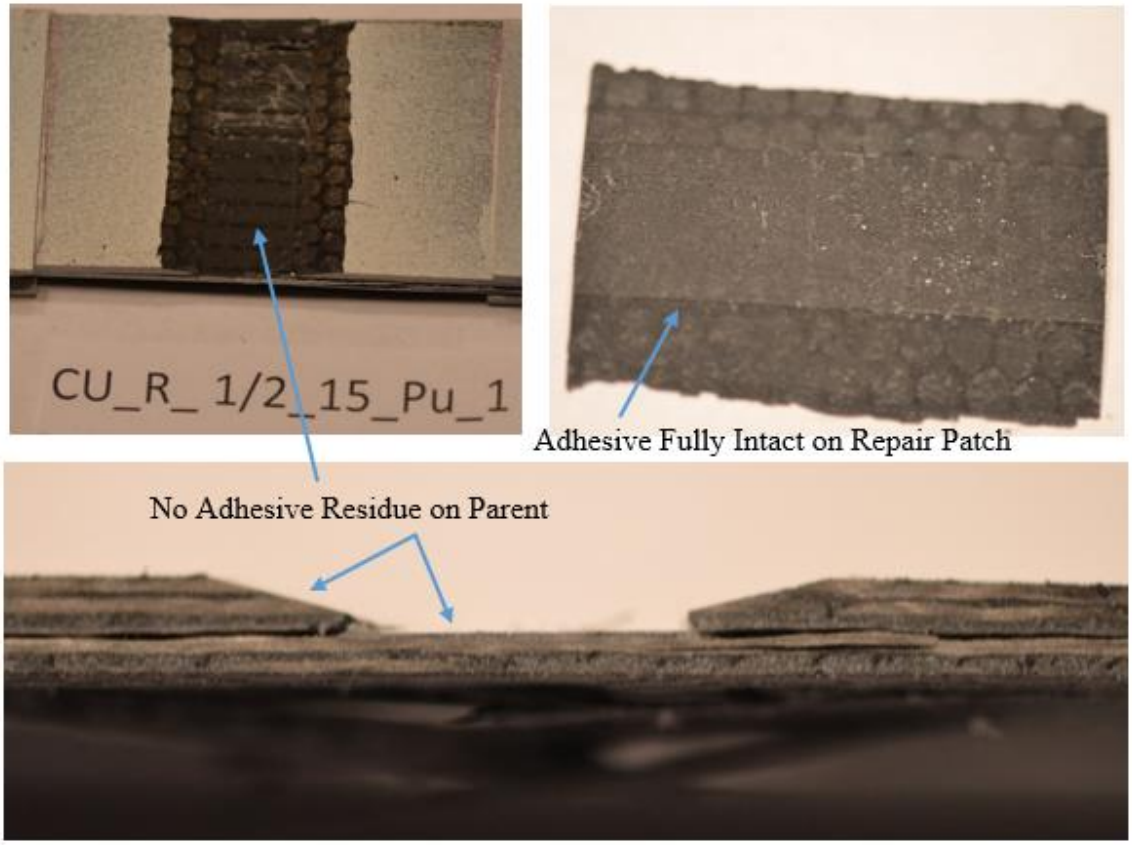

Figure 58: Adhesive Failure Mode in the Polyurethane Adhesive Specimens

of polyurethane is best utilized for filling gaps less than 0.5 mm. A bondline thickness of approximately 0.6 mm implemented in the repair specimens may have been outside the limitations of the adhesive. It is important to note that the results of this testing should not be used to characterize all polyurethane adhesives nor should polyurethane be ruled out as a possible adhesive for composite repair.

Stress and Strain Comparison

Stress and strain values recorded at adhesive failure are listed in Table 21 and plotted in Figure 59. When compared in the same repair configuration, the Epoxy

Table 21: Adhesive Comparison in 15 Degree, 50% Repair Specimen at Adhesive Failure

Adhesive	Failure Stress (ksi)	Far Field Strain Y (%)	Max Von Mises Strain (%)	Failure Mode
Epoxy	14.27	0.12	2.75	Cohesive
Polyurethane	3.92	0.06	0.96	Adhesive
MA	4.15	0.03	2.61	Cohesive

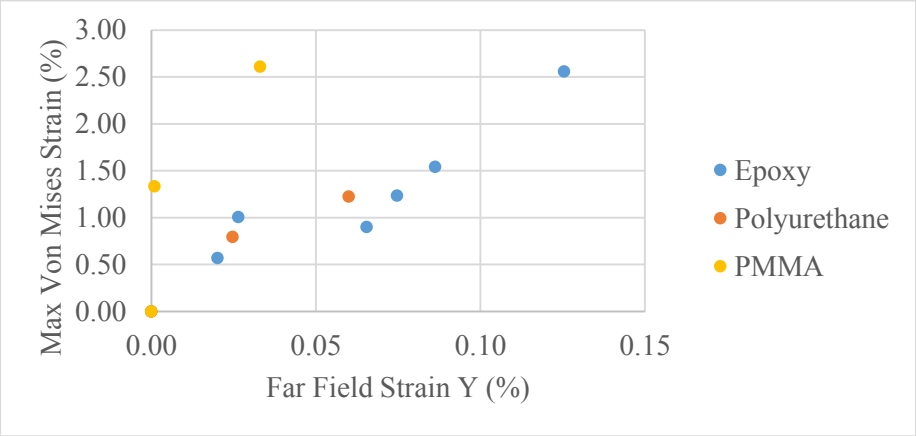

Figure 59: Max Von Mises Strain vs Far-field Strain Adhesive Comparison in 15 Degree, 50% Repair Specimen at Adhesive Failure

adhesive proved to be over three times stronger on average than the MA and Polyurethane adhesives. Despite the low failure stress and far-field strain Y, the MA exhibited similar max Von Mises strains as the epoxy, suggesting that the max Von Mises strain failure criteria could be applied to other adhesive types. Due to the adhesive failures exhibited by the Polyurethane, the test results cannot be compared to the other adhesives.

Joint to Repair Comparison

Test results from the 5 and 15 degree unidirectional Carbon joint and repair specimens were compared to analyze the ability of a joint to represent a repair at the coupon level. Table 22 shows a side-by-side comparison of parameters evaluated at

Table 22: Joint vs Repair Comparison at the Adhesive Failure Stage with Carbon Uni Adherend and Epoxy Adhesive

	5 Degree			15 Degree		
	Joint	50% Repair	75% Repair	Joint	50% Repair	75% Repair
Strength (ksi)	31.8	25.53	25.23	15.5	14.27	10.17
Far Field Strain Y (%)	0.27	0.22	0.23	0.15	0.13	0.12
Max Von Mises Strain (%)	2.62	2.52	2.88	2.83	2.75	2.63

adhesive failure. Far field data reflects strains in the parent composite while Von Mises data reflects strains in the adhesive. Max Von Mises strains in the adhesive remained consistent between joint and repair, Figures 60 and 61. In both the 5 and 15 degree configurations it is interesting to note that the joint specimens resulted in higher strengths and far-field strains than the repair specimens. The repair test results indicate that strength and far-field strain are not influenced by depth. Since a joint is simply a 100% through thickness repair, these values should be more closely related. The two configurations were tested on different Instron machines with different feed rates. The slower feed rates administered in the joint testing could have led to relatively higher average strength and strain results. A broad spectrum of adhesive failure strength values was observed in the 5 degree joint and 5 degree, 50% repair specimens. Four 5 degree joints were tested. The resulting standard deviation was 4.5. Among the three 5 degree

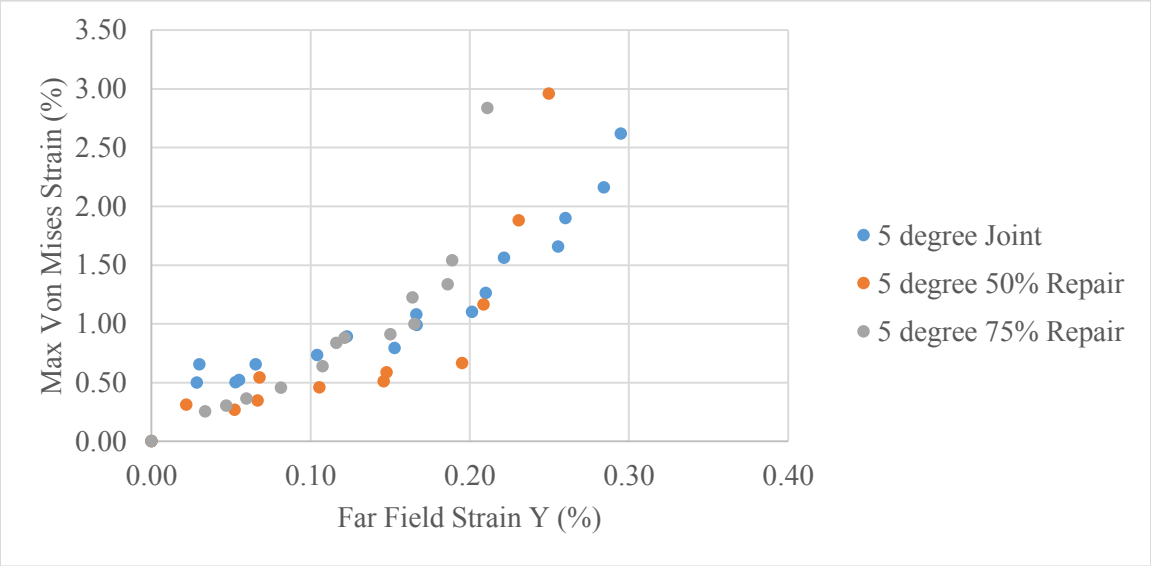

Figure 60: Max Von Mises Strain vs Far-field Strain in 5 Degree Joint and Repair Specimens with Carbon Uni Adherend and Epoxy Adhesive

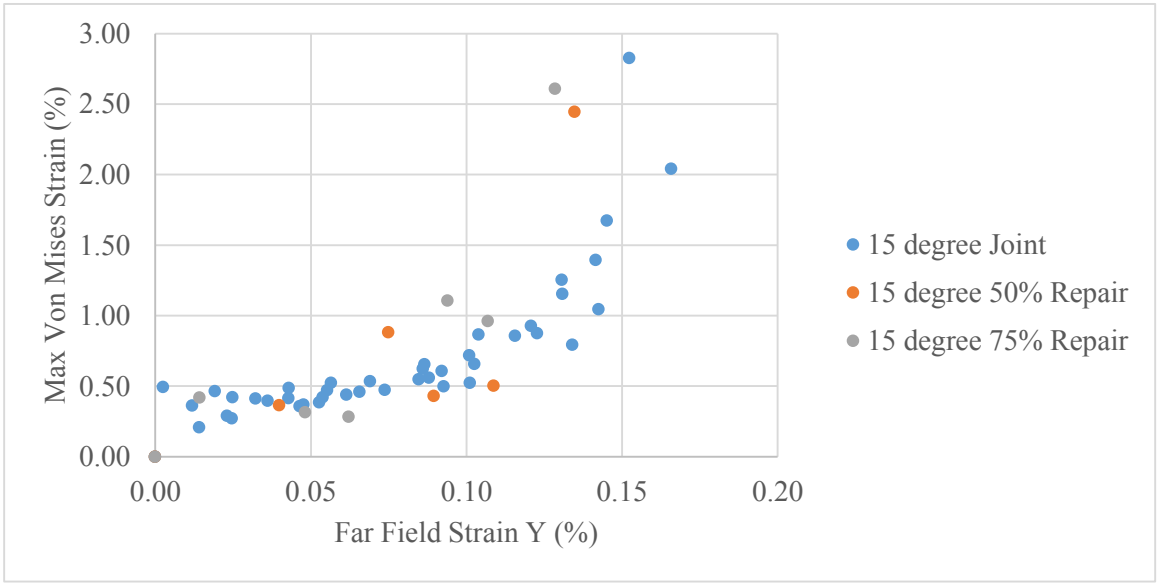

Figure 61: Max Von Mises Strain vs Far-field Strain in 15 Degree Joint and Repair Specimens with Carbon Uni Adherend and Epoxy Adhesive

50% repair specimens a standard deviation of 3.97 was calculated. Taking this into account, the failure results could in fact be more closely related than the averages present.

In spite of the differences in average strength and far-field strain values, the test results support the legitimacy of joints as a simplified representation of scarf repair when applied to the design of the adhesive bondline. A joint cannot accurately represent the damage progression and ultimate failure of a repaired structure. After failure of the bondline, the repair specimens continued to carry loads up to three times that of the joints before destruction.

Load shedding, a theory that un-scarfed surrounding parent plies would strengthen the repair, did not appear to be a factor. The specimens were only imaged along the thickness. The manner in which the adhesive fails along the width remains to be fully understood. It is possible that a repair fully surrounded by the parent composite would experience an increased strength due to load shedding. The exposed edges of the bondline in the repair specimens for this study do not allow for this analysis. However, the benefit of these exposed edges is the ability to image the strains throughout the adhesive bondline and composite parent to compare with 2D finite element models.

Finite Element to Experimental Comparison

Two dimensional finite element analysis was conducted on the Carbon adherend-Epoxy adhesive joint and repair configurations as well as the Carbon adherend-MA adhesive repair configuration using the MATLAB partial differential equation (PDE) tool. The polyurethane adhesive configuration was not modeled due to the unsuccessful test results of the polyurethane specimens. The failure criteria of 2.7% max Von Mises strain was imposed on the adhesive bondline of the model. Average far-field strain and

stress were calculated at the point of failure. Table 23 reveals the results along with percent differences from experimental test data.

Table 23: Experimental to FEA Comparison at Adhesive Failure for Carbon Uni Adherend Joint and Repair Configurations

Configuration	Max Von Mises Strain FEA (%)	Max Von Mises Strain Exp (%)	% Diff	Ave Far Field Strain Y FEA (%)	Ave Far Field Strain Y Exp (%)	% Diff	Ave Stress FEA (ksi)	Ave Stress Exp (ksi)	% Diff
EP/5/50%	2.7	2.52	7%	0.27	0.25	8%	26.28	25.53	3%
EP/5/75%	2.7	2.68	1%	0.24	0.23	4%	23.96	25.23	5%
EP/15/50%	2.7	2.75	2%	0.12	0.13	8%	11.3	14.27	26%
EP/15/75%	2.7	2.63	3%	0.11	0.12	9%	10.2	10.17	0%
MA/15/50%	2.7	2.61	3%	0.02	0.03	50%	1.68	4.15	147%
EP/5/Joint	2.7	2.62	3%	0.19	0.27	42%	19	31.8	67%
EP/15/Joint	2.7	2.83	5%	0.09	0.15	67%	9.15	15.5	69%
EP/25/Joint	2.7	1.54	43%	0.08	0.11	38%	8.1	8.92	10%

In the "Configuration" column, the first designation is the adhesive, followed by the scarf angle, and the final designation being the through thickness value. "EP" denotes Epoxy and "MA" denotes methacrylate.

Maximum Von Mises Strain: Repairs

The average max Von Mises strain over the 5degree, 75% through thickness experimental repair specimens was only 1% off of the average value over all the repair specimen. Thus, this configuration was used as a baseline for the model and then extended to the remaining configurations. This baseline provided excellent correlation to experimental values for fair-field strain and stress at adhesive failure with percent differences of 4% and 5% respectively. When extended to the other three epoxy adhesive

repair configurations, the FEA model continued to show good correlation with all but one value resulting in less than 10% difference compared to experimental data. There are a few factors that could have attributed to the large differences in the stress values for the 15 degree, 50% repair model including manufacturing and data collection errors. The image sampling rate for the DIC was two seconds. It is possible that adhesive failure may have occurred between images resulting in higher recorded values for the experimental data. The first occurrence of damage was difficult to capture visually. Test results showed that through thickness had little effect on the adhesive failure. However, FEA results show a decreasing trend in strength and far-field strain as the depth of repair increases. Figures 62-69 show the Von Mises strain overlays from the DIC at the stage just prior to the first visual observation of damage in the adhesive bondline in the repair adhesive. The DIC images are shown in comparison with the respective FEA model. The same color scale applies to both the FEA and experimental images. These figures show excellent correlation in Von Mises strain values and distributions through the specimen, as well as location of the max Von Mises strain and subsequent failure.

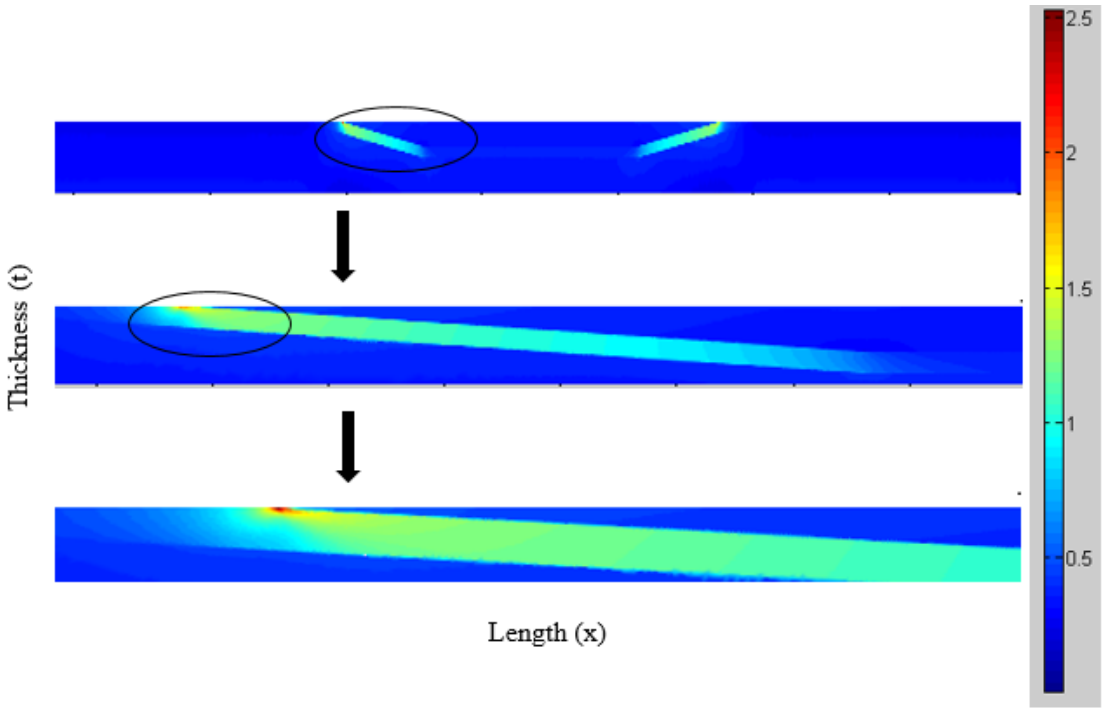

Figure 62: Von Mises Strain (%) in 5 Degree, 50% Repair Carbon Uni with Epoxy Adhesive FEA Model

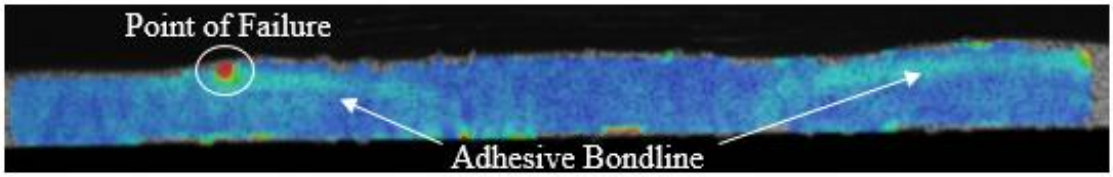

Figure 63: Von Mises Strain (%) in 5 Degree, 50% Repair Carbon Uni with Epoxy Adhesive Experimental ARAMIS DIC Results

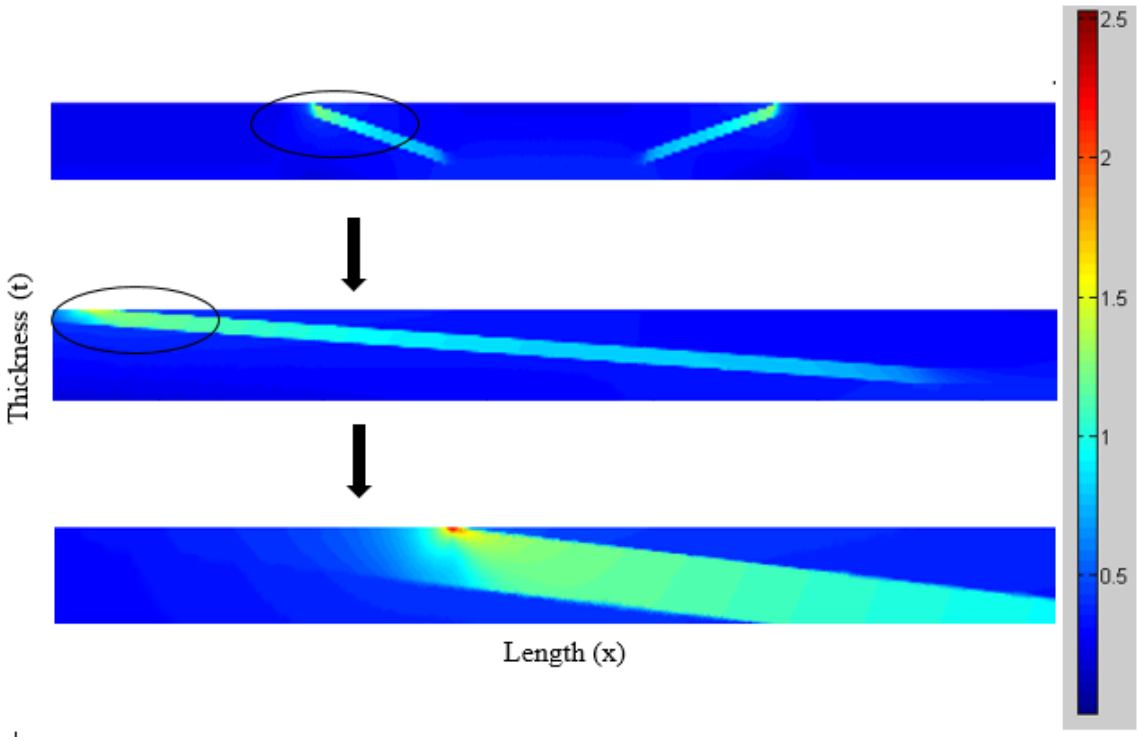

Figure 64: Von Mises Strain (%) in 5 Degree, 75% Repair Carbon Uni with Epoxy Adhesive FEA Model

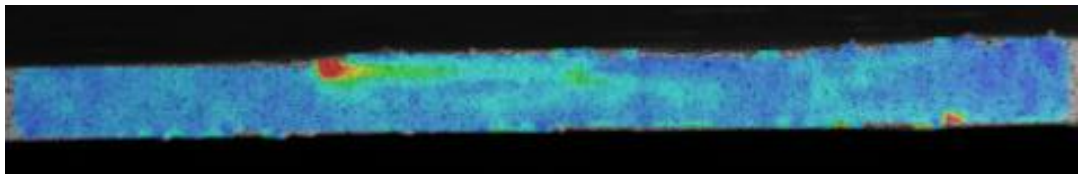

Figure 65: Von Mises Strain (%) in 5 Degree, 75% Repair Carbon Uni with Epoxy Adhesive Experimental ARAMIS DIC Results

*Half of the repair was imaged due to the extended length. Symmetry is assumed.

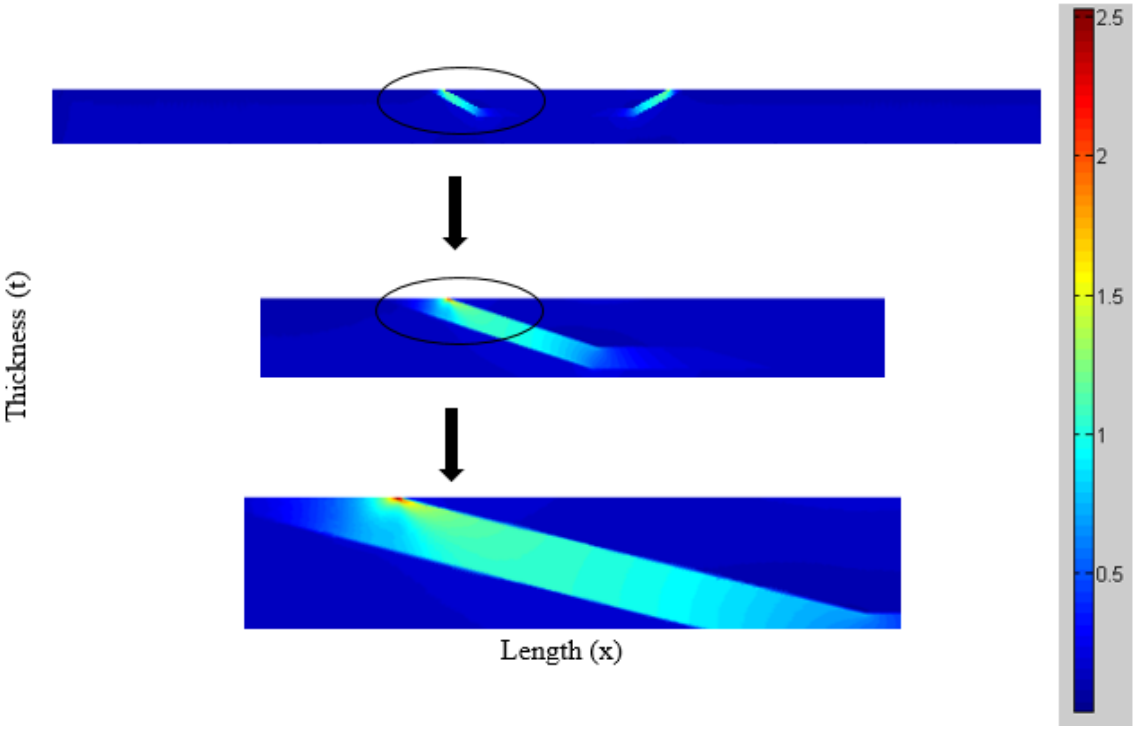

Figure 66: Von Mises Strain (%) in 15 Degree, 50% Repair Carbon Uni with Epoxy Adhesive FEA Model

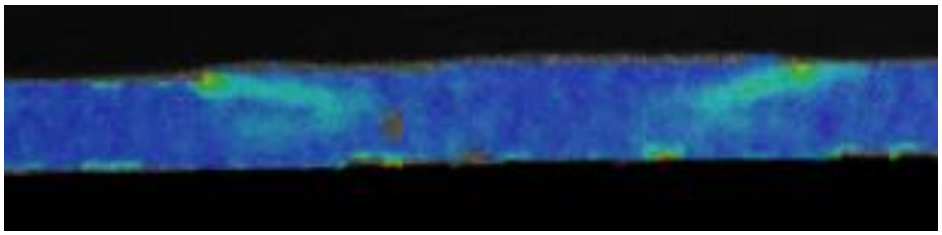

Figure 67: Von Mises Strain (%) in 15 Degree, 50% Repair Carbon Uni with Epoxy Adhesive Experimental ARAMIS DIC Results

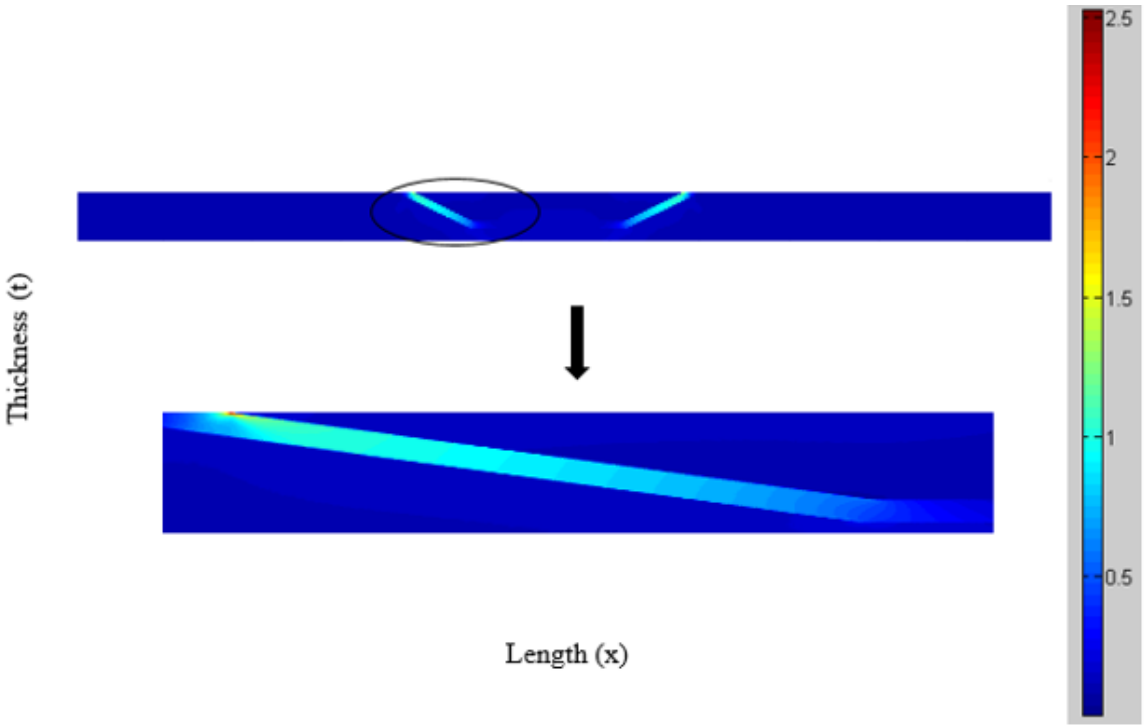

Figure 68: Von Mises Strain (%) in 15 Degree, 75% Repair Carbon Uni with Epoxy Adhesive FEA Model

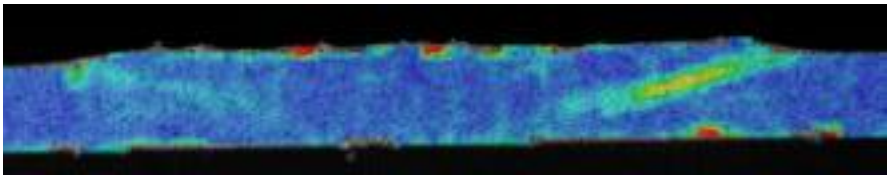

Figure 69: Von Mises Strain (%) in 15 Degree, 75% Repair Carbon Uni with Epoxy Adhesive Experimental ARAMIS DIC Results

Far Field Strain vs Max
Von Mises Strain: Repairs

Figure 70 shows FEA results for far-field strain plotted against max Von Mises strain in relation to the spread of experimental test results for the repair configurations. Although following a different trend, the finite element analysis falls reasonably within the spread of the experimental results in all cases. Due to the strictly linear elastic material assumptions of the FEA model and the use of a yield criteria as an ultimate

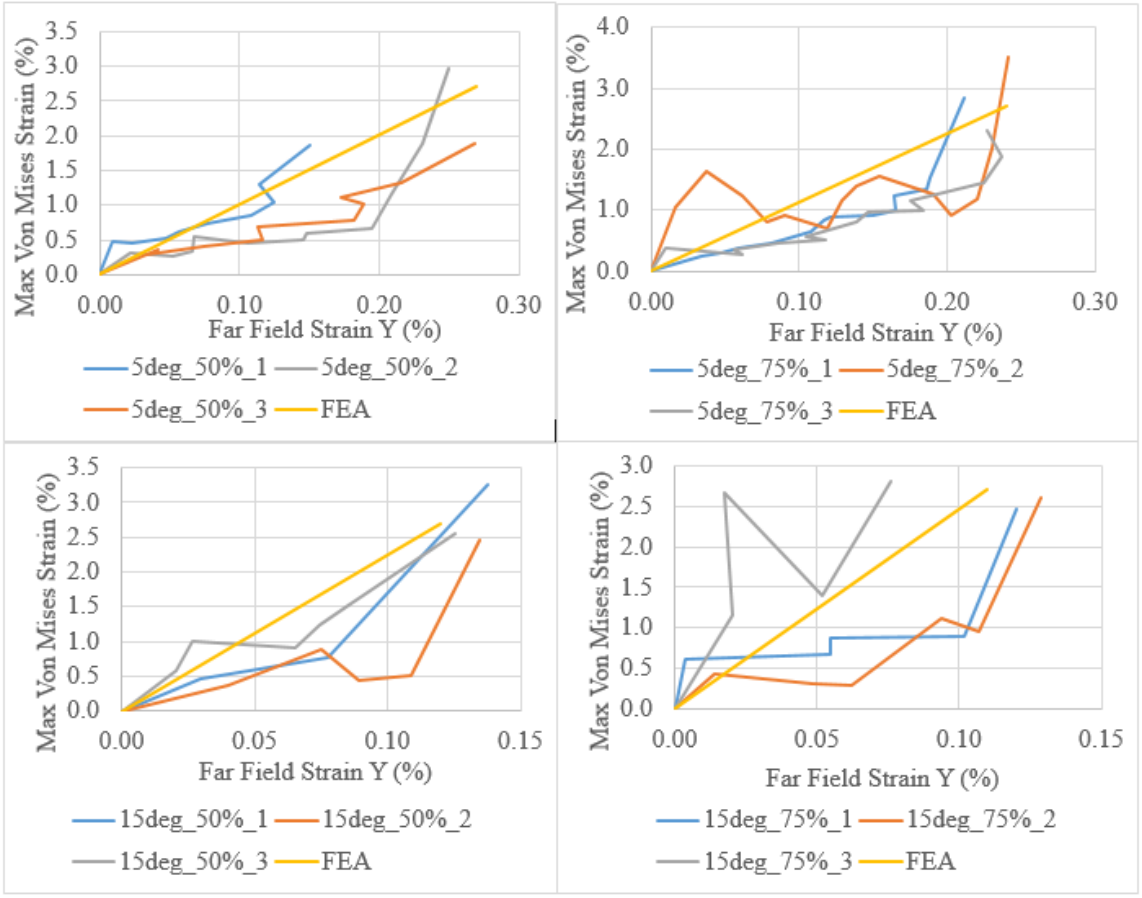

Figure 70: Max Von Mises Strain vs Far-field Strain Comparison between FEA and Experimental Results for Repair Configurations
Top Left: 5 Degree, 50% Repair, Top Right: 5 Degree, 75% Repair, Bottom Left: 15 Degree, 50% Repair. Bottom Right: 15 Degree, 75% Repair

failure criteria, the strain follows a linear trend with a slope greater on average than the elastic region of the test results. In reality, the adhesive, as a ductile material, undergoes plastic deformation resulting in yielding behavior when subject to tensile loading. This yielding is proportionally small when considering the elastic limit strains in relation to failure strains and thus the elastic assumption allows for acceptable correlation for the adhesive behavior.

FEA Adhesive Comparison

Comparing the MA adhesive to the Epoxy adhesive repair models, the Von Mises strains are definitively observed through the entirety of the bondline, including the non-angled portion, Figures 71-72. The epoxy adhesive models show very small values of

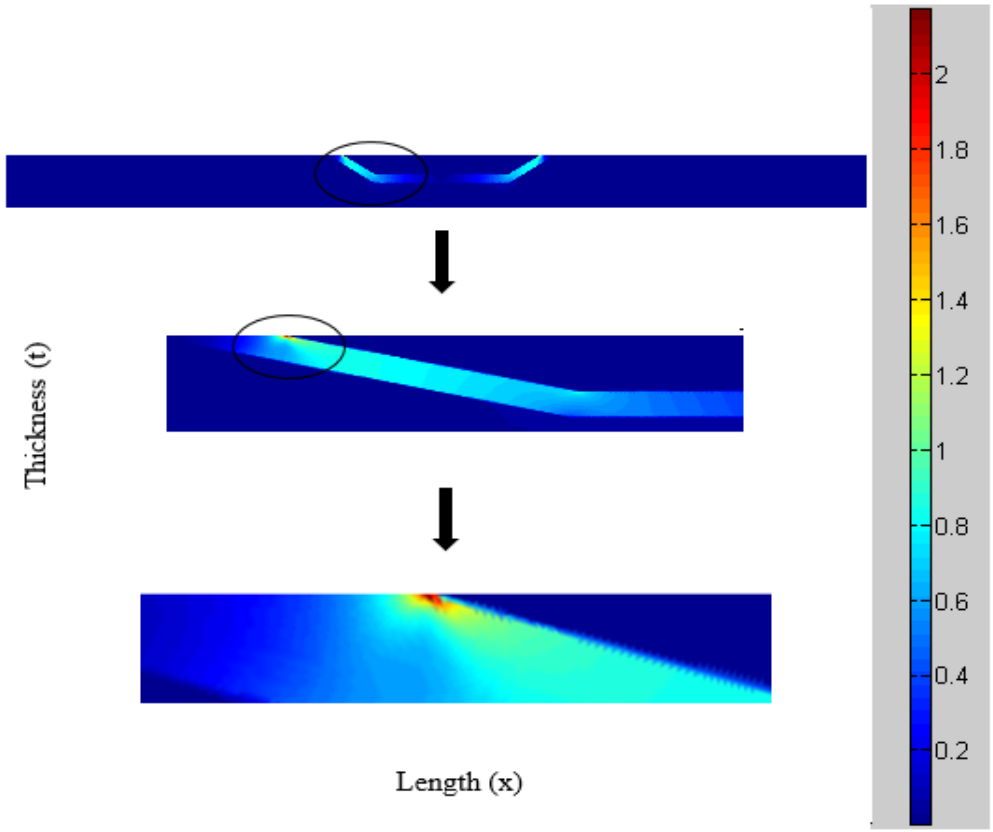

Figure 71: Von Mises Strain (%) in 15 Degree, 50% Repair Carbon Uni with MA Adhesive FEA Model

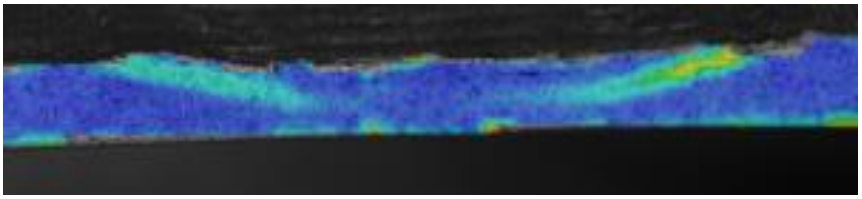

Figure 72: Von Mises Strain (%) in 15 Degree, 50% Repair Carbon Uni with MA Adhesive Experimental ARAMIS DIC Results

Von Mises strain in the non-angled bondline. The MA adhesive experiences increased strains in this area due to the lower elastic modulus. In relation to the experimental test results, the MA finite element model was less accurate than the Epoxy model. Far-field strain values in both experimental and FEA results were on the order of 0.03% and 0.02%. These extremely low values lead to high percent differences when compared in Figure 23. The stress results differed by nearly 150%, but again the values are very low, on the order of a few hundred kips. Actual numerical differences may be relatable. Only two MA specimens were tested since one of the intended test specimens was damaged during the manufacturing process. More testing is needed on the MA adhesive to achieve conclusive results on adhesive failure conditions.

FEA Joint Comparison

Model runs on the Carbon adherend-Epoxy adhesive joint configurations yielded anticipated results showing a distinct trend in strength and far-field strain reduction as through thickness increases from 50% in a repair to 100% in a joint for each scarf angle. As expected, strength and far-field strain values decreased as scarf angle increased. A reduction of 52% was observed moving from a 5 degree joint to a 15 degree joint with a 12% reduction moving from the 15 to 25 degrees. This nonlinear decrease was also observed in the experimental results. Von Mises strain overlay comparisons for the Carbon adherend joints are shown in Figures 73-78.

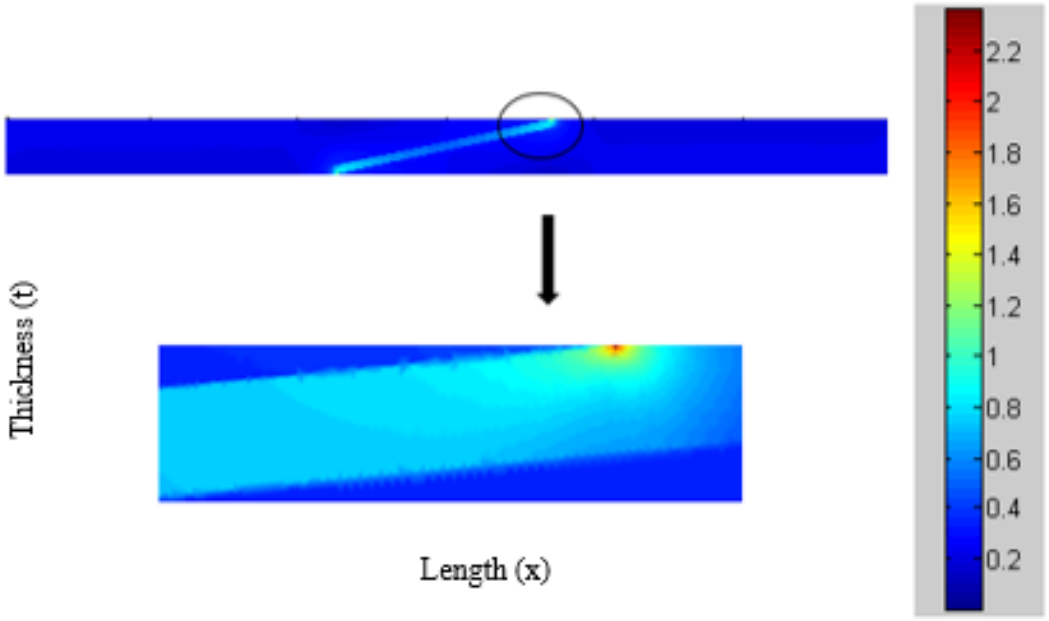

Figure 73: Von Mises Strain (%) in 5 Degree Carbon Uni, Epoxy Adhesive Joint FEA Model

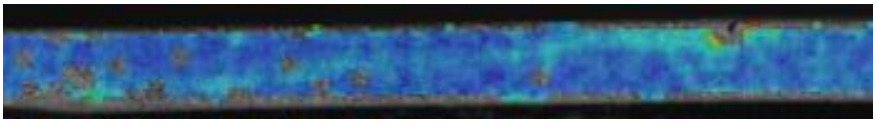

Figure 74: Von Mises Strain (%) in 5 Degree Carbon Uni, Epoxy Adhesive Joint Experimental ARAMIS DIC Results

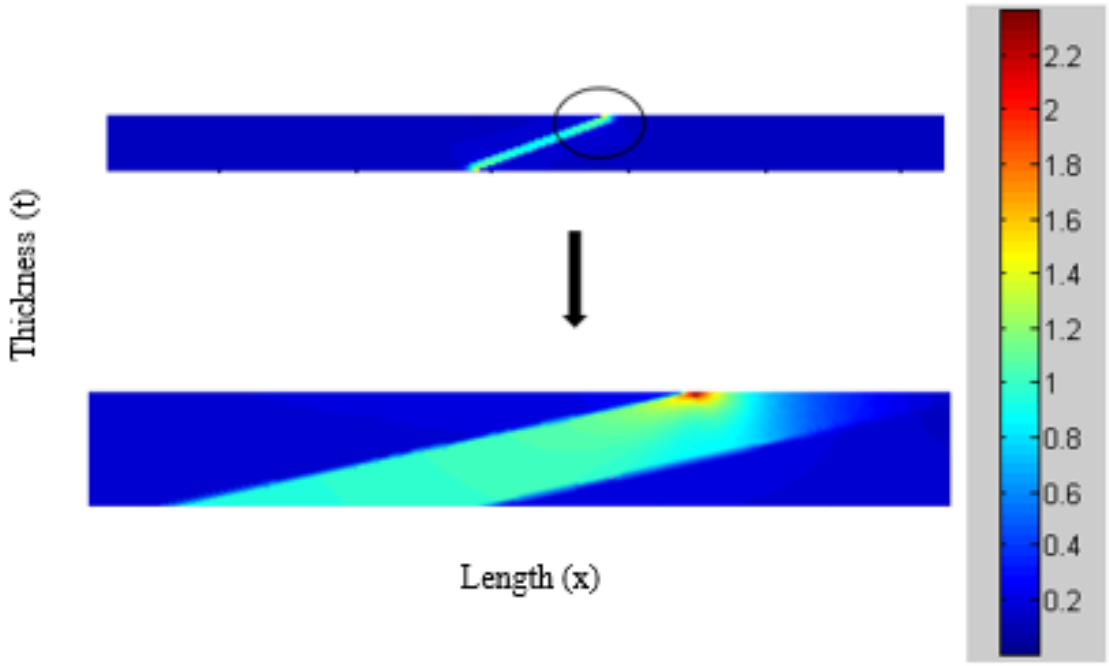

Figure 75: Von Mises Strain (%) in 15 Degree Carbon Uni, Epoxy Adhesive Joint FEA Model

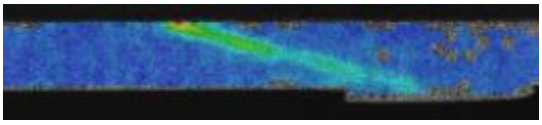

Figure 76: Von Mises Strain (%) in 15 Degree Carbon Uni, Epoxy Adhesive Joint Experimental ARAMIS DIC Results

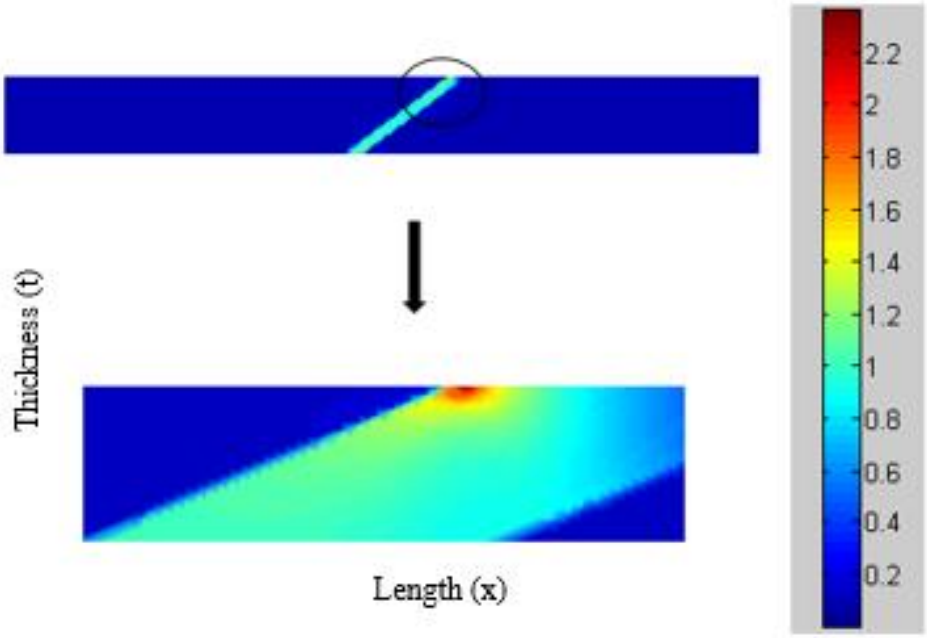

Figure 77: Von Mises Strain (%) in 25 Degree Carbon Uni, Epoxy Adhesive Joint FEA Model

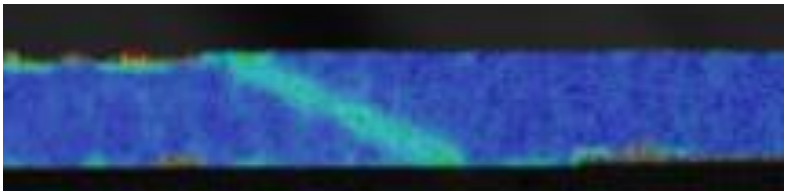

Figure 78: Von Mises Strain (%) in 25 Degree Carbon Uni, Epoxy Adhesive Joint Experimental ARAMIS DIC Results

The FEA model provides a good correlation to the trends in strength and strain as scarf angle is varied in a joint. However, actual values did not show good correlation with 40-60% differences as reported in Figure 23. The low confidence in comparisons of the experimental repair and joint data is likely driving these results. Since the FEA model was built from repair data it follows that difficulties would exist in correlating to joint experimental data. The repair and joint configurations experienced different failures. Adhesive failure to coupon failure in the joints occurred in a quick brittle

fashion, while for the repairs, the coupon continued to carry loads after the adhesive failed. Testing feed rates, data collection, and consistency with defining the point of adhesive failure could have all played a role in the lack or correlation to the experimental joint results. An important observation is the location of the maximum Von Mises strain value. The failure does not occur in the center of the adhesive, but very close to the interface with the composite adherend in both the joint and repair configurations. It is assumed that the same failure location occurred in the experimental specimens although it is difficult to tell the adhesive from the adherend material due to the paint scheme necessary for DIC imaging. While the location of failure was in close proximity to the interface, these configurations all exhibited cohesive failures. The damage likely initiated within the adhesive, then progressed along the path of least resistance to the adherend-adhesive interface where the stiffness differentiation between the materials creates a high stress concentration.

The images reveal that the strain distribution through the length of the adhesive decreases as the scarf angle increases. In the 5 degree joint model, Figure 73, there is a high strain concentration on the ends of the scarf with distinctly lower strain values in the center. As the scarf angle is increased to 25 degrees, Figure 77, the strain becomes more uniform along the length of the scarf. For all scarf angles, the distribution is symmetric about the center thickness of the coupon. The Von Mises strain distribution through the center of the adhesive joint was extracted from the FEA models and normalized through the thickness, Figure 79. The peak strains on the ends of the joint are far lower than the max Von Mises failure criteria of 2.7% since the strain concentration associated with the

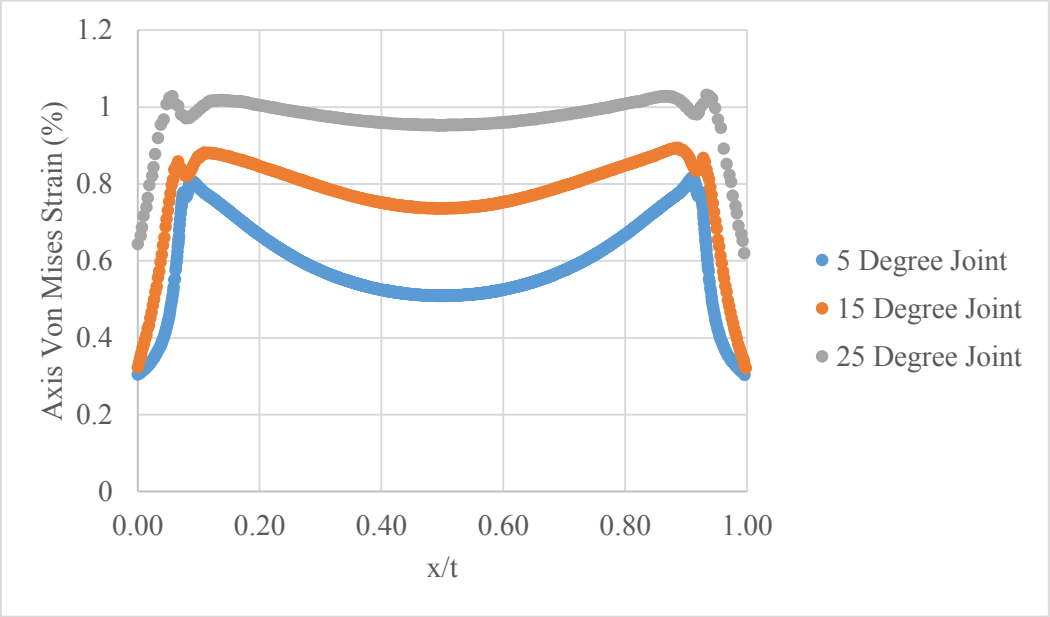

Figure 79: Joint FEA Von Mises Strain Distribution Through the Center of the Epoxy Adhesive

failure was not observed along the centerline. This figure depicts the distribution trends as scarf angle is varied as well as trends along the length of the scarf itself. The repair model experienced a symmetric strain distribution about the center of the repair. Distributions observed in experimental images did not maintain symmetry as in the FEA models. In general, a higher strain concentration developed more quickly on one end of the scarf than the other. This is either the result of non-uniformities in adhesive application throughout the bondline, or possible defects such as voids or porosity in the adhesive due to the manufacturing method. In the experimental repair specimens, the scarfed edges of the repair did not fail simultaneously as the FEA would predict. There was no pattern observed as to which of the two angled regions failed first leading to the belief that the primary factor is manufacturing.

DISCUSSION

Industry Application

Manufacturing Flaws

For industry applications such as wind power, knowledge and understanding of a repaired composite structure can enhance decision making in the field. Damaged structures and flaws induced by manufacturing processes drive the need for repair parameters to be defined. In many cases, the strength restored by a repair is less than the strength lost due to a defect and thus leaving the flaw unrepaired would achieve a longer life span. Blade Reliability Collaborative (BRC) research conducted at Montana State University investigated the strength lost due to manufacturing defects including in-plane waves, out-of-plane waves, and porosity. Table 24 lists a sampling of strength knockdowns for varying defects and 4-ply composite layups.

Table 24: Strength Knockdowns for Manufacturing Flaws in 4-Ply Composite Layups

Flaw Parameter	Composite Layup	Strength Knockdown
12 Degree Out-of-Plane Wave	Carbon Uni	14%
11 Degree Out-Of-Plane Chain Waves	Hybrid Triax	25%
4 Degree In-Plane Proximity Waves	Glass Triax	33%
6 Degree In-Plane Chain Waves	Glass Uni	37%
2-4% Porosity	Glass Triax	0%

This study suggests that the adhesive bondline in a scarf repair will initiate damage at 7% of the original strength of the structure when loaded in tension. This is a knockdown of 93% in comparison to the knockdowns in Table 24. After the repair bondline has failed, the point at which the parent composite material will initiate damage

is dependent on the depth of the repair. For a repair depth of two plies this point occurred at 15% of the original strength. Ultimate failure occurred at 40% of the strength of the original unflawed control specimen. This is a strength knockdown of 60%. When compared to the flaw parameters listed in Table 24, the best decision considering static tensile load cases is to leave the flaws un-repaired. For load cases involving compression or taking into account fatigue, a bonded repair may fair better than a flaw if the bond remains intact. The harmful effect of fiber waviness can become compounded under fatigue.

2D Joint Mechanics Methods

Current industry standards for full strength restorations require a scarf repair scheme with a scarf angle less than 3 degrees and an adhesively bonded patch of the same parent layup. Design methodologies define ultimate load per unit width as 1.5 times the allowable load per unit width, $P_{ult} = P_{all} * 1.5$ with the allowable load given by

$$P_{all} = \frac{2t}{\tan\theta} + D \tag{27}$$

Where t is the laminate thickness, D is the hole diameter, and θ is the scarf angle. Applied to the repair specimens manufactured for this study and extended to one to three degree scarf angles, the predicted ultimate failure stresses are calculated and listed in Table 25. Laminate thickness, t, of 0.15 inches and a hole diameter, D, of 0.5 inches was used to represent the Carbon Uni repair specimen. Ultimate stress was calculated by dividing the ultimate load by the approximate average cross sectional area of the tested repair specimens.

Table 25: Current Design Analysis of Scarf Repairs of Varying Angles

Scarf Angle (deg)	P_{all} (Per Unit Width)	P_{ult} (Per Unit Width)	Ultimate Stress (ksi)
1	17.69	26.53	82.91
2	9.09	13.64	42.61
3	6.22	9.34	29.18
5	3.93	5.89	18.42
15	1.62	2.43	7.59

Experimental testing for 5 and 15 degree scarf repairs resulted in ultimate stresses of approximately 25.5ksi and 10.5ksi respectively. These results indicate that current analysis leads to an overdesigned repair by 27.7%. This overdesign along with the 1.5 factor of safety between ultimate load and allowable load has resulted in extremely conservative repair practices. Given a 15 degree scarf angle, the ultimate load per unit width found in experimental testing is equivalent to the allowable load of a 6 degree scarf angle according to this analysis. The allowable load per unit width of a scarf angle considered to give "full strength restoration" can actually be achieved with a 6 degree scarf angle. The ultimate stress values for the 5 and 15 degree angles listed in Table 25 correlate well with the FEA results from the joint models suggesting this analysis was derived from a 2D joint geometry. FEA models showed a decreasing trend in strength as through thickness was increased for a given scarf angle. Experimental results from repair test coupons propose that strength is independent of through thickness. Thus, the use of 2D joint geometry to analyze non-through thickness 3D repair may in reality lend itself to an over design of nearly 28%.

To Repair or Not to Repair

Analyzing the failure in coupon level repair specimens can aid in optimizing design for repair and develop a more accurate standard for certification in the wind turbine industry. An optimized repair results in less time and material removal ultimately saving on cost. Location of the repair and the associated stresses and strains related to the loading conditions on that particular region of the structure is important in the decision to repair or scrap a blade. If the damaged area is subject to high tensile strains a repair will be unsuccessful and the structure should be scrapped or a bolted repair in place of an adhesive bond should be considered. Bolted repairs, while not typically practiced in the wind turbine industry, are best suited for thick structures that undergo high stresses. This research indicates that an adhesively bonded repair will only regain approximately 7% of the original strength of the structure before the bond fails. In light of this, bolted repairs, used frequently in the composite aerospace industry, may need to be implemented in wind turbines in place of bonded repairs. If the region typically experiences strains less than a fifth of the parent's max strain, there is a possibility that a successful bonded repair can be achieved. The optimal angle for the scarf repair can be based on the realized strains at the location of damage.

Failure Criteria for Certification Standards

Independent of scarf angle and depth of repair, the max allowable Von Mises strain for the adhesive is 2.7% and can used as a failure criteria in composite repair analysis. Germanischer Llyod, a wind turbine certification agency, states that for a repair to be certified the scarf ratio, $\frac{l_s}{t_s}$, must be calculated by

$$\frac{\sigma_{Mat}}{\tau} = \frac{l_s}{t_s} * \chi \tag{28}$$

Where σ_{Mat} is the tensile strength of the repair material, x=1 for hand laminate, 1.05 for tempering, and 1.15 for cure under vacuum and tempering. In this calculation, a failure criteria of permissible shear strength, τ, is set to 9 N/mm^2 for shop repairs and 7 N/mm^2 for in field repairs. The use of shear strength as a failure criteria is most applicable to ductile failures. As observed in experimental testing, the adhesive failure actually occurred in a more brittle matter likely due to the stress concentrations induced by the composite laminate. In addition, actual torsion testing has proven the Von Mises-Hencky maximum-distortion-energy theory to be 15% more accurate than the maximum-shear stress theory. Using a maximum Von Mises strain failure criteria in place of the maximum shear stress accounts for the multi-stress state induced by the scarf angle and can lead to more accurate repair design and analysis.

Geometric and Material General Conclusions

Geometry. Certain trends pertaining to geometric configurations and material choice can be drawn from this study. It is evident that decreasing the scarf angle will in turn increase the strength of an adhesively bonded scarf repair. The deeper the damage, the more material will need to be removed to achieve smaller angles and therefore, a one to three degree scarf angle is not always realistic in practice. Five and fifteen degree angles showed the best correlations using maximum Von Mises strain theory as a failure criterion. However, angles greater than this may be more suited for a Max Normal

Stress/Strain theory as stresses become dominated by the normal direction with higher angles.

Adherend Material. Material choice will greatly influence the behavior of a repair. When considering adherends, the behavior of the repaired structure will reflect that of the parent as seen in Figure 44. A repaired carbon structure will be stronger and stiffer, while a repaired glass structure will have a higher strain to failure.

Adhesive Material. Examining adhesives, it is apparent that an epoxy adhesive will result in the strongest, stiffest bond under tension. Brittle adhesives, such as epoxy, showed increased adhesion when paired with a brittle parent, such as carbon. Thus, it is possible that MA, a more ductile adhesive, would pair better with a glass adherend which has a higher strain to failure. Failure criteria should be derived for the individual adhesive type. It is interesting to note that the maximum Von Mises failure criteria of 2.7% derived for the Momentive Epikote Epoxy matches the published specification of bending ultimate strain of the adhesive. The bending ultimate strain parameter can be used as a starting point for development of adhesive specific Von Mises failure criteria to be used in repair design and predictive modeling.

Repair Design Optimization Process

Optimization of a repair design should begin with the initial considerations of the parent material and the stress-strain field of the location of the damage under normal operating loads and conditions. Next, an adhesive can be selected that is compatible to the parent material and loading condition. Epoxy based adhesives should be considered

for tensile loading conditions. Mechanical properties of other adhesives are comparable to Epoxy in pure shear and can be considered for structures stressed under this condition. Finally, the scarf angle can be designed based on the strength needs at the location of the repair. Higher stresses will require smaller angles. Adhesive specific Von Mises failure criteria can be used to determine the strength of the bonded repair.

As described in Table 1, numerous factors must be considered in designing the strength of a repair. This research analyzed the effects of scarf angle, depth of repair, adhesive type, and parent composite layup, and adhesive-adherend compatibility. Based on experimental and FEA results, the most important factors influencing the strength of a repair are scarf angle and adhesive type. Smaller scarf angles resulted in stronger adhesive bonds. The smallest angle analyzed was five degrees and it is postulated that decreasing the angle to as far as one degree will continue to significantly increase the strength of the bonded joint or repair. Adhesive type directly correlated to repair strength. The strongest specimens in tension correlated to the adhesive with the highest tensile strength. Choosing an adhesive with excellent mechanical properties for a particular loading condition will result in the strongest repair design.

SUMMARY AND CONCLUSIONS

This study developed and tested coupon level composite scarf repair specimens to compare against joint configurations in a tensile loading condition with three primary objectives. Static tensile testing led to the following conclusions for each given objective.

Objective I

Objective I: Quantify the effects of scarf angle, depth of repair, and material compatibility on failure in adhesively bonded joints and repair coupons to enhance decision making for the service industry.

i) Joint testing of varying adherends with an epoxy adhesive in 5, 15, and 25 degree angles primarily resulted in adhesive failure modes for glass adherends and cohesive failure modes for carbon adherends. This suggests that carbon is more compatible with epoxy than glass, possibly due to the more brittle nature of epoxy in comparison to other adhesives.

ii) The adhesive is the limiting factor in the strength of a repair, restoring only 7% of the initial tensile strength of the laminate. The location of the damage should dictate the design of the repair. In a low strain area, a bonded repair is sufficient. Knowledge of the typical strain field of a structure can help optimize the angle of the scarf repair. For areas subject to higher strains, other repair designs should be considered such as the addition of cover plies or a bolted repair. Data for small scarf angles

ranging from 1-3 degrees would be necessary to determine the threshold of tensile far-field strain on an adhesively bonded repair.

iii) Manufacturing defects inherent in composite fabrication can lead to a knockdown of strength in the laminate. Depending on the severity of the flaw, in many cases, the laminate will maintain a higher static tensile strength left un-repaired than the strength restored by an adhesively bonded repair. Other loading conditions, including fatigue, may reveal the superiority of a repair.

iv) Based on the results of this study recommendations for preliminary decision making in the service industry are outlined on the following flow chart, Figure 80. Examples of use are given below.

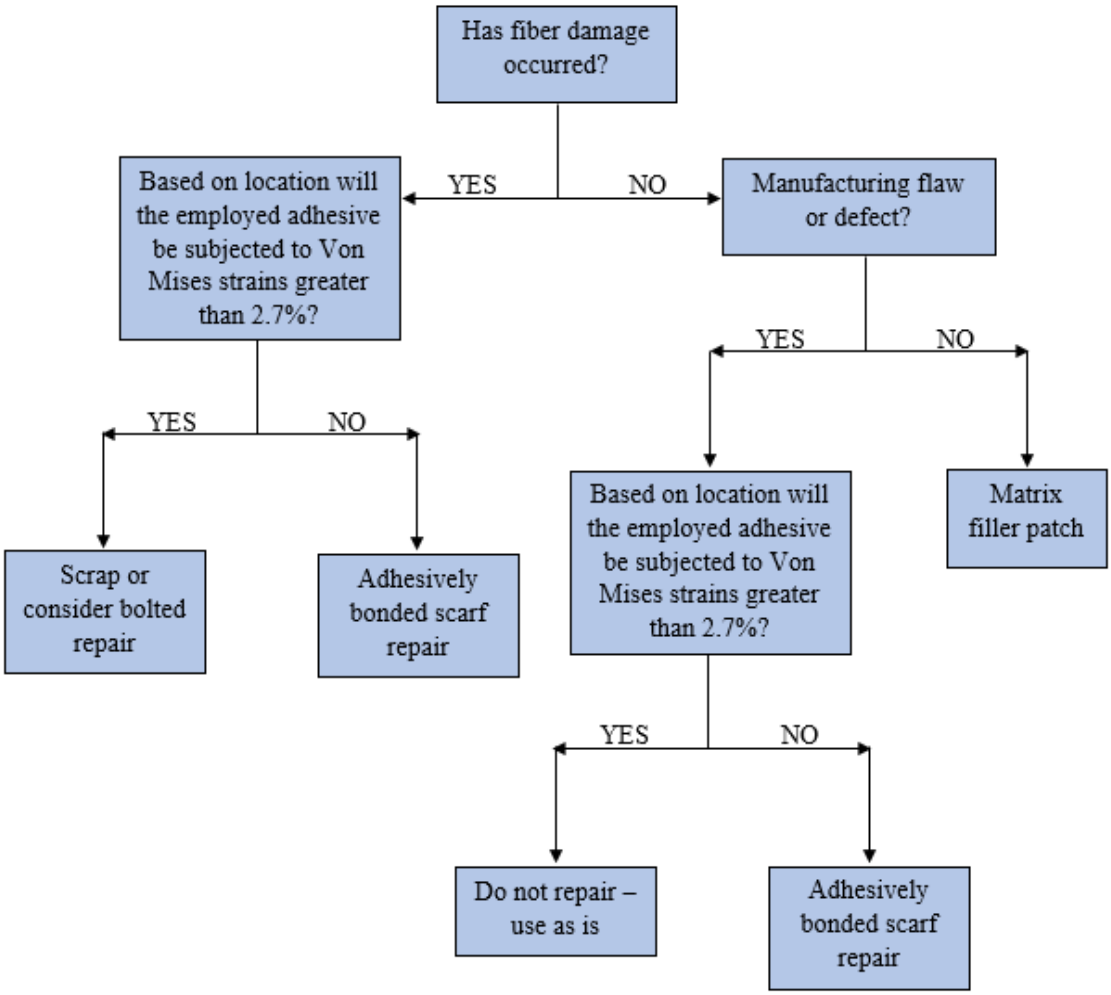

Figure 80: Decision Making Flow Chart For Adhesively Bonded Scarf Repairs

a. Example 1: A carbon wind turbine blade incurs impact damage in the field on low pressure side near the trailing edge of the blade. Upon visual assessment damage to the fibers is noted. Model runs indicate that the span-wise location of the damage does not experience high stresses under typically loading conditions such that the addition of an adhesive bondline would be subjected to max Von Mises strains of approximately

1.5%. Following figure 80, an adhesively bonded scarf repair could successfully be implemented for this case.

b. Example 2: Pre-shipment quality control inspection of a glass wind turbine blade reveals a 10 degree in-plane fiber wave caused by a manufacturing defect. The location of the flaw is shown through computer modeling to be in an area of moderate stress for the anticipated loads. An adhesive introduced to the location would experience Von Mises strains exceeding 2.7%. An adhesively bonded repair would fail in this scenario and as Figure 80 indicates, the best decision is to use the blade "as is."

Objective II

Objective II: Validate current composite repair standards in the use of 2D joint models to analyze 3D repair scenarios and derive a geometry independent failure criterion to more accurately predict the adhesive failure in the bondline of a scarf repair and correlate the criterion with finite element modeling.

i) Geometry considerations in scarf repair design are dictated by the following rules: 1) Scarf angle affects ultimate bondline strength but not the ultimate strength of the structure. 2) The number of plies removed in a scarf, or percent through thickness of a repair, affects the ultimate strength of a structure but not bondline strength. Thus, joints give an accurate

representation of failure in the adhesive bondline of a scarf repair, but not on the ultimate failure of the structure.

ii) Maximum shear stress failure criteria from 2D scarf joint analysis drives the wind turbine industry standards for repair set by the certifying agency, Germanischer Lloyd. This standard results in a conservative analysis, overestimating the design of the repair by 27.7%. An alternative approach to the maximum shear stress criteria is the maximum Von Mises strain criteria applied to the adhesive bondline. Test results show a maximum Von Mises strain of 2.7% to be geometry independent and more accurate in predicting failure than the certification agency prescribed maximum allowable shear strain of 9 MPa.

iii) Finite element analysis utilizing MATLAB's PDE Tool of 2D scarf repair models implementing the maximum Von Mises strain failure criteria showed good correlation to experimental test data.

iv) Load shedding to the parent composite plies through the thickness of the repair test specimen did not occur. Previous studies suggest load shedding may play a role for parent material adjacent to the repair width and length-wise.

Objective III

Objective III: Visually characterize the strain field and damage progression through the thickness of an adhesively bonded scarf repair and joint using ARAMIS data image correlation.

i) Damage in a composite scarf repair progresses through three distinct phases. The adhesive bondline in the repair patch fails first. A crack initiates in the parent between the last ply in the scarfed area and the first parent ply to remain intact. This crack progresses until the composite has fully delaminated between these plies until finally, only the non-scarfed parent plies are left to carry the load.

Future Work

Extended Research

Composite repair research remains in a ground breaking stage for low cost structures such as wind turbine blades. The diversity of possibilities provides numerous research opportunities. This study provides a foundation for the characterization of failure and optimization of repair techniques in composite structures. Further areas of research that would complement this study would include variations of bondline thickness, a comparison of film and paste adhesives, testing and modeling of joint and repair coupons with scarf angles between one and three degrees, and testing of scarf repair coupons under compression, bending, and fatigue load conditions. A bonded scarf repair is limited by the adhesive in regards to restoration of strength. For areas of high

stress within a structure options for strengthening the bondline will be imperative to repair design. The addition of cover plies over the repair for purposes other than an environmental seal should be explored with more criticality. Fiber orientation, number of plies, and compatibility of the materials with the parent structure could be key factors in strength restoration.

Joint and Repair Coupon Manufacturing Processes

Manufacturing processes for joint and repair coupons used in this study are open to refinement based on lessons learned throughout development. While processes used in this study were meant to reflect those performed in real world situations, a more robust manufacturing technique could result in increased strength values. The epoxy adhesive was mixed by hand, a technique which affords air the possibility of a non-uniform mixture leading to voids and porosity. Mixing the adhesive in a centrifuge and refining the application technique possibly with a cartage gun would eliminate these uncertainties and potential flaws. This would especially be beneficial for coupons that experienced adhesive failure modes as these modes could have been caused by a void at the adherend-adhesive interface. The bonding technique employed for the joints was sufficient for angles of 5 degrees and larger, but would become challenging when applied to smaller angles due to the bondline length required by the geometry. Use of a co-cured composite ply sandwiching the bondline may provide increased structural integrity. Utilizing a fixture during the cure cycle would provide for more accurate coupons. The ARAMIS DIC system requires the specimen to be painted in a speckling pattern for data gathering

purposes. The bondline was covered with the paint scheme inhibiting the visual distinction between adhesive and adherend. This lead to difficulty in deciphering fracture location and failure mode. It is recommended to mark the bondline interfaces for future DIC testing to aid in analysis of post-test images. Future work on the improvement and parameterization of manufacturing process for adhesively bonded repair techniques is a highly recommended area of study based on this research.

Additional Testing

Augmenting Current Results. Additional testing is also recommended for joint configurations in an effort to better define the point of initial adhesive damage. Due to the quick and brittle nature of the joint failures there was great difficulty identifying this point, leading to FEA model correlation problems and an inability to accurately compare joint and repair experimental results. This study was able to accurately capture the strain distributions through the joint. To augment this data, it is recommended for future testing imaging frequency be increased and the control volume of the ARAMIS be decreased to focus exclusively on the bondline edge of the thickness plane where the initial damage is predicted to occur. The smaller control volume with the ARAMIS will allow for more sub images distributed over a smaller area resulting in an increase of correlation data points and ultimately higher resolution images and strain overlays. With the increased resolution and imaging frequency it may be possible to capture adhesive damage initiation prior to coupon failure. Increasing the resolution and frequency should also be applied to additional testing on 15 degree, 50% through thickness repair specimens. It is

recommended that this configuration receive more testing due to its unconformity with the FEA model.

Adhesive Investigation. Further work with varying structural paste adhesives including additional work with the MA and Polyurethane adhesives used in this study warrant investigation. The limited specimen sample size for these adhesives inhibited conclusive results. Understanding the Von Mises limit of these adhesives will begin to shed light on the relationship between mechanical properties and failure criteria.

Subscale Testing. Development of time, cost, and resource efficient design parameters begins at the coupon level. Knowledge gained at the coupon level can then be applied at a sub-scale level, and then finally to a full scale structure. The findings from this study regarding scarf angle, through thickness variations, damage progression through the repair, and failure criteria can now be applied to a sub-scale test specimen. This specimen would allow for the repair to be fully enclosed by non-damaged parent sections giving further understanding to the possibility of a load shedding phenomenon. Another benefit to the sub-scale test level is the ability to vary the location of the repair. Threshold values of strain can be identified for the repair and applied to the structure for a given loading condition, thus revealing locations in which a bonded repair will be sufficient or a stronger repair design should be considered.

Finite Element Modeling

Finite element modeling is essential for predicting failure in any design. An accurate model increases confidence in prediction and leads to an efficient design. This

study conducted a 2-dimensional finite element analysis limited to bulk isotropic material properties which are able to fully characterize the adhesive but are a poor characterization of the composite laminate. Thus, the model used in this study is only useful in understanding failure at the adhesive bondline and is unable to model the damage progression experienced in the parent composite. The next step for finite element analysis is to extend the maximum Von Mises failure criteria from this study to a 3-dimensional Cohesive Zone Model (CZM). Cohesive Zone Models, evolutionary to fracture mechanics, models crack initiation and propagation as it takes place over an extended crack tip resisted by cohesive tractions. It is beneficial in the ability to predict behaviors of un-cracked materials. Other fracture mechanics models require the presence of an initial crack to predict fracture behavior. A CZM analysis will provide greater insight and predictive capabilities into the damage initiation and crack progression of the parent laminate in an adhesively bonded repaired structure.

Concluding Remarks

A multitude of variables exist within composite repair and very little data is available to fully characterize a repair's response to different loading conditions. Due to the lack of research in the area, standards in the wind turbine industry outline a conservative approach to certification of adhesively bonded repairs. The results of this study suggest that a maximum Von Mises failure criterion would result in a more accurate failure prediction of the adhesive bondline. Optimization of materials, scarf angles, bondline thickness, and other influential parameters will achieve the most

efficient composite repair design taking into account the location of the repair on a given structure. The most important of these parameters being scarf angle and adhesive selection. As additional experimental testing and finite element analysis of composite repair techniques adds to the knowledge base, the wind turbine industry will be better equipped to optimize repair design and to make decisions regarding when to repair, scrap, or take no action in response to manufacturing defects and damages in blades.

REFERENCES

[1]Wood, Karen, "Blade Repair: Closing the Maintenance Gap," Composites Technology, 2011.

[2]Wang, C.H.,Gunnion, A., "Design Methodology for Scarf Repairs to Composite Structures," Defence Science and Technology Organisation, 2006.

[3]Heslehurst, R.B., Analysis and modeling of damage and repair of composite materials in aerospace, Numerical analysis and Modeling of Composite Materials, Chapman & Hall, 1996.

[4]Lekou, D.J., Vionis, P., "Report on Repair Techniques for Composite Parts of Wind Turbine Blades," Optimat Blades, 2002.

[5]Tomblin, John, Seneviratne, Waruna, Yoon-Khian, Yap, "Shear Stress-Strain Data for Structural Adhesives," DOT/FAA/AR-02/97, November 2002.

[6]Hoke, Michael, J, "Adhesive Bonding of Composites," Abaris Training Inc, 2005.

[7]Hunstman Corporation, "Users Guide to Adhesives," Freeman MFG & Supply Co., 2007.

[8]Davies, P., Sohier, L., Cognard, J.-Y, et al, "Influence of adhesive bond line thickness on joint strength," International Journal of Adhesion and Adhesives, 2009.

[9]Cripps, David, Gurit, "Resin Comparison – Advantages and Disadvantages of Polyesters, Vinylesters, and Epoxies," http://www.netcomposites.com/guide/resin-comparison/18tComposites, 2014.

[10]Henkel, "Microplast Technology for Wind Turbines," http://www.henkel-ap.com/Macroplast_Technology_for_Wind_Turbines.htm,2014.

[11]Tomblin, J.S., Yang, C., Harter, P., "Investigation of Thick Bondline Adhesive Joints," DOT/FAA/Ar-01/33, June 2001.

[12]Germanischer Lloyd, "Rules for Classification and Construction, Materials and Welding," 2006.

[13]Hibbeler, R.C., Mechanics of Materials, 4th Edition, Prentice Hall, 2000.

[14]Barbero, Ever J., Introduction to Composite Materials Design, 2nd Edition, CRC Press, 2011.

[15]Srinivasa, V., et al, "Development of Damage Tolerant Adhesive Bonded Repair," CSIR-National Aerospace Laboratories-Bangalore, 2013.

[16]Kumar, S.B., et al, "Tensile Failure of Adhesively Bonded CFRP Composite Scarf Joints," Nanyang Technological University, 2013.

[17]Shih-Pin, Chou, "Finite Element Application for Strength Analysis of Scarf-Patch-Repaired Composite Laminates," Wichita State University, December, 2006.

[18]Tomblin, John S., et al, "Bonded Repair of Aircraft Composite Sandwich Structures," DOT/FAA/AR-03/74, February, 2004.

[19]Parker, John Wesley. *Development and implementation of a low cost image correlation system to obtain full-field in-plane displacement and strain data [electronic resource]/by John Wesley Parker*. Diss. Montana State University-Bozeman, College of Engineering, 2009.

[20]Momentive, "Epikote MGS BRP 135G Technical Datasheet," March 2009.

[21]Permabond Engineering Adhesives, "PT326 Polyurethane Adhesive Provisional Technical Datasheet," April 2010.

[22]Plexus Structural Adhesives, "MA 550 Technical Data Sheet," March, 2006.

[23]TWI Ltd, "Adhesive Design Toolkit," DTI, 2006.

[24]Samborsky, D.D., SNL/MSU/DOE June 25 2013 Composite Material Database, Version 22.0.